UNIVERSITÀ DEGLI STUDI DI TRENTO

Facoltà di Scienze Matematiche, Fisiche e Naturali

Dipartimento di Fisica

Tesi di Dottorato di Ricerca in Fisica
Ph.D. Thesis in Physics

Quantum Transport of Charges and Excitations through Macromolecules

Supervisor:
Prof. Pietro Faccioli

Candidate:
Elia Schneider

DOTTORATO DI RICERCA IN FISICA, XXVII CICLO
Trento,

Contents

Introduction

The investigation of real-time dynamics of charged and neutral quantum excitation propagating through macromolecular systems is receiving growing attention due to its potentially countless applications in nano-scale (opto-)electronics and in biophysics.

Semiconductor materials are nowadays fundamental in electronics and optoelectronics. The industrial interest is to constantly reduce the dimension of integrated circuits in order to obtain more powerful, lighter and less power consuming microchips. Recent efforts are aimed to understand the feasibility of organic and biological polymeric systems or aggregates as a route for boosting these requirements and thus, becoming the new paradigm in electronics and optoelectronics.

In this contest, the strategy of studying bulk macroscopic properties is not adequate. Atomistic approaches are essential to understand structural and transport properties of molecular electronic devices, revealing as an important and general techniques for facing on open problems in traditional semiconductor devices. Furthermore, as opposed to electric conduction in semiconductors, charge transport in soft condensed matter can be significantly influenced by molecular vibrations and by the surrounding environment. Consequently, any reliable investigation of quantum transport through biological macromolecules has to include environmental effects.

Whether quantum mechanics is needed to understand biological processes is a question that researchers have been asking since quantum mechanics has been founded. In his famous book *What is life?*, Erwin Schrödinger firstly observed that, since our understanding of the stability and structure of molecules is based on quantum mechanics, quantum phenomena are crucial for the stability of living beings and for their cellular processes. Recently, some experimental evidences have been revealed that quantum mechanics is not only fundamental to explain the properties of molecules and of their reactions, but also that some biological phenomena rely on quantum mechanisms to achieve functionality or to accomplish specific processes. These phenomena are studied in a new area of research called *quantum biology*.

At present, the most discussed phenomenon in quantum biology is the energy transport in photosynthetic complexes, that govern the light-harvesting processes in plants. Recent experimental works revealed long-lived coherent quantum energy transport in photosynthetic protein-pigment complexes at room temperature. This discovery has triggered a huge activity aimed at clarifying the interplay between quantum coherence, transfer efficiency and environment-driven noise.

In these fields, namely organic electronics and quantum biology, several models have been developed. All of these approaches have been described in the framework of open quantum systems.

Quantum transport in biomolecules and organic materials has been extensively studied with a phenomenological approach, in which the dynamics of the quantum excitation is described by simple models, such as one-body Hamiltonians. In these models, the fluctuation and dissipation generated by the molecular vibrations and by the heat bath are collectively represented by means of an effective bosonic bath. These effective approaches provide computationally efficient tools to investigate the general mechanisms underlying the long-range charge transport in macromolecules and the loss of quantum coherence in macromolecules. On the other hand, the lack of chemical detail makes it difficult to obtain quantitative predictions on quantum transport properties.

Complementary theoretical approaches have been developed which encode more information about the chemical structure of the macromolecule. For this reason, they are in principle better

suited to obtain quantitative predictions. These models are generally based on combining the Schrödinger equation for the one-body wave function of the quantum excitation with molecular dynamics simulations for the motion of the atomic nuclei. Quantum excitation dynamics in these models can be investigated in detail through extensive numerical simulations. On the other hand, the lack of analytic insight makes it difficult to identify the physical mechanisms involved in the transport dynamics.

In the present thesis, we develop and apply a microscopic theoretical framework to describe quantum transport in macromolecules, which combines chemical detail with analytic insight.

The quantum field path integral representation is adopted to describe the dynamics of the system's reduced density matrix. The path integral formalism is convenient because it makes it possible to describe molecular vibrations at the classical level, and to rigorously trace out the atomic coordinates from the density matrix in the small oscillation limit. The final result is a microscopic field theory describing the dynamics of biomolecular open quantum systems. In this theory, fluctuation-dissipation effects and thermal oscillations of the molecule are taken into account through effective interaction terms, derived from first principles.

Depending on the time and space scales we are interested in, there are different ways to study the quantum propagation by means of the effective theory mentioned above.

In the short-time and short-distance regime, we derive Feynman diagrams to perturbatively compute the effects of the dissipative coupling between a propagating quantum excitation, heat bath and atomic degrees of freedom.

In the long-time and long-distance regime, this problem is tackled by using the renormalization group formalism to systematically coarse-grain the dynamics. The result is a rigorous "low-energy" approximation of our initial microscopic field theory.

In the intermediate regime, the resummation scheme is applied to go beyong the perturbative approach without losing microscopic details. In this particular regime, comparison between theoretical predictions and experimental results is feasible and of particular interest for those who want to study long-lived coherence phenomena.

This thesis is organized as follows:

Chapter 1 gives a general overview about quantum transport in biomolecules. In particular, basic concepts about open quantum systems are introduced. Then, applications of this framework to the study of charge transport in organic substances and energy transfer in photosynthetic complexes are reviewed.

Chapter 2 describes a microscopic theoretical framework for the investigation of quantum transport in macromolecules, combining chemical detail with analytic insight. Firstly, the microscopic Hamiltonian for quantum transport is introduced. Secondly, the dynamics of the whole system are described by a path-integral representation, and, through appropriate approximations, our Quantum Transport Field Theory (QTFT) is derived. The results of this chapter have been published in Ref. [1]

Chapter 3 discusses a perturbation theory to solve the QTFT developed in Chapter 2, in short-distance and short-time regime. Using the standard Feynman diagram technique the leading order correction due to molecular vibrations and environmental effects is computed. As a first illustrative application of this formalism, a simple model to describe intra-chain charge propagation in a polymer is developed. The results of this chapter have been published in Ref. [1]

Chapter 4 deals with the long-distance and long-time limit. The renormalization group is adopted to systematically coarse-grain the dynamics. We show that, in this regime the transport dynamics reduces to a modified diffusion process. The analytic expression for the probability

density is derived and discussed. Finally, an illustrative application of this framework to hole propagation in homo-DNA is given. The results of this chapter are published in Ref. [2]

Chapter 5 describes the intermediate time regimes. To this goal, a non-perturbative method based on a Bethe-Salpeter type of resummation scheme is developed. In the Markovian limit we recover a Lindblad quantum master equation, while in the non-Markovian case imposing a series of approximations we find an analytic expression for the time evolution of the density matrix. We use it to study the exciton dynamics in a dimer model. Finally, we apply this method to simulate 2D-Photon Echo Spectroscopy experiments on a simple model of a dimer. The results of this chapter are not yet conclusive, a few improvements are needed befor to published them in a future article.

Chapter 1

Quantum Transport in Biomolecular Systems

Transport phenomena concern exchange of mass, energy or momentum between, or through, observed and studied systems. In classical physics, one of the most studied cases of transport is the diffusion process, a fundamental mechanism for several biological functions. In the quantum world, we can study similar transport phenomena involving molecular transfer of charged or neutral quantum excitations inside or between macromolecules [3].

In both regimes, the theoretical framework to investigate transport phenomena in biomolecules is that of open systems, in which effects caused by the molecule-environment interaction are taken into account. Regarding quantum transport, the coupling between the system (**S**) and the environment, or reservoir (**R**) makes the problem challenging even for system with a few degrees of freedom.

In section 1.1 we introduce this theoretical framework, called *open quantum system* (see Fig. 1.1). There are several fields of application for this theoretical tool, ranging from quantum optics to nuclear physics. In the following sections, we show two example systems, which could be investigated by means of the effective theory developed in this thesis. They both have a solvent as environment, but the kind of excitations transferred is different. In section 1.2, we present a study of exciton energy transfer in a photosynthetic complex or polymer. We show recent experimental observations regarding long-lived coherence study in these systems and we highlight current open questions in this field of research. In section 1.3 we introduce the problem of studying the charge transport in organic compounds, like DNA or polymers, focusing on two possible application of molecular wires and Organic Thin-Film Transistor (OTFT).

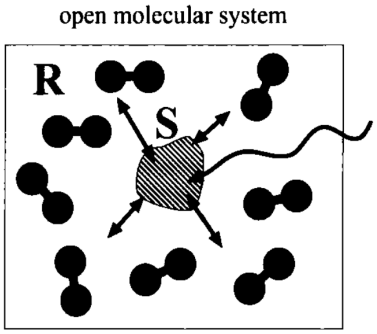

Figure 1.1: An open molecular system **S** interacting with its environment (reservoir) **R**. In addition the system may be influenced by an external field (wiggly line). Figure taken from Ref. [3]

1.1 Biomolecules as Open Quantum Systems

Any biological system should be described as an open quantum system due to the coupling with an uncontrollable environment, which perturbs it in a non-negligible way. However, most of the interesting systems are too complicated to be investigated directly by microscopical quantum laws.

A possible approach to these systems consists in seeking a simpler and effective probabilistic description, where relevant variables are governed by modified quantum laws. Environmental degrees of freedom are effectively taken into account by including additional dissipative and stochastic terms in the dynamics.

1.1.1 Closed and Open Quantum System

Let us consider a physical *closed* system $\mathbf{S}$, described by the Hermitian Hamiltonian $\hat{H}_{\mathbf{S}}(t)$, and introduce the density matrix

$$\rho(t) = \sum_{\alpha} \omega_{\alpha} |\psi_{\alpha}(t)\rangle\langle\psi_{\alpha}(t)| \,,$$

where the ω_{α} are positive weights and the $|\psi_{\alpha}(t)\rangle$ are normalized state vectors which evolve in time according to Schrödinger equation, whose solution with initial condition $|\psi(t_0)\rangle$ is

$$|\psi(t)\rangle = \hat{U}(t, t_0)|\psi(t_0)\rangle \,,$$

where the time-evolution operator reads

$$\hat{U}(t, t_0) = \mathrm{T}_{\leftarrow} \exp\left[-\frac{i}{\hbar}\int_{t_0}^{t} ds\, \hat{H}(s)\right] .$$

In the previous equation, $\mathrm{T}_{\leftarrow}$ denotes the chronological time-orderer operator which orders any product of time-dependent operators in the exponential expansion, in such a way that their time-arguments increase form left to the right. Applying the time-evolution operator to an initial density matrix, we can compute it at any time t

$$\rho(t) = \hat{U}(t, t_0)\rho(t_0)\hat{U}^{\dagger}(t, t_0) \,,$$

and differentiating the previous equation, we obtain the *Liouville-Von Neumann* equation

$$i\hbar \frac{d}{dt}\rho(t) = \left[\hat{H}_{\mathbf{S}}(t), \rho(t)\right] .$$

All formulas showed so far describe the dynamics of a *closed* system, whose evolution is unitary, time reversible and, if the system is isolated, energy conserving.

Having briefly summarized some basic equations describing the Hamiltonian dynamics of a closed quantum system, let us now turn to the notion of an open quantum system [4, 5].

In general terms, coupling the system $\mathbf{S}$ to another quantum system $\mathbf{R}$ called environment, bath or reservoir, yields an open quantum system. The combination of both systems $\mathbf{S} + \mathbf{R}$ is still closed and it follows the dynamics of the following unitary Hamiltonian

$$\hat{H}(t) = \hat{H}_{\mathbf{S}}(t) \otimes \mathbb{1}_{\mathbf{R}} + \mathbb{1}_{\mathbf{S}} \otimes \hat{H}_{\mathbf{R}}(t) + \hat{H}_{\mathrm{int}}(t) \,,$$

where $\hat{H}_{\mathbf{S}}(t)$ is the self-Hamiltonian of the open system $\mathbf{S}$, $\hat{H}_{\mathbf{R}}(t)$ is the free Hamiltonian of the reservoir $\mathbf{R}$, and $\hat{H}_{int}(t)$ describes the coupling between system and environment.

Usually, the environment has infinite degrees of freedom and it is unfeasible to explicitly compute the evolution of this part of the total system. The common way to investigate the interesting dynamics of the subsystem $\mathbf{S}$ consists in tracing out the reservoir's degrees of freedom,

$$\rho_{\mathbf{S}}(t) = \mathrm{Tr}_{\mathbf{R}}\left[\rho(t)\right] ,$$

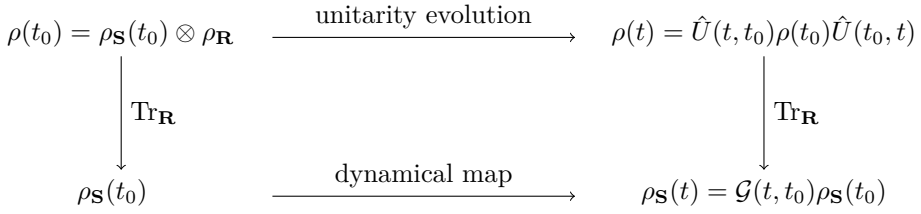

Figure 1.2: A scheme showing the relation between the dynamical map $\mathcal{G}$ and the time-evolution operator U.

obtaining the density matrix of the so called *reduced system* **S**. Due to the interaction with the environment, the dynamics of the reduced system can no longer be represented by unitary Hamiltonian dynamics. Therefore, we need to introduce a dynamical map $\mathcal{G}(t,t_0)$ which returns the time evolution for a given initial density matrix:

$$\rho_{\mathbf{S}}(t) = \mathcal{G}(t,t_0)\rho_{\mathbf{S}}(t_0)\,.$$

Let us point out that, besides, the loss of unitarity, the dynamics described by $\mathcal{G}$ dissipates energy, includes decoherence effects and it is no longer reversible.

1.1.2 Dynamical Maps: *Master Equation, Propagating Function, and Atomistic Simulation*

The exact computation of the dynamical map introduced in the previous section is a major challenge. Here we give a survey of common approaches employed to study the dynamics of the reduced density matrix [6], dividing them into three general methodologies.

Master equations

Master equation approaches provide equations for the propagation of the density matrix, by tracing out environmental degrees of freedom. These methods are usually based on the projection operator technique [7, 8], yielding a set of integro-differential equations:

$$i\hbar\,\frac{d}{dt}\rho_{\mathbf{S}}(t) = \sum_{m=1}^{N}\int_{t_0}^{t} ds\mathcal{K}_m(t,s)\rho_{\mathbf{S}}(s)\,.$$

An analytic formulation of the kernel function $\mathcal{K}_m(t,s)$ is known only in a few cases, thus approximations or numerical methods are required.

In the case of a system coupled linearly to an environment described by a set of harmonic oscillators, accurate approaches have been developed. A recent non-perturbative method suitable for a large range of problems is *hierarchy equations of motion* [9, 10]. It consists of the introduction of auxiliary operators $\hat{\Phi}_k$ and auxiliary matrices $\sigma^{\vec{n}}$ which account for the environment effects.The resulting master equation reads

$$i\hbar\,\frac{d}{dt}\rho_{\mathbf{S}}(t) = \left[\hat{H}_{\mathbf{S}},\rho_{\mathbf{S}}\right] + \sum_{k=1}^{N}\hat{\Phi}_k\sigma^{\vec{e}_k}(t)\,.$$

This method has been proved capable of reproducing known approximations in different regimes [12]. On the other hand, it is computationally expensive, and it scales badly with the size of the system **S** and with the complexity of the reservoir.

Another promising approach for system coupled linearly with a bath, recently proposed by Plenio and co-workers [13, 14], consists in an exact mapping of the environment onto an infinite

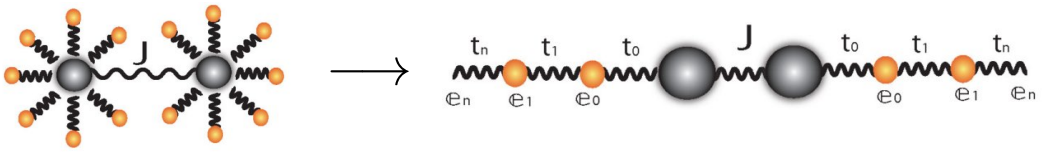

Figure 1.3: On the left a dimer system interacting with its surrounding environment, on the right the mapping onto a 1D chain. Figure taken from Ref. [13].

one-dimensional chain (see Fig. 1.3). In this way, the time-adaptive density matrix renormalization group (t-DMRG) technique can be applied to efficiently integrate the time evolution of the system-environment dynamics. This method is suitable for any choice of temperature, environment and system **S**. Furthermore, the truncation of the chain introduces a known and controllable error.

The main limitations of these two approaches are the impossibility to go beyond linear interaction between the system and the environment, and to have a directly relation between the microscopic world and the effective Hamiltonian used.

Propagating functions methods

A variety of methods are based on the propagating functions describing the time evolution of the density matrix of the system **S**. Generally, the core of these approaches is to numerically solve a formal real time path integral, combining some analytic manipulation of the action with the time discretization yielded by Trotter decomposition [15, 16]. In this way, memory, dissipative, and decoherence effects due to the environment are accounted for. A general time evolution described by propagating functions reads

$$\rho_{\mathbf{S}}(s',s'',t) = \int \prod_{i=0}^{N_s} \mathcal{D}s_i' \int \prod_{j=0}^{N_s} \mathcal{D}s_j^{''} \; \langle s'|e^{-\frac{i}{\hbar}H^{eff}(t_{N_s})\delta t}|s'_{N_s}\rangle \dots \langle s'_1|e^{-\frac{i}{\hbar}H^{eff}(t_0)\delta t}|s'_0\rangle$$
$$\langle s'_0|\rho_{\mathbf{S}}(0)|s''_0\rangle \; \langle s''_0|e^{\frac{i}{\hbar}H^{eff}(t_0)\delta t}|s''_1\rangle \dots \langle s''_{N_s}|e^{\frac{i}{\hbar}H^{eff}(t_{N_s})\delta t}|s''\rangle \; I(s',s'_{N_s},\dots,s'_0;s',s''_{N_s},\dots,s''_0;\Delta t)\,,$$

In the previous formula $H^{eff}(t_i)$ is the modified Hamiltonian at time t_i and I is a functional which takes non-Markovian effects into account. Below, we discuss two examples which are particularly close to the approach presented in this thesis.

In the Path Integral Monte Carlo method [17, 18], the environment is integrated out by encoding its influence on the system **S** in the *Feynman Vernon functionals* [19]. The dynamics of the reduced density matrix $\rho_{\mathbf{S}}$ is obtained by performing real time Monte Carlo simulation. Unfortunately, this technique is affected by the "dynamical sign problem", which originates from the quantum interference between different time paths, causing a small signal-to-noise ratio in the stochastic average. To mitigate this problem, Ankerhold used a technique suggested in Ref. [20], which exploits special symmetries of the influence functional. This approach is accurate but computationally expensive.

A second approach based on propagating functions is the Partial Linearized Density Matrix propagation [21, 22]. This method consists in a series of approximations that yields a mixed classical-quantum dynamics. The whole system consists by an electronic Hamiltonian which described quantum transport interacting with a generic environment. The quantum environmental dynamics in path integral representation is described by reservoirs coordinate R' and R'', which are transformed in mean and difference variables

$$\bar{R} = \frac{1}{2}\left(R' + R''\right)\,, \qquad\qquad Z = \left(R' - R''\right)\,.$$

Taking only linear terms in Z in the transformed action, a modified classical limit for the bath is recovered. Thus, by averaging over a large number of trajectories, it is possible to study the quantum dynamics of the reduced system **S**. This approach is generally applicable for arbitrary

system-bath interactions, in particular beyond the linear interaction with the environment, and can be readily applied to include non-Markovian effects. However, being a mean field approach, it cannot accurately take into account the "back reaction" between the classical and the quantum degrees of freedom.

Atomistic simulation approaches

Molecular modeling approaches are ab-initio simulations of both system and reservoir. These techniques combine molecular dynamics simulations for the environmental dynamics with the time integration of the Schrödinger equation, based on quantum electronic structure calculations, for the reduced system [23, 24, 25, 26]. The open quantum system dynamics can be investigated in great detail through extensive numerical simulations, but the main problem in these methods is to find the correct way to describe how classical and quantum degrees of freedom interacts during simulations.

In the following section, we present two examples in which the open quantum system theory presented above finds its application.

1.2 Exciton Energy Transfer in Biomolecules

In the past few years, the investigation on the transport of electronic excitations across biological systems has seen a renewed interest. The enthusiasm about quantum effects in biology [27, 28], is motivated both by fundamental questions and by related technological perspectives, for instance the improvement of solar cells efficiency.

The comprehension of fundamental mechanisms underlying the efficient energy transfer during the first steps in the photosynthetic process is still an open problem. Recent theoretical and experimental works [29, 30] suggest that quantum effects could play a crucial role for this biological function.

1.2.1 Experimental Evidences

Photosynthesis is the biological function that provides energy for all plants and many other organisms. Even in extreme conditions, when there is little sunlight, this mechanism works so efficiently that it makes life possible [30].

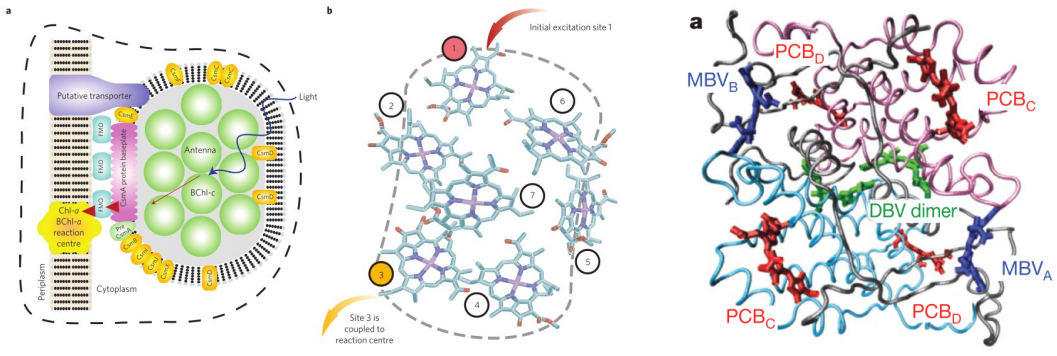

Figure 1.4: **Left panel**: diagram of the photosynthetic apparatus of green sulfur bacteria. Sunlight creates an excitation in this antenna that is transferred (red arrows) to the reaction center through one of several FMO complexes. **Central panel**: the molecule structure of one of the FMO pigment-protein complexes determined through X-ray diffraction. **Right panel**: X-ray structure determined through X-ray diffraction. Figures taken from Ref.s [27] and [34].

The energy of the sun, in the form of photons, is absorbed by light-harvesting antennas as an electronic excitation. This excitation is then transported from each antenna to a reaction center where charge separation creates more stable forms of chemical energy [31].

Researchers are particularly interested in light-harvesting apparatus of bacteria living in low-light conditions, because these organisms need to exploit a very efficient energy transportation mechanism in order to survive in such extreme conditions. One of the most well studied light-harvesting apparatus is the photosynthetic complex of green-sulfur bacteria, see Fig. 1.4. This structure includes a very large chlorosome antenna which collects any photon reaching the bacterium. After absorption, the energy is transferred to the reaction center through a specialized structure called the Fenna-Matthews-Olson (FMO) complex. The FMO complex is the most interesting part because of its high efficiency energy transfer, which is almost 100%. This means that almost every photon that is absorbed is successfully transferred to the reaction center, even though the intermediate electronic excitations are very short-lived (~ 1 ns).

From the experimental point of view, the fundamental mechanisms underlying the efficient energy transport are investigated by ultrafast spectroscopic techniques, which make possible to study the exciton transfer with high time resolution (~ 10 fs). In particular, 2D-Photon Echo Spectroscopy (2DPE) experiment is a suitable method to investigate the quantum coherence dynamics, i.e. the superposition of excitonic states during the energy transfer, thus if quantum effects play some role in this process [32]. Indeed, experimental observation employing this technique showed long-lived oscillatory features during this energy transfer in photosynthetic complexes [30, 33, 34], which have been interpreted as quantum coherent energy transfer.

This experimental method consists in the illumination of the molecular sample by three consecutive ultrashort laser pulses, and in the reception of a four photon. Varying the time delays between the four pulses, one can organize the data in a series of two 2DPE map for any difference time delay between the second and the third pulse, called *population time*. In Fig.s 1.5a and 1.5d we show two 2DPE maps. Studying diaganal and antidiagonal slice of any map, we can identify the beating signal interpreted as long quantum coherence dynamics. In Fig.s 1.5b and 1.5e we show the variation of the antidiagonal and diagonal slice of the 2DPE map for different time population, while in Fig.s 1.5c and 1.5f we show the oscillating signal in the cross peaks marked in the respective 2DPE maps.

This experimental discovery opened a large number of questions about the exciton energy transfer in natural and artificial light-harvesting complexes. If at physiological temperatures, environmental thermal fluctuations are not negligible, then which is their role in the exciton energy

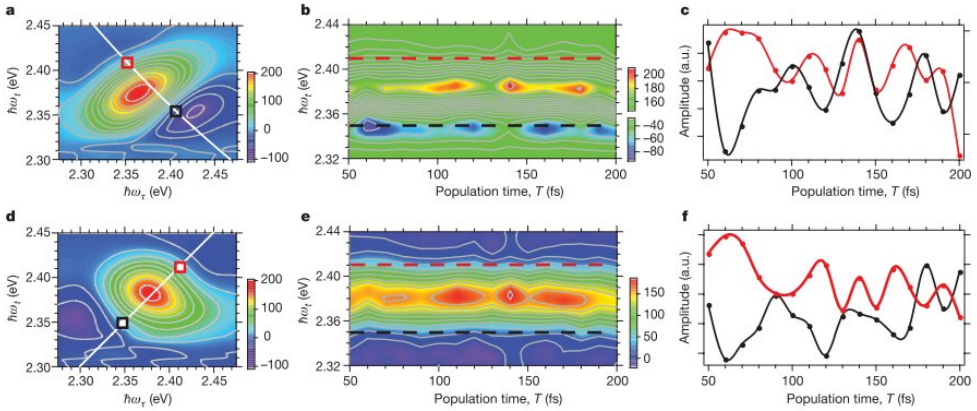

Figure 1.5: 2DPE spectroscopy data for cryptophyte antenna proteins. Figures taken from Ref. [34], where firstly was reported the detection of a long-lived coherence at room temperature in light-harvesting complex through a beating signal in a 2DPE spectroscopy experiment.

transfer? At room temperature, it was expected that quantum coherence could survive only a few femtoseconds in biological systems. Therefore, a reasonable question would be which is the right time scale for quantum coherence during the energy transfer and under which conditions coherence can survive for such a long time. Once the connection between fluctuations and energy transfer is understood, it would be interesting to assess the conditions in which the most efficient excitation energy transfer is realized. Finally, the most general question is whether quantum mechanics plays an important role in the physiology of living beings.

1.2.2 Vibrations and Exciton Energy Transport

In the past few years, several theoretical papers have been written in order to answer the questions presented above, focusing in particular on the role played by vibrations [35].

Recently, significant efforts have been devoted to numerically simulating the exciton energy transfer in the FMO complex in different conditions of noise and disorder. The most important and robust mechanism which has been discovered is the Environment-Assisted Quantum Transport (ENAQT) [36, 37, 38]. This concept shows that a highly efficient transport in an open quantum system can be obtained thanks to the interaction with a fluctuating environment. Both plots in Fig. 1.6 show the relation between the transport efficiency in the FMO complex and the dephasing rate, which is the inverse of the time it takes for the electronic excitation to lose quantum coherence, i.e the evolution between a pure state to a mixed state. Both plots demonstrate that optimal performances are found for an intermediate level of dephasing noise, and that three dephasing regimes can be defined: Anderson localization at low dephasing, ENAQT at intermediate dephasing, and Zeno regime at high dephasing.

As firstly suggested by Anderson [39], the degree of intrinsic static disorder in a system controls[1] the electronic wavefunction localization, proving that above a disordered threshold the eigenstates of the system Hamiltonian are localized in space[2]. As a consequence the quantum transport in this system is hindered, since overlapping between states is the element which makes possible coherent transfer. Therefore, at low noise level, where the dynamics is described at full quantum level by coherent hopping between sites, Anderson localization suppresses the quantum transport, as we can observe in Fig. 1.6.

For larger dephasing rate, we observe that noise enhances the efficiency of the quantum trans-

[1] The intrinsic static disorder is related to the variations in the excitonic energy levels of different sites and in the hopping probability.

[2] The degree of localization mainly depends on the ratio between the variation in the energies and the hopping strength: for a small ratio the system should exhibit weak localization, while strong localization should take place for a large ratio.

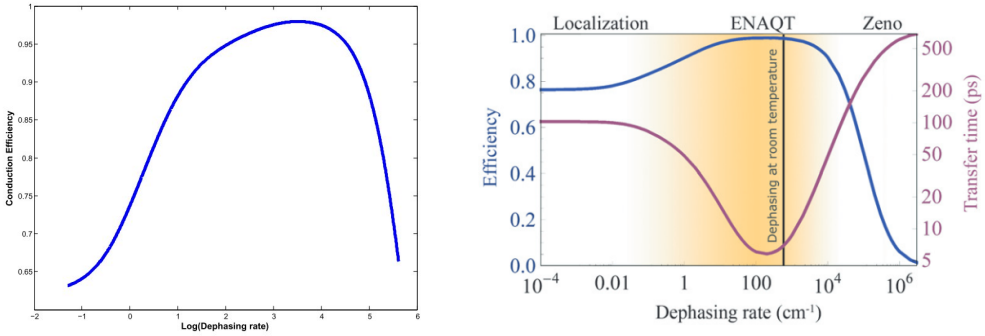

Figure 1.6: **Left panel**: plot of the conductivity of the FMO complex versus the overall strength of the dephasing noise. **Right panel**: efficiency (blue) and transfer time (red) as a function of the pure-dephasing rate for the FMO complex. Figures taken from Ref.s [35] and [36].

port. A possible explanation is that the dephasing mechanism, besides destroying quantum coherence, delocalizes quantum states allowing the excitation to propagate through the system [36]. The dynamical noise broadens energy levels, enhancing the wave function overlap, i.e. the hopping probability, between sites. An alternative interpretation is that the dephasing mechanism suppresses the destructive interference, allowing some paths that would be enviable without the noise [38]. The ENAQT mechanism is akin to the stochastic resonance [40], a phenomenon in which a signal, that is normally too weak to be detected, can be enhanced by adding white noise.

On the contrary, at very high noise level the quantum transport is again suppressed. This suppression by high dephasing can be interpreted as an example of the "watchdog effect" (i.e. quantum Zeno effect). In this regime, the environment constantly measures the system, hindering the quantum transport of the excitation through the FMO complex.

An extensive investigation of different regimes [41, 42, 43, 44] and of numerical solutions of increasing accuracy [10, 23, 45] has been performed, confirming the illustrated ENAQT principle.

On the other hand, the origin and the role played by long-lived coherence as experimentally observed are still an object of debate in the literature.

One of the open questions concerns the unambiguous determination of the nature of the observed long-lived coherence in 2DPE spectroscopy among pure vibrational, mixed exciton-vibrational (vibronic), or predominantly excitonic. In several papers [46, 47, 48, 49] the theoretical tools devised for the study of the time evolution of the density matrix have been used to reproduce 2DPE experimental maps and to clarify the origin of the observed long-lived coherence. Plenio first suggested a solution, arguing that a non-trivial spectral structure of protein fluctuations can generate a non-equilibrium processes that leads to the spontaneous creation and sustenance of excitonic coherence [29]. Thus, the coupling between long-lived nuclear vibrational modes and the excitation dynamics preserves the excitation quantum coherence for a longer time than expected. This particularity is closely related to the non-Markovian property of the thermal bath (long-memory effects) [10, 29]. Although this solution is not definitive, it remains the most valid suggestion to explain the nature of long-lived coherence in light-harvesting complexes.

The issue about the role of quantum coherence in the excitation transfer process is more complex. In several 2DPE experiments for different FMO complexes, long-lived quantum coherence has been observed [47]. This fact seem to suggest a strong relation between long-lived coherence and high efficiency in the excitation energy transfer. This assumption has been strongly criticized. One of the most common observations is that coherence is created only by ultrashort laser pulses used in the experiments, and incoherent light sources, such as the Sun, would not produce the same effect. At present, only a few experimental and theoretical studies [51, 50] tried to elucidate this critical point with no definitive conclusions.

Another open debate concerns the classical or quantum nature of the highly efficient excitation transport. In Ref. [52] it is shown that a highly efficient noise-assisted energy transport can be found also in purely classical systems. Instead, in Ref. [53] it is demonstrated that the energy transfer in FMO complex can occur and be enhanced from non-classical fluctuations of collective molecular motions.

1.3 Charge Transport in Organic Compounds

Organic electronics has emerged as a promising field of research and technological development. On the applied research side, organic semiconductors promise the advent of fully flexible and cheap electronic devices [54, 55]. Furthermore, molecular structures have the following major advantages. A very small size (between 1 and 100 nm), enabling the reduction of the size of integrated circuits. They also offer the chance of exploiting intermolecular interaction to form and modify structures by nanoscale self-assembly, and the opportunity to take advantages of multiple distinct stable geometric structures with different optical and electronic properties. On the basic research side, theories developed from the fifties on to describe charge transport in molecular crystal proved to be inadequate for the investigation of the majority of high mobility molecular semiconductors, opening a new fascinating research field [56, 57]. The only similarity between organic and inorganic

semiconductors is the the energy difference between the highest occupied levels and the lowest unoccupied levels (the energy gap). The electronic structure, the interaction between nuclear and electronic degrees of freedom and the role of defect states are so different in organic molecule that new methodologies have been developed in order to investigate the mechanisms of molecular charge transport [24, 58].

In the following sections, we focus on two specific areas of molecular electronics, namely molecular wires and Organic Thin-Film Transistors (OTFT). In both examples, understanding how molecules transport charge is fundamental to improve performances and design of new devices. Furthermore, dynamical fluctuations are an important factor governing the charge transfer, since they can favor or hinder the charge/hole migration.

1.3.1 Molecular Wires

Nowadays one of the challenges in organic electronics consists in building devices made of individual molecules [59]. To achieve this goal, it will be necessary to completely control and understand the electron transport through a molecule attached to electrodes, namely the charge transport in a molecular wire (see Fig 1.7).

A simplified picture of electron transport through molecular wires consists in a combination of a strongly distance-dependent *tunneling mechanism* and a weakly distance-dependent *incoherent transport* [60].
In the tunneling mechanism, during the transfer, no electrons or holes ever actually reside on the molecular wire, i.e. molecular orbitals are used solely as a coupling medium to connect donors and acceptors. The relation between the length of the molecular wire and the tunneling rate [61] is exponential:

$$W_{tun} \;=\; \nu_{tun}\, e^{-\beta\, r_{\mathrm{DA}}}\,,$$

where k_0 is the pre-exponential frequency factor for the tunneling transitions between neighboring sites and β is the falloff parameter. Therefore, in the case of a long molecular bridge this mechanism becomes inefficient.

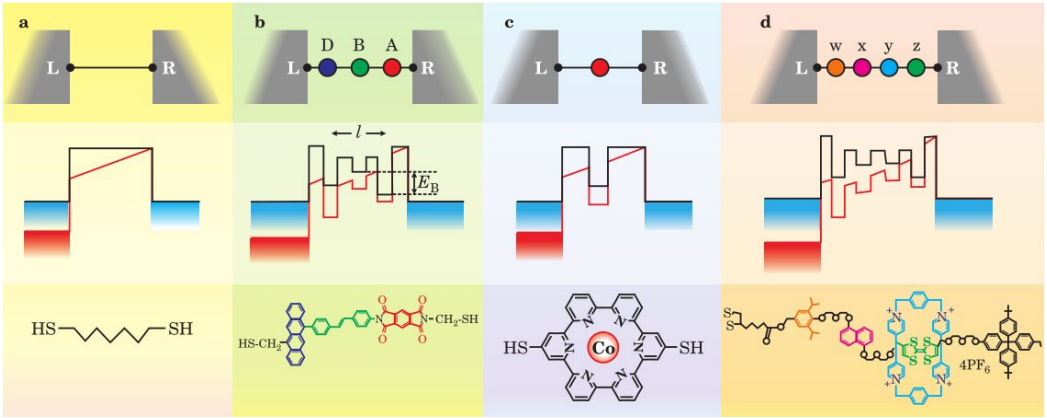

Figure 1.7: Examples of molecular transport junctions: (**a**) a linear chain of saturated C-C bonds, (**b**) a donor-bridge-acceptor, (**c**) a molecular quantum dot system, (**d**) a macromolecule, like a protein or a DNA chain. The top panels depict molecules with various localized, low-energy molecular orbitals (colored dots) bridging two electrodes L (left) and R (right). In the middle panels, the black lines are unperturbed electronic energy levels; the red lines indicate energy levels under an applied field. The bottom panels depict representative molecular structures. Figure taken from Ref. [54].

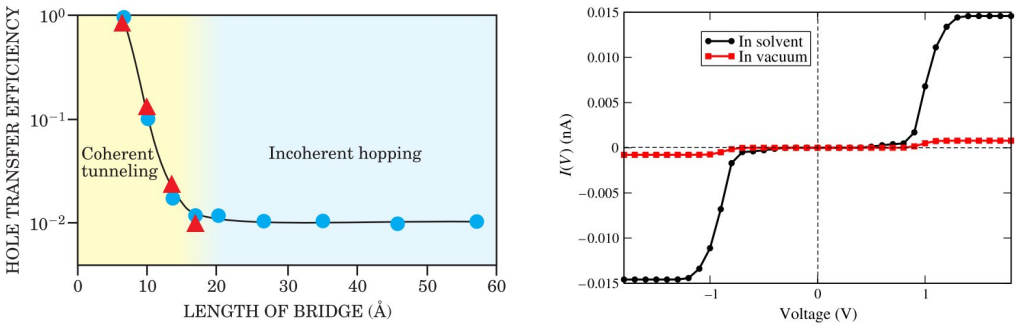

Figure 1.8: **Left panel**: experimental (triangles and circles) and theoretical (solid line) results for the relative rate of hole transfer in between guanine-cytosine (GC) base pairs on DNA oligomers [54, 61]. **Right panel**: Electrical current for a DNA chain both in vacuum (without solvent) and including the solvent [56, 62].

On the contrary, the incoherent charge transfer involves thermal activated jump between molecular orbitals along the wire. The simplest assumption to describe the hopping rate is the Arrhenius law,

$$W_{hop} \;=\; \nu_{therm}\; e^{-\dfrac{\Delta}{k_{\rm B}T}}\,,$$

where ν_{therm} is the pre-exponential frequency factor for the thermally activated release of a hole temporarily localized on a molecular orbital, Δ is the energy gap, $k_{\rm B}$ is the Boltzmann constant, and T is the temperature.

Exponential decay in the conductance with increasing distance has been directly seen in DNA molecules folded into hairpin shapes, and the transition to incoherent hopping has been seen in measurements of the efficiency of hole transfer along the molecule. In Fig. 1.8 we observe the transition from tunneling to the thermally activated mechanism.

In last years, some works focused on the treatment of dynamical effects in the charge transport along molecular wires by building in information from quantum chemical calculations and Molecular Dynamics [24, 25, 62]. This hybrid approach consists in the computation of the charge transfer parameters along nanosecond Molecular Dynamics trajectories, including solvation effects by means of a Quantum Mechanics/Molecular Mechanics (QM/MM) coupling scheme. In Fig. 1.8 we show one of the main results of this approach, consisting in the considerable enhancement of the current upon inclusion of solvent molecular fluctuations.

1.3.2 Organic Thin-Film Transistors

OTFTs are Metal-Insulator-Semiconductor Field-Effect Transistors (MISFET) in which the semiconductor is a conjugated organic material (see Fig. 1.9). In these devices, the semiconductor is separated from the metal electrode by a thin insulating layer (the gate dielectric, G). Whenever a voltage difference between the gate dielectric and the semiconductor is applied a thin sheet of mobile electronic charges is created in the semiconductor in the proximity of the interface. With two metal contacts attached to the semiconductor (the source contact, S, and the drain contact, D), the electric current flowing through the transistor can therefore be chosen in a wide range, simply by adjusting the gate voltage. Both for organic and inorganic MISFETs, the transistor performance mainly depends on the charge carrier mobility, μ, on the current modulation (or on/off ratio, I_{on}/I_{off}) and on the stability after a prolonged exposure to ambient conditions of the $I-V$ characteristic [63, 64].

Among the features listed above, the field effect mobility, or charge mobility, is the macroscopic key quantity that characterizes the charge transport in semiconductors. The room temperature

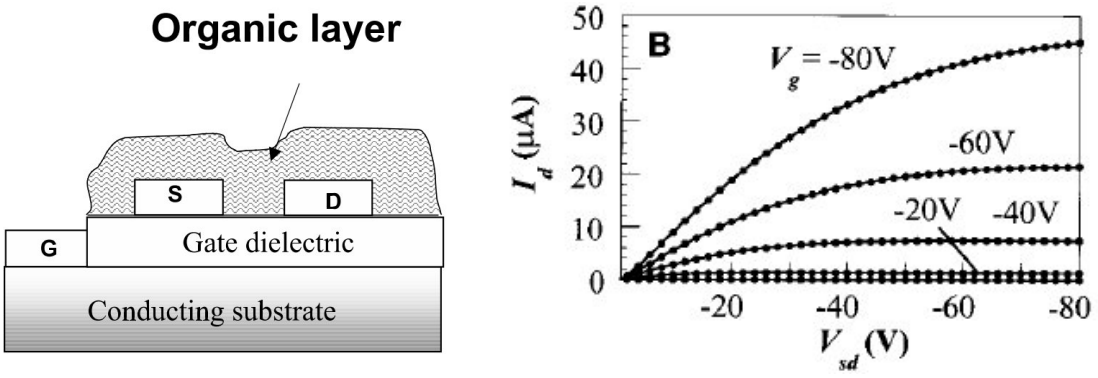

Figure 1.9: **Left panel**: typical OTFT device structure. **Right panel**: $I - V$ characteristic of a typical OTFT. Figure taken from Ref.s [66] and [68].

charge mobility of the most conductive organic semiconductor is a few tens of $\mathrm{cm^2V^{-1}s^{-1}}$ [65], while the value for silicon is an order of magnitude larger. As a consequence of this upper limit on the mobility that can be achieve with organic molecules, OTFTs cannot rival the performance of MISFETs based on inorganic semiconductors. However, OTFTs can be competitive candidates for thin-film transistor alternative applications requiring large area coverage, structural flexibility, low temperature processing, and especially low cost production [63]. Additionally, the use of OTFT as a sensor device has been considered [66, 67].

Most of the theoretical studies on charge transport in organic semiconductors are focused on reproducing the experimental measured charge mobilities for different molecules and polymers.
An operative definition for the charge mobility is the following. In the absence of any external potential, the charge transport can be modeled as a purely diffusive motion [55], described by the simple equation

$$\langle x^2 \rangle \;=\; nDt\,,$$

where $\langle x^2 \rangle$ is the mean-square displacement of the charge, D represents the diffusion coefficient, t is the time, and n denotes an integer number equal to 2, 4, or 6 for one-, two-, and three-dimensional (1D, 2D, and 3D) systems respectively. Thus charge mobility is related to the diffusion coefficient via the Einstein-Smoluchowski equation:

$$\mu \;=\; \frac{eD}{k_{\mathrm{B}}T}\,, \tag{1.1}$$

where k_{B} is the Boltzmann constant and e the electron charge. Upon applying an external electric field of amplitude E, the motion of the charge acquires a drift velocity v. The mobility can be thus alternatively defined as

$$\mu \;=\; \frac{v}{E}\,. \tag{1.2}$$

Eq.s (1.1) and (1.2) are the relations which are needde in order to evaluate the charge mobility by dynamic simulations or time of flight experiments, respectively.

Charge carrier mobilities are influenced by many factors, including molecular packing, disorder, presence of impurities, temperature, electric field, charge carrier density, size/molecular weight, and pressure [55]. Among these aspects, disorder is the most studied in the literature by means of simplified models [69, 70, 71, 72] or ab-initio simulations [73, 74, 75].

We distinguish between two different kinds of disorder in organic semiconductors: *static disorder* or *dynamic disorder* [76]. Generally, disordered materials are described by random electronic

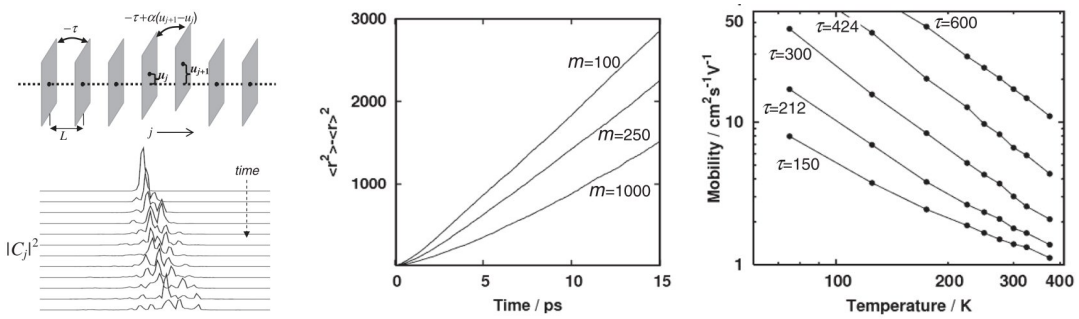

Figure 1.10: **Left panel**: scheme of the model used to describe the charge transport in organic semiconductors and example of time evolution of the probability density in the model considered in Ref. [69]. **Central panel**: plot of the temperature averaged squared displacement versus time. **Right panel**: temperature dependence of the charge carrier mobility for the model system introduced in Ref. [69]. Figures taken from Ref. [69].

Hamiltonians, depending on the molecular configuration. In the case that the evolution of the molecule is much slower than the dynamics of the charge carrier, the latter effectively experiences a static landscape. This is considered the *static disorder* case, which leads to statically localized states. The inverse time scale limit, when the electronic disorder evolves faster than the charge dynamics, is the definition of the *dynamic disorder* caused by nuclear motions.

The transport of charge carriers through *static disordered* materials is typically modeled by using charge carrier hopping theories. These approaches are based on the evaluation of the rate of charge transfer between localized states and on the computation of the density of states. Given these two information, the charge transport features are obtained as a function of the applied voltage, temperature and gate bias by solving a master equation as follows,

$$\frac{\partial}{\partial t}P_i(t) = -\sum_{j\neq i} W_{ji}P_i(t)\left[1-P_j(t)\right] + \sum_{j\neq i} W_{ij}P_j(t)\left[1-P_i(t)\right]$$

where $P_i(t)$ is the probability that site i is occupied by a carrier at time t and W_{ij} is the transition rate between sites.

To capture the physics of charge transport in the presence of *dynamic disorder*, a solution proposed by Troisi is to use a one dimensional semiclassical model [69]. This model consists of a tight-binding electronic Hamiltonian, in which the coupling between nearest neighbors is modulated by nuclear displacements (see Fig. 1.10). The time evolution of the charge carrier follows the ordinary Schrödinger equation, whereas the nuclear dynamics can be described by the Newton equation,

$$m\ddot{u} = -Ku_j - \frac{\partial}{\partial u_j}\langle\psi(t)|H^{el}|\psi(t)\rangle\,,$$

where u_j represents the molecular configuration, m is the mass of a site, K is a spring constant, and the last term represents the force caused by the presence of a charge ($\langle\psi(t)|H^{el}|\psi(t)\rangle$ is the electronic energy). The results obtained in Ref. [69], reported in Fig. 1.10, are in good agreement with measured charge mobility in molecular crystals.

Partially ordered organic semiconductors form an important class of systems where neither the static nor the dynamic disorder limit is strictly valid. The charge transport behavior observed in these systems is complicated by the presence of nuclear modes with a very broad range of timescales. To deal with this intermediate regime, both methods can be extended. In the first case, the parameters of the master equation needs to be updated along the time evolution, simultaneously solving the nuclear dynamics and the charge evolution. On the other hand, the semiclassical model can be extended by adding the effect of a random force $R^{(k)}(t)$ and a friction coefficient $\gamma^{(k)}$ to

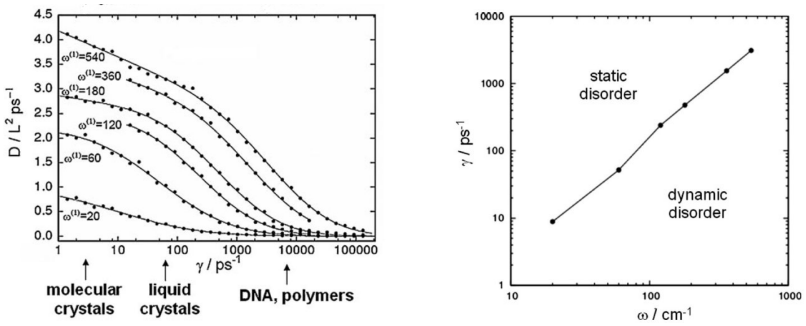

Figure 1.11: **Left panel**: the diffusivity of the charge in the model presented with different characteristic frequencies and friction coefficients. A transition is observed between dynamic disorder (high mobility/molecular crystals) and static disorder (low mobility/polymers). **Right panel**: the phase diagram of the transition between static and dynamic disorders. Figures taken from Ref.s [76] and [77].

the deterministic Newton equation,

$$m^{(k)}\ddot{u}^{(k)} = -m^{(k)}(\omega^{(k)})^2 u_j^{(k)} - m^{(k)}\gamma^{(k)}\dot{u}_j^{(k)} + R^{(k)}(t) - \frac{\partial}{\partial u_j^{(k)}}\langle\psi(t)|H^{el}|\psi(t)\rangle\,,$$

where $u_j^{(k)}$ represents the k-th nuclear mode with mass $m^{(k)}$ and frequency $\omega^{(k)}$. An interesting property of this model is that by varying γ it describes the transition from the dynamic ($\gamma \to 0$) to the static disorder ($\gamma \to \infty$) [77]. This transition is evident in the falling of the diffusion coefficient as γ increases, with a point of inflexion indicating the onset of static localization (see Fig. 1.11). While this model provides a good qualitative description of the charge transfer mechanism, it is inadequate to describe large devices or to investigate possible bottlenecks of the charge dynamics: for this purpose a more microscopic description is required.

Chapter 2

Dynamics of Electronic Excitations in Macromolecules

In this chapter, we introduce our approach to study quantum transport in macromolecules, based on the coherent path integral representation of the density matrix evolution. This formalism is convenient because it allows us to deal with the dynamics of the atomic nuclei at the classical level, while keeping a fully quantum description of the dynamics of the electronic excitations.
We show how, using this formalism, it is possible to obtain a system of equations of motion which couple the quantum electronic dynamics and the nuclear mechanics. Otherwise, by integrating out the atomic nuclei dynamics we derive an effective theory which is defined in terms of electronic excitations only [1].

2.1 Microscopic Hamiltonian for Quantum Transport

An entirely ab-initio approach to quantum transport in macromolecules requires solving the time-dependent Schroedinger equation for all nuclei and all electrons in the molecule and in the solvent. The extremely high computational cost limits such ab-initio description to very small systems, consisting of a few atoms. Solving the quantum transport process in macromolecules To reduce the computational complexity of the problem we adopt a standard simplified framework, consisting of two main approximations:

- the electronic problem is coarse-grained at the *tight-binding approximation* level,
- the dynamics in the absence of quantum excitations is described by the lowest *Born-Oppenheimer energy surface*.

In such an approach, the molecule is first partitioned into several fragments, hereby labeled by an index $\mathbf{m}$. This partition of the molecule must be defined in such a way that the electron density is significantly more delocalized within each molecular fragment than over different fragments [80]. Then, the so-called frontier orbitals $|\phi_{\mathbf{m}}\rangle$ are calculated by solving the Schrödinger equation for a reduced portion of the molecule, centered at the fragment $\mathbf{m}$. The system's wave function is then obtained by diagonalizing the Hamiltonian projected onto the space of the frontier orbitals $|\phi_{\mathbf{m}}\rangle$.

For example, in studying electronic hole transport in DNA, the molecular fragments can be chosen to coincide with the base-pairs and their Highest Occupied Molecular Orbitals (HOMOs) can be obtained by solving the Schrödinger equation for an isolated pair [81]. The propagation of the charge carriers through the molecule is then modeled as the hopping of holes between neighboring base-pairs. In general, it is convenient to choose the dimensionality of the molecular fragment index $\mathbf{m}$ according to the topology of the system under consideration. In Fig. 2.1 we show a practical example of coarse-grained model applied on a conjugate polymer.

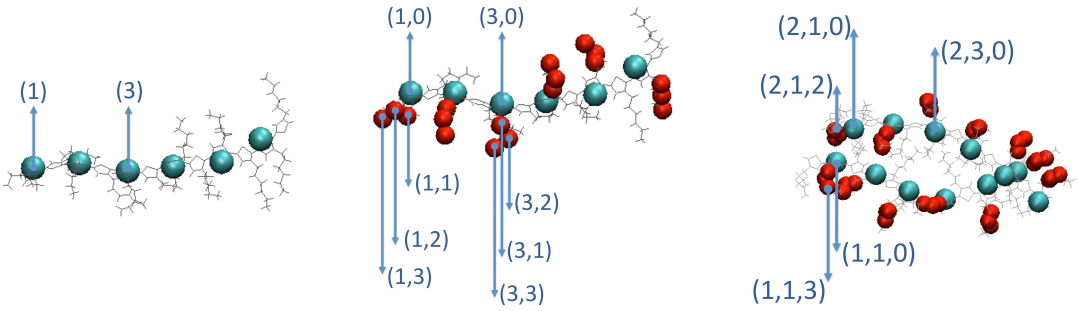

Figure 2.1: Labeling of molecular fragments in molecules with different topology. In linear polymers, the fragments among which the charge hops form an effective one-dimensional system (left panel). In branched polymers, a two dimensional representation may be introduced in order to account for propagation along the side chains (center panel). In polymer assemblies a third index may be used to label the different molecules (right panel).

In our approach of modeling the quantum propagation through an open macromolecular system, we consider three coupled sub-systems: the *quantum excitation* propagating through the molecule, the *molecule*, and the surrounding *environment*. Therefore, the dynamics of the entire system is modeled by the following quantum Hamiltonian:

$$\hat{H} = \hat{H}_{TB} + \hat{H}_M + \hat{H}_B + \hat{H}_{MB}. \tag{2.1}$$

In the following, we will introduce and comment any terms of this equation.

2.1.1 Quantum Excitation Hamiltonian

In Eq. (2.1), quantum transport is described by $\hat{H}_{MC}$, which is a *tight-binding* Hamiltonian for the quantum excitation that reads

$$\hat{H}_{TB} = \sum_{\mathbf{m},\mathbf{n}}^{N_{frag}} f_{\mathbf{mn}}[Q]\ \hat{a}^\dagger_{\mathbf{m}}\hat{a}_{\mathbf{n}}. \tag{2.2}$$

In this definition the discrete vectors $\mathbf{m}$, $\mathbf{n}$ label the different fractional molecular orbitals. The set of all atomic nuclear coordinates is collectively represented by the configuration space vector Q,

$$Q(t) \equiv (q_1, \ldots, q_{3N}) = (r^1_x(t), r^1_y(t), r^1_z(t); \ldots; r^N_x(t), r^N_y(t), r^N_z(t)).$$

where $r^i = (r^i_x, r^i_y, r^i_z)$ are the Cartesian coordinates of the $i-$th atom. The $\hat{a}^\dagger_{\mathbf{m}}$ ($\hat{a}_{\mathbf{m}}$) operators create (annihilate) a quantum state at the molecular fragment $\mathbf{m}$. For sake of definiteness, in this chapter we shall focus on the propagation of fermionic excitations, which are relevant for studying charge transport[1]. The generalization to bosons is straightforward. Correspondingly, the creation and annihilation operators are assumed to obey the anti-commutation relations

$$\{\hat{a}_{\mathbf{m}}, \hat{a}_{\mathbf{n}'}\} = \{\hat{a}^\dagger_{\mathbf{m}}, \hat{a}^\dagger_{\mathbf{n}}\} = 0, \qquad \{\hat{a}_{\mathbf{m}}, \hat{a}^\dagger_{\mathbf{n}}\} = \delta_{\mathbf{lm}}\,.$$

Depending on the specific molecular system, it may be necessary to include also the coupling between different molecular orbitals. This can be done by introducing additional creation-annihilation operators, i.e. different types of excited states for each orbital.

[1] In particular we consider electron holes in HOMOs, which are relevant for many molecular charge transfer phenomena.

The quantity $f_{\mathbf{mn}}[Q]$ is commonly split in two: the hopping matrix elements $T_{\mathbf{mn}}[Q]$ and on-site energies $e_{\mathbf{m}}[Q]$:

$$f_{\mathbf{mn}}[Q] \equiv T_{\mathbf{mn}}[Q](1-\delta_{\mathbf{mn}}) + e_{\mathbf{n}}[Q]\,\delta_{\mathbf{mn}}. \tag{2.3}$$

The parameters $T_{\mathbf{mn}}$ and $e_{\mathbf{m}}$ are obtained from the fragment orbitals $|\phi_{\mathbf{m}}\rangle$ and $|\phi_{\mathbf{n}}\rangle$, and they depend parametrically on the configuration vector Q. These quantities are defined by

$$T_{\mathbf{mn}}[Q] \equiv \langle\phi_{\mathbf{m}}|\hat{\mathcal{H}}_{el.}|\phi_{\mathbf{n}}\rangle, \tag{2.4}$$

$$e_{\mathbf{m}}[Q] \equiv \langle\phi_{\mathbf{m}}|\hat{\mathcal{H}}_{el.}|\phi_{\mathbf{m}}\rangle, \tag{2.5}$$

where $\hat{\mathcal{H}}_{el}$ is the electronic Hamiltonian (for example, the Kohn-Sham Hamiltonian of density functional theory). In literature, we can find several methods to compute the parametric value of $e_{\mathbf{m}}$ and $T_{\mathbf{mn}}$, depending on which transport phenomena we are studying. In the case of charge transport along biomolecules, one of the most used is a DFT-scheme which has been developed by *Elstner et al.* [82]. To study energy excitation transfer, we can compute Eq.s (2.4) and (2.5) following the collective electronic oscillator procedure developed by Mukamel [83, 84] or the theoretical framework proposed by Troisi [85].

Finally, we stress that the transfer matrix elements $f_{\mathbf{mn}}$ depend on the molecular configuration Q. This dependence means that the dynamics of the atomic coordinates and that of the quantum fermions are coupled.

2.1.2 Macromolecule and Solvent Hamiltonian

The Hamiltonian $\hat{H}_M$ in Eq. (2.1) governs the conformational dynamics of the atomic nuclei in the absence of quantum excitations and reads

$$\hat{H}_M \equiv \frac{\hat{P}^2}{2M} + \hat{V}[Q], \tag{2.6}$$

where the P is the momentum canonically conjugated to the configuration vector Q. $V[Q]$ is the molecular potential energy, evaluated in the Born-Oppenheimer approximation. This includes the interaction between the different atoms within the molecule and possibly with the external fields. We stress that the potential energy $V[Q]$ in Eq. (2.6) depends only on the molecular configuration. This is equivalent to taking the adiabatic limit for the dynamics, and to assume that the location of the quantum excitation does not alter in a significant way the interaction between the atomic nuclei.[2] Notice that, for sake of notational simplicity, in the definition (2.6) we are assuming that all atoms have the same mass M. The generalization to different atomic masses is straightforward and will not be discussed here.

The part of the Hamiltonian $\hat{H}_B + \hat{H}_{MB}$ describes the coupling of the molecule with a thermal heat bath in the Leggett-Caldeira model [86], i.e. through an infinite set of harmonic-oscillators coupled to each atomic coordinate:

$$\hat{H}_B = \sum_{\alpha=1}^{3N}\sum_{j=1}^{\infty}\left(\frac{\hat{\pi}_j^2}{2\mu_j} + \frac{1}{2}\mu_j\omega_j^2\hat{x}_j^2\right), \tag{2.7}$$

$$\hat{H}_{MB} = \sum_{\alpha=1}^{3N}\sum_{j=1}^{\infty}\left(-c_j\hat{x}_j\hat{q}_\alpha + \frac{c_j^2}{2\mu_j\omega_j^2}\hat{q}_\alpha^2\right). \tag{2.8}$$

$X = (x_1, x_2, \ldots)$ and $\Pi = (\pi_1, \pi_2, \ldots)$ are the harmonic oscillator coordinates and momenta, μ_j and ω_j denote their masses and frequencies and c_j are the couplings between atomic and heat bath

[2] In some case of interest, the validity of this approximation has been questioned and corrections to the adiabatic regime have been proposed. However, in this thesis we shall not deal with these complications.

variables. The last term in Eq. (2.8) is a standard counter-term introduced to compensate the renormalization of the molecular potential energy which occurs when the heat bath variables are traced out [87]. This elimination consists in a Gaussin integral over the heat bath variables that interacting linearly with the molecule cre
Even thought it's simplicity, a reservoir composed of harmonic oscillator with linear coupling is rather general and often provides an appropriate description of a realistic environment. Indeed, the model introduce in Eq.s (2.8) and (2.7) has widely been used to model dissipation, both to describe quantum phenomena, like quantum tunneling [88], and to describe classical dynamics, like Langevin's equation [89]. In addition, as we shall see, this model allows us to recover the standard Langevin equation, for the classical dynamics of atomic nuclei

The Hamiltonian in Eq. (2.1) define a closed quantum system. In the next section, we introduce the path integral representation for the density matrix evolution.

2.2 Path Integral Representation of Quantum-Diffusive Dynamics

Let us define the reduced density matrix which describe the quantum transport through a macromolecule as

$$\rho_{\mathbf{ij}} = \frac{\mathrm{Tr}[\ |\,\mathbf{i}\rangle\langle\mathbf{j}\,|\,\hat{\rho}(t)\ ]}{\mathrm{Tr}\ \hat{\rho}(t)} = \frac{\mathrm{Tr}[|\,\mathbf{i}\rangle\langle\mathbf{j}\,|\,e^{-\frac{i}{\hbar}\hat{H}t}\ \hat{\rho}(0)\ e^{\frac{i}{\hbar}\hat{H}t}]}{\mathrm{Tr}\ \hat{\rho}(0)}\,, \tag{2.9}$$

which depends only on the quantum excitation's degrees of freedom. As introduced in Section 1.1, all the molecular and heat-bath degrees of freedom will be traced out, obtaining an QTFT including fluctuation-dissipation effects. In Eq. (2.9), $\hat{\rho}(0)$ is the initial density matrix, which is taken to be in the factorized form

$$\hat{\rho}(0) = \rho^0\ \otimes\ e^{-\frac{1}{K_B T}\hat{H}_M}\ \otimes\ e^{-\frac{1}{K_B T}\hat{H}_B}. \tag{2.10}$$

where $\rho^0 = \sum_{\mathbf{ij}} \rho^0_{\mathbf{ij}}\ |\,\mathbf{i}\rangle\langle\mathbf{j}\,|$. Equation (2.10) corresponds to assuming that, at the initial time, the molecular degrees of freedom and the heat bath degrees of freedom can be considered separately equilibrated at the same temperature. Hence, the normalization factor at the denominator reads

$$\mathrm{Tr}\ \hat{\rho}(0)\ =\ Z_M(\beta)\ \times Z_B(\beta)\,,$$

where Z_M and Z_B are the quantum partition functions for the molecule and heat bath degrees of freedom.

Let us now derive a path integral expression for numerator in eq. (2.9). We begin by noting that the conformational dynamics of the atomic nuclei in the molecule can be reasonably well described in the classical limit. In contrast, the hopping of the quantum excitations from molecular site to molecular site requires a fully quantum description. In view of this important difference, we choose to adopt the standard first-quantized representation for the dynamics of the atomic coordinates and for the harmonic oscillators in the heat bath, while we use a second-quantized representation of the quantum excitation dynamics (see Appendix A.1).
This choice is motivated because the field-theoretic description for the quantum excitation allows to obtain a simpler final representation of the reduced density matrix. Moreover, the coordinate representation for the atomic degrees of freedom is most convenient in order to take the classical limit.

The path integral representation of the reduced density matrix (2.9) is obtained by performing the Trotter decomposition of the forward- and backward- time evolution operators $e^{-i\hat{H}t}$ and $e^{i\hat{H}t}$ and of the imaginary-time evolution operators $e^{-\frac{1}{K_B T}\hat{H}_M}$ which appear in Eq.s (2.9) and (2.10). In

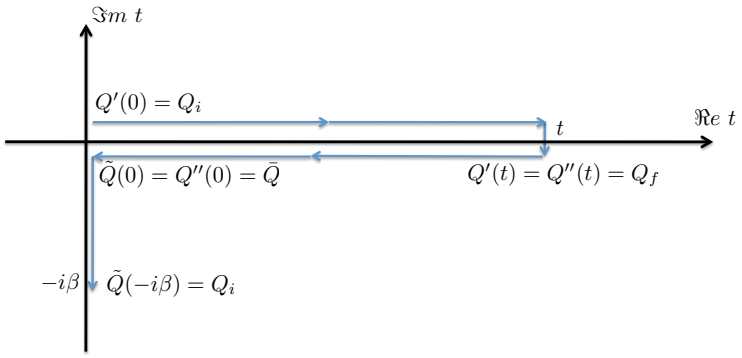

Figure 2.2: Boundary conditions of the molecular configurations (and heat bath state) paths defined on the Keldysh contour appearing in the path integral (2.11) and (2.16).

practice, each time evolution is split in a series of n infinitesimal intervals, then at every discrete time t_i the following completeness identity is introduced

$$1 \;=\; \int dQ \int dX \int \left(\prod_{\mathbf{k}=1}^{N_{frag}} \frac{d\phi_{\mathbf{k}} d\phi_{\mathbf{k}}^*}{2\pi i} \right) e^{-\sum_{l=1} \phi_{\mathbf{l}} \phi_{\mathbf{l}}^*} |Q, X, \Phi\rangle \, \langle Q, X, \Phi| \,,$$

where the states $|Q, X, \Phi\rangle$ collect the set of all coherent states (constructed from the annihilation operators associated to each molecular fragment, $\hat{a}_{\mathbf{k}}$), the set of the eigenstates of the molecular coordinate operator $\hat{Q}$ and the set of eigenstates of the heat bath generalized coordinate operator $\hat{X}$. Then, at each step we use the *Trotter* expansion,

$$e^{\epsilon \sum_k A_k} = \prod_k e^{-\epsilon A_k} + o\left(\epsilon^2\right) \,,$$

and finally we perform the continuum limit $n \to \infty$ (details in Ref. [90]). After this manipulation and assuming an initial condition $\rho^0 = |\mathbf{k}_i\rangle\langle\mathbf{k}_i|$[3], the reduced density matrix in Eq. (2.9) in path integral form reads

$$\begin{aligned}
\rho_{\mathbf{ij}}(t) = \frac{1}{\mathrm{Tr}\left[\hat{\rho}(0)\right]} \int dX_f \int dX_i \int d\bar{X} \int_{\bar{X}}^{X_i} \mathcal{D}\tilde{X} e^{-S_B[\tilde{X}]} \int dQ_f \int dQ_i \int d\bar{Q} \int_{\bar{Q}}^{Q_i} \mathcal{D}\tilde{Q} e^{-S_E[\tilde{Q}]} \\
\int_{X_i}^{X_f} \mathcal{D}X' \int_{Q_i}^{Q_f} \mathcal{D}Q' \int \mathcal{D}\phi' \mathcal{D}\phi'^* \; \phi'_{\mathbf{i}}(t) \phi'^*_{\mathbf{k}_i}(0) \; e^{-\phi'^*_m(0)\phi'_m(0)} \; e^{\frac{i}{\hbar}\left(S_{MC}[Q',\phi',\phi'^*] + S_{MB}[Q',X']\right)} \\
\int_{\bar{X}}^{X_f} \mathcal{D}X'' \int_{Q_f}^{\bar{Q}} \mathcal{D}Q'' \int \mathcal{D}\phi'' \mathcal{D}\phi''^* \phi''_{\mathbf{k}_i}(0) \phi''^*_{\mathbf{j}}(t) \; e^{-\phi''^*_m(t)\phi''_m(t)} \; e^{-\frac{i}{\hbar}\left(S_{MC}[Q'',\phi'',\phi''^*] + S_{MB}[Q'',X'']\right)} .
\end{aligned} \tag{2.11}$$

In this equation, $\phi'_{\mathbf{l}}(t)$ and $\phi''_{\mathbf{l}}(t)$ are the Grassmann quantum fields associated to the coherent states propagating forward and backwards in time respectively[4]. In the path integral (2.11), the $Q'(t)$, $Q''(t)$ (and $X'(t)$, $X''(t)$) variables represent the configuration of the molecule (and respectively the heat bath state) propagating forward and backwards in time, while the $\tilde{Q}(t)$ (and $\tilde{X}(t)$) variables are associated with the evolution of the same molecule (and of the heat bath state) along the imaginary-time direction. All these paths can be collectively represented by a path variable integrated along the so-called Keldysh contour (see Fig. 2.2).

[3] This condition could be relaxed, summing linearly contribution to any initial condition.

[4] As usual, the path integral (2.11) is defined over Grassmann fields or complex fields, depending on whether propagating excitation is a fermion or a boson.

The action functionals appearing at the exponents in Eq. 2.11 read

$$S_{MC}\left[Q,\phi,\phi^*\right] = \int_0^t dt' \left\{ \frac{M\dot{Q}(t')^2}{2} - V[Q(t')] + \phi^*_{\mathbf{l}}(t') \left(i\hbar \frac{\partial}{\partial t'} \delta_{\mathbf{lm}} - f_{\mathbf{lm}}[Q(t')] \right) \phi_{\mathbf{m}}(t') \right\}, \quad (2.12)$$

$$S_B[X] = \int_0^\beta d\tau \left\{ \sum_j \left(\frac{\mu_j \dot{x}_j(\tau)^2}{2} + \frac{1}{2}\mu_j \omega_j^2 x_j^2(\tau) \right) \right\}, \quad (2.13)$$

$$S_E[X] = \int_0^\beta d\tau \left\{ \left(\frac{M\dot{Q}(\tau)^2}{2} + V[Q(t')] \right) \right\}, \quad (2.14)$$

$$S_{MB}[X,Q] = \int_0^t dt' \left\{ \sum_j \frac{\mu_j}{2} \left(\dot{x}_j^2(t') - \omega_j^2 x_j^2(t') \right) + \sum_{\alpha\ j} \left(c_j x_j(t') q_\alpha(t') - \frac{c_j^2}{2\mu_j \omega_j^2} q_\alpha^2(t') \right) \right\}. \quad (2.15)$$

Let us point out that, throughout this thesis we shall adopt Einstein's notation and implicitly assume the summation over all bold repeated indexes, except for the initial exciton position $\mathbf{k}_i$ which is held fixed.

2.2.1 Feynman-Vernon Functional

We note that the path integrals over the harmonic oscillator variables X in Eq. (2.11) are Gaussian. Therefore, the path integral X can be carried out analytically [87], and we obtain

$$\begin{aligned} \rho_{\mathbf{ij}}(t) = & \frac{1}{\mathrm{Tr}\left[\hat{\rho}(0)\right]} \int dQ_f \int dQ_i \int d\bar{Q} \int_{\bar{Q}}^{Q_i} \mathcal{D}\tilde{Q} e^{-S_E[\tilde{Q}]} \int_{Q_i}^{Q_f} \mathcal{D}Q' \int_{Q_f}^{\bar{Q}} \mathcal{D}Q'' \\ & \int \mathcal{D}\phi' \mathcal{D}\phi'^* e^{-\phi'^*_{\mathbf{m}}(0)\phi'_{\mathbf{m}}(0)} \int \mathcal{D}\phi'' \mathcal{D}\phi''^* e^{-\phi''^*_{\mathbf{m}}(t)\phi''_{\mathbf{m}}(t)} \left(\phi'_{\mathbf{i}}(t)\phi'^*_{\mathbf{k}_i}(0)\ \phi''_{\mathbf{k}_i}(0)\phi''^*_{\mathbf{j}}(t) \right) \\ & \times e^{-\Phi_{FV}[Q',Q'']}\ e^{\frac{i}{\hbar}\ S_{MC}[Q',\phi',\phi'^*] - \frac{i}{\hbar} S_{MC}[Q'',\phi'',\phi''^*]}, \end{aligned} \quad (2.16)$$

where functionals which appear at the exponent are defined in Eq.s (2.14) and (2.12), while $\Phi_{FV}[Q',Q]$ is the so-called Feynman-Vernon influence functional [19], which describes the fluctuation and dissipation induced by the coupling with the heat-bath and reads:

$$\begin{aligned} \Phi_{FV}[Q',Q''] = & \frac{1}{\hbar} \int_0^t dt' \int_0^{t'} dt'' \Big\{ \left[Q'(t') - Q''(t') \right] \left[\mathcal{B}(t'-t'')Q'(t'') - \mathcal{B}^*(t'-t'')Q''(t'') \right] \Big\} \\ + & i\frac{\bar{\mu}}{2\hbar} \int_0^t dt' \left[Q'^2(t') - Q''^2(t') \right], \qquad \left(\bar{\mu} = \sum_j \frac{c_j^2}{m_j \omega_j^2} \right) \end{aligned}$$

$\mathcal{B}(t)$ is a two-point correlation function which encodes the physics of the coupling of the molecular coordinates with the heat-bath and reads:

$$\mathcal{B}(t) = \int \frac{d\omega}{\pi} J(\omega) \left[\coth\left(\frac{\omega\hbar}{2k_B T} \right) \cos(\omega t) - i \sin(\omega t) \right],$$

where $J(\omega)$ is the spectral density, that is defined by

$$J(\omega) = \frac{\pi}{2} \sum_n \frac{c_n^2}{\mu_n \omega_n} \delta(\omega - \omega_n).$$

We note that time scales at which thermal oscillations are damped and memory effects are relevant can be tuned by varying the frequencies of the virtual harmonic oscillators in Eq. (2.8) and

equivalently in the spectral density $J(\omega)$. In particular, here we consider the so-called Ohmic bath limit, in which the $\mathcal{B}(t)$ reduces to

$$\mathcal{B}(t) \to L^{ohm}(t) = \frac{2k_BTM\gamma}{\hbar}\delta(t) + \frac{i\ M\gamma}{2}\ \frac{d}{dt}\delta(t)\,,$$

which consists in assuming a memoryless damping kernel. Indeed, it is well known that, in the classical limit for the molecular motion, this choice for $L(t)$ leads to a Langevin dynamics with friction coefficient γ (see e.g. Ref. [87]). Hence, Eq. (2.16) represents a quantum generalization of the stochastic dynamics of the molecule, which includes also the time-evolution of the quantum state described by the tight-binding Hamiltonian (2.2).

2.3 Classical Molecular Dynamics Limit

A reasonable approximation to simplify the problem consists in taking the classical limit for the dynamics of the molecular atomic coordinates. This limit is motivated by the final aim of the model to describe quantum transport in Macromolecule at room temperature, i.e. we assume that we don't need to include quantum effects in the macromolecular dynamics.

2.3.1 Semiclassical Variables

In order to recover the classical limit, we perform the following change of variable, i.e. we express the path integral (2.16) in a form in which forward and backward molecular paths $Q'(t)$ and $Q''(t)$ are replaced by their average and difference, respectively:

$$R(t) = \frac{1}{2}\left(Q^{'}(t) + Q^{''}(t)\right)\,, \qquad y(t) = Q^{'}(t) - Q^{''}(t)\,.$$

The path $R(t)$ coincides with the diagonal elements of the molecular density matrix, in coordinate space, and is therefore called *quasiclassical path*. On the contrary, $y(t)$ path corresponds to off-diagonal terms, which describe quantum and thermal fluctuations. After change of variable, the Eq. (2.16) reads

$$\begin{aligned}\rho_{\mathbf{ij}}(t) \ \equiv\ & \frac{1}{\mathrm{Tr}\,[\hat{\rho}(0)]}\int \mathcal{D}\phi^{'}\mathcal{D}\phi^{'*}\phi^{'}_{\mathbf{i}}(t)\phi^{'*}_{\mathbf{k}_i}(0)\ e^{-\phi^{'*}_{\mathbf{m}}(0)\phi^{'}_{\mathbf{m}}(0)}\ e^{iS_0[\phi^{'},\phi^{'*}]} \\ & \int \mathcal{D}\phi^{''}\mathcal{D}\phi^{''*}\ \phi^{''}_{\mathbf{k}_i}(0)\phi^{''*}_{\mathbf{j}}(t)\ e^{-\phi^{''*}_{\mathbf{m}}(t)\phi^{''}_{\mathbf{m}}(t)}\ e^{-iS_0[\phi^{''},\phi^{''*}]} \\ \times \int dQ_f \int d\bar{Q} \int dQ_i \int_{\bar{Q}}^{Q_i} & \mathcal{D}\tilde{Q}e^{-S_E[\tilde{Q}]} \int_{\frac{1}{2}(Q_i+\bar{Q})}^{Q_f} \mathcal{D}R \int_{Q_i-\bar{Q}}^{0} \mathcal{D}y\ e^{i\Phi^{'}_{FV}[R,y]}\ e^{\frac{i}{\hbar}\mathcal{W}[R,y,\phi^{'*},\phi^{'},\phi^{''*},\phi^{''}]}, \quad (2.17)\end{aligned}$$

where the functionals at the exponent are defined as

$$S_0[\phi,\phi^*] = \int_0^t dt'\phi^*_{\mathbf{n}}(t')\left[i\ \frac{\partial}{\partial t'}\delta_{\mathbf{nm}}\right]\phi_{\mathbf{m}}(t')\,, \quad (2.18)$$

$$\begin{aligned}\mathcal{W}[R,y,\phi^{'*},\phi^{'},\phi^{''*},\phi^{''}] = & \int_0^t dt'\left\{M\dot{R}\cdot\dot{y} - V\left[R+\frac{y}{2}\right] + V\left[R-\frac{y}{2}\right]\right. \\ & \left. -\ \left(f_{\mathbf{nm}}\left[R+\frac{y}{2}\right]\phi^{'*}_{\mathbf{n}}\phi^{'}_{\mathbf{m}} - f_{\mathbf{nm}}\left[R-\frac{y}{2}\right]\phi^{''*}_{\mathbf{n}}\phi^{''}_{\mathbf{m}}\right)\right\}\,, \quad (2.19)\end{aligned}$$

$$\Phi^{'}_{FV}[R,y] = \int_0^t dt'\left\{\frac{M\gamma K_BT}{\hbar^2}y^2(t') + \frac{iM\gamma}{\hbar}\ \dot{R}\cdot y\right\}. \quad (2.20)$$

In the path integral representation (2.17), the time evolution of the quantum excitation-molecule system in contact with a dissipative heat bath follows directly from the quantum Hamiltonian defined in Eq. (2.1), without any further approximation. In particular, the molecule's conformational

dynamics and the quantum excitation propagation are described at the fully quantum level. In addition, there is no restriction either on the strength of the coupling between the molecular vibrations and the quantum excitation, nor on the amplitude of the conformational changes which the molecule can undergo within the time interval t.

Clearly, computing such a path integral is a formidable task and further approximations are needed. In section 2.3.2, we discuss the classical limit for the dynamics of the molecular atomic coordinates. In section 2.4, we apply the *saddle-point* approximation to Eq. (2.17) in order to derive a set of coupled equations, which describe the quantum and stochastic evolution at mean field level of the reduced density matrix $\rho_{\mathbf{ij}}$ and the molecular configuration R. In section 2.5, we go beyond mean field approximation, integrating out exactly both integral paths over y and R, in the small oscillation limit, obtaining the formulation of an QTFT.

2.3.2 Onsager-Machlup Functional

In the absence of the quantum charge, from the path integral representation (2.17) we can obtain the Onsager-Machlup path integral representation of the Langevin dynamics of the molecule in its heat bath. To prove this, let us provisorily drop all the coherent field.

To this end, let us point out that the saddle-point equations which are derived by functionally differentiating the exponent in Eq. (16) with respect to R, y, ϕ', ϕ'' lead to the condition $y(t) = 0$ for all t (see derivation in Appendix A.2). Following the discussion in Ref. [87], we impose the classical limit on the molecular motion by assuming that the path $y(t)$ remains close to its saddle-point configuration (hence represents a small fluctuation) and by imposing the boundary-condition $y(0) = 0$. Expanding the functionals in the exponent to quadratic order in y, the resulting expression reads

$$\frac{1}{Z_M(\beta)} \int dQ_f \int dQ_i \int_{Q_i}^{Q_i} \mathcal{D}\tilde{Q} e^{-S_E[\tilde{Q}]} \mathcal{P}_t(Q_f|Q_0) = 1\,,$$

where

$$\mathcal{P}_t(Q_f|Q_0) = \int_{Q_0}^{Q_f} \mathcal{D}R \int \mathcal{D}y \; e^{-\frac{i}{\hbar}\int_0^t dt' \left[\; y(t')\cdot\left(M\ddot{R}(t')+M\gamma\dot{R}(t')+\frac{\partial}{\partial r}V[R(t')]\right) \; - \; \frac{i\;k_B T M\gamma}{\hbar} y^2(t') \right]}\,,$$

which corresponds to the conditional probability to reach a configuration Q_f after a time t starting from a configuration Q_0. Performing the Gaussian integration over y, the path integral $\mathcal{P}_t$ reduces to

$$\mathcal{P}_t(Q_f|Q_0) = \int_{Q_i}^{Q_f} \mathcal{D}R \; e^{-S_{OM}[R]}\,,$$

where $S_{OM}[R]$ is the Onsager-Machlup functional [91], which assigns a statistical weight to the stochastic trajectories in the Langevin dynamics by[5]:

$$S_{OM}[R] = \frac{\beta}{4M\gamma} \int_0^t dt' \; \left[M\ddot{R} + \frac{\partial}{\partial R} V(R) + M\gamma\dot{R} \right]^2 .$$

Finally, we take the saddle-point approximation for the path integral $\mathcal{D}\tilde{Q}$, which corresponds to taking the classical limit also for the partition function of the initial molecular configuration. The result is

$$\int dQ_f \int dQ_i \frac{e^{-\beta V[Q_i]}}{Z_M[\beta]} \int_{Q_i}^{Q_f} \mathcal{D}R \; e^{-S_{OM}[R]} = \int dQ_f \int dQ_i \; P_t(Q_f, Q_i) \; \rho_0(0) = 1\,,$$

where $\rho_0(Q_i) = \frac{e^{-\beta V[Q_i]}}{Z_M[\beta]}$ is the initial distribution of molecular configurations. We recognize that this is the normalization condition on the solution of the Fokker-Planck equation, expressed in path integral form [92, 93] and it is the starting point of the so-called dominant-reaction pathway approach to investigate the long-time dynamics of macromolecules [94, 95].

[5] See Appendix A.3 for the derivation of the functional S_{OM} from the Langevin dynamics.

2.4 Quantum and Stochastic Equations of Motion

In this section, in order to derive a set of mean-field equations both for the molecular dynamics and the quantum transport, we return to consider the complete path integral in Eq. (2.17).

The derivation consists in estimating the path integral over the coherent field in the lowest order saddle-point approximation, while the integral over the molecular coordinate y is computed beyond mean field level, i.e. including effects of leading-order around the saddle-point solution $y(t) = 0$ (as we showed in the previous section). All the detailed calculation are shown in Appendix A.2 and A.3. The final set of quantum and stochastic differential equation is the following [78]:

$$\begin{cases} M\frac{d^2}{dt^2}R_\alpha = -M\gamma\frac{d}{dt}R_\alpha - \frac{\partial}{\partial R^\alpha}\Big(V[R] + \mathrm{Tr}[\hat{\rho}\ \hat{f}[R]]\Big) + \eta_\alpha(t) \\ \\ \frac{d}{dt}\hat{\rho} = -\frac{i}{\hbar}\left[\hat{f}[R],\ \hat{\rho}\right], \end{cases} \tag{2.21}$$

where $\hat{f}_{\mathbf{lm}}[R] = f_{\mathbf{lm}}[R]$ corresponds to the transfer integral in Eq. (2.3), and $\eta^\alpha(t)$ is the usual white delta-correlated Gaussian noise of the Langevin dynamics,

$$\langle \eta^\alpha(t) \cdot \eta^\beta(0)\rangle = 6\frac{k_B T}{M\gamma}\ \delta^{\alpha\beta}\ \delta(t).$$

Since the motion of the molecular degrees of freedom is stochastic, the quantum excitation probability density at different times is obtained from the average over many independent trajectories, which may turn out to be a computationally challenging procedure.

2.5 Quantum Transport Field Theory for the Reduced Density Matrix

In this section we derive the most important result of this thesis, an effective theory approach to describe the quantum transport in macromolecule. To this end, we return to the path integral expression in Eq. (2.17), in which no approximations have been introduced, and we integrate out the molecular coordinate y and R, in the limit of small oscillation around the mechanical equilibrium for R path, and around the classical limit for the variable y (see section 2.3).

The final result is a rigorous effective theory, which is formulated exclusively in terms of the degrees of freedom associated to the quantum excitation and is fully consistent with the fluctuation-dissipation relationship. This way, one does not need to perform MD simulations, and average over multiple realization of the dynamics.

2.5.1 Small Oscillation Limit

Let us note that the quantum transport dynamics is in general much faster than the characteristic time scales for major conformational transitions of macromolecular systems (typically ranging from few nanoseconds to many seconds or even larger). Hence, during the time intervals which are relevant for quantum propagation phenomena, the molecule can be assumed to follow at most only small oscillations around the mechanical equilibrium configuration Q_0, which is defined as the global minimum of the molecular potential energy $V(Q)$. In this small-oscillation limit, it is convenient to introduce the atomic displacement variables

$$\delta r(t) = R(t) - Q_0\,,$$

and regard both the $\delta r(t)$ and $y(t)$ as small quantities of the same order. In the expansion of the $\mathcal{W}$ functional in Eq. (2.19) up to quadratic order in δr and y we obtain a term

$$\begin{aligned} V\left[R - \frac{y}{2}\right] - V\left[R + \frac{y}{2}\right] &= \frac{1}{2}\mathcal{H}_{ij}\left(\delta r - \frac{y}{2}\right)_i\left(\delta r - \frac{y}{2}\right)_j - \frac{1}{2}\mathcal{H}_{ij}\left(\delta r + \frac{y}{2}\right)_i\left(\delta r + \frac{y}{2}\right)_j \\ &= \delta r_i y_j \mathcal{H}_{ij} + \dots\,, \end{aligned}$$

where $\mathcal{H}_{ij} \equiv \frac{\partial^2}{\partial Q_i \partial Q_j} V(Q)|_{Q=Q_0}$ is the Hessian matrix of the potential energy at the point of mechanical equilibrium.

A small deviation from the equilibrium configuration Q_0 generates a small change in the hopping matrix elements and in the on-site energies which define the tight-binding Hamiltonian (2.2). To the leading-order in the Taylor expansion in powers of δr and y we have:

$$\begin{aligned} f_{\mathbf{nm}}\left[r-\frac{y}{2}\right] &= f^0_{\mathbf{nm}} + f^i_{\mathbf{nm}}\left(\delta r_i - \frac{y_i}{2}\right) + \dots , \\ f_{\mathbf{nm}}\left[r+\frac{y}{2}\right] &= f^0_{\mathbf{nm}} + f^i_{\mathbf{nm}}\left(\delta r_i + \frac{y_i}{2}\right) + \dots , \end{aligned}$$

where $f^0_{\mathbf{nm}} \equiv f_{\mathbf{nm}}(Q_0)$ and $f^i_{\mathbf{nm}} \equiv \frac{\partial}{\partial Q^i} f_{\mathbf{nm}}(Q)|_{Q=Q_0}$ are the tight-binding parameters, and respectively their derivatives, evaluated on mechanical equilibrium configuration.

In the small oscillation regime, the path integral over y is of Gaussian type and can be performed analytically

$$\begin{aligned} \rho_{\mathbf{ij}}(t) \;\equiv\; \frac{1}{\mathrm{Tr}\,[\hat{\rho}(0)]} \int & \mathcal{D}\phi^{'}\mathcal{D}\phi^{'*}\phi^{'}_{\mathbf{i}}(t)\phi^{'*}_{\mathbf{k}_i}(0)\; e^{-\phi^{'*}_{\mathbf{m}}(0)\phi^{'}_{\mathbf{m}}(0)}\; e^{iS_0[\phi^{'},\phi^{'*}]} \\ & \int \mathcal{D}\phi^{''}\mathcal{D}\phi^{''*}\;\phi^{''}_{\mathbf{k}_i}(0)\phi^{''*}_{\mathbf{j}}(t)\; e^{-\phi^{''*}_{\mathbf{m}}(t)\phi^{''}_{\mathbf{m}}(t)}\; e^{-iS_0[\phi^{''},\phi^{''*}]} \\ & \times \int \mathcal{D}\delta r\; e^{\frac{i}{\hbar}S[\delta r,\phi^{'*},\phi^{'},\phi^{''*},\phi^{''}]} e^{-\frac{\beta}{2}\delta r_i(0)\mathcal{H}_{ij}\delta r_j(0)}, \end{aligned} \tag{2.22}$$

where the functional integral over $\delta r(t)$ is unrestricted also at time 0 and time t and the $\mathcal{S}$ functional reads

$$\begin{aligned} \mathcal{S}[\delta r,\phi^{'*},\phi^{'},\phi^{''*},\phi^{''}] &= \frac{i\;\hbar\beta}{4M\gamma}\int_0^t dt'\;\left[M\delta\ddot{r}_i + \mathcal{H}_{ij}\delta r_j + M\gamma\delta\dot{r}_i + \frac{1}{2}f^i_{\mathbf{nm}}(\phi^{'*}_{\mathbf{n}}\phi^{'}_{\mathbf{m}} + \phi^{''*}_{\mathbf{n}}\phi^{''}_{\mathbf{m}})\right]^2 \\ &+ \int_0^t dt'\;\left(f^0_{\mathbf{nm}} + f^i_{\mathbf{nm}}\delta r_i\right)(\phi^{'*}_{\mathbf{n}}\phi^{'}_{\mathbf{m}} - \phi^{''*}_{\mathbf{n}}\phi^{''}_{\mathbf{m}}). \end{aligned} \tag{2.23}$$

In order to compute the Gaussian integration over δr too, it is convenient to introduce the differential operator $\hat{L}$ and its Hermitian conjugate $\hat{L}^\dagger$, which depend on the molecular coordinate indexes i, j:

$$\left[\hat{L}\right]_{ij} = M\left(\partial^2_{t'} + \gamma\partial_{t'}\right)\delta_{ij} + \mathcal{H}_{ij}\,, \qquad \left[\hat{L}^\dagger\right]_{ij} = M\left(\partial^2_{t'} - \gamma\partial_{t'}\right)\delta_{ij} + \mathcal{H}_{ij}\,.$$

Note that, in $\hat{L}$ and $L^\dagger$, the time-derivatives are defined to act on the right. Using such operators, the functional in Eq. (2.23) can be rewritten as

$$\begin{aligned} \mathcal{S}[\delta r,\phi',\phi^{'*},\phi'',\phi^{''*}] &= \frac{i\;\hbar\beta}{4M\gamma}\int_0^t dt'\;\delta r_i(t')[\hat{L}^\dagger\cdot\hat{L}]_{ij}\;\delta r_j(t') \\ &+ \frac{i\;\hbar\beta}{4M\gamma}\int_0^t dt'\;f^i_{\mathbf{nm}}\;(\phi^{'*}_{\mathbf{n}}(t')\phi^{'}_{\mathbf{m}}(t') + \phi^{''*}_{\mathbf{n}}(t')\phi^{''}_{\mathbf{m}}(t'))\;[\hat{L}]_{ij}\;\delta r_j(t') \\ &+ \frac{i\;\hbar\beta}{16\gamma M}\int_0^t dt'\;f^i_{\mathbf{nm}}\;(\phi^{'*}_{\mathbf{n}}(t')\phi^{'}_{\mathbf{m}}(t') + \phi^{''*}_{\mathbf{n}}(t')\phi^{''}_{\mathbf{m}}(t'))\;(\phi^{'*}_{\mathbf{l}}(t')\phi^{'}_{\mathbf{h}}(t') + \phi^{''*}_{\mathbf{l}}(t')\phi^{''}_{\mathbf{h}}(t'))\;f^i_{\mathbf{lh}}. \\ &- \int_0^t dt'\;f^i_{\mathbf{nm}}\;(\phi^{'*}_{\mathbf{n}}(t')\phi^{'}_{\mathbf{m}}(t') - \phi^{''*}_{\mathbf{n}}(t')\phi^{''}_{\mathbf{m}}(t'))\;\delta r_i(t') \\ &- \int_0^t dt'\;f^0_{\mathbf{nm}}\;(\phi^{'*}_{\mathbf{n}}(t')\phi^{'}_{\mathbf{m}}(t') - \phi^{''*}_{\mathbf{n}}(t')\phi^{''}_{\mathbf{m}}(t'))\,. \end{aligned} \tag{2.24}$$

We note that, in Eq. (2.24) the first term corresponds to the Onsager-Machlup action introduced in section 2.3 and the last term describes the quantum transport of our quantum excitation in absence of coupling with the molecular dynamics, while the other terms correspond to interaction

terms. Furthermore, we observe that the second and third of them vanish in the classical limit $\hbar\beta \to 0$.

The path integral (2.22) describes the coupled dynamics of the nuclear coordinates and of the quantum excitation in the molecule. It is instructive to first consider this density matrix time evolution in the limit in which the couplings between the quantum excitation and the molecular degrees of freedom are completely neglected. In this case, the path integral factorizes as

$$\rho_{\mathbf{ij}}(t) \simeq \left[G_0^{>}(\mathbf{i},t|\mathbf{k}_i)\cdot G_0^{>\dagger}(\mathbf{j},t|\mathbf{k}_i)\right]\left\{\frac{1}{Z_M(\beta)}\int \mathcal{D}\delta r\, e^{-\frac{\beta}{4M\gamma}\int_0^t d\tau (M\delta\ddot{r}-\gamma\delta\dot{r}+\mathcal{H}_{ij}\delta r_j)^2} e^{-\frac{\beta}{2}\delta r_i(0)\mathcal{H}_{ij}\delta r_j(0)}\right\}$$
$$= \left[G_0^{>}(\mathbf{i},t|\mathbf{k}_i)\cdot G_0^{>\dagger}(\mathbf{j},t|\mathbf{k}_i)\right]. \tag{2.25}$$

In this equation,

$$G_0^{>}(\mathbf{n},t|\mathbf{k}_i) \equiv \langle \mathbf{n}|\, e^{-i\hat{H}_0 t}\,|\mathbf{k}_i,\rangle, \qquad \text{with} \quad \hat{H}_0 \equiv f_{\mathbf{lm}}(Q_0)\,\hat{a}^\dagger_{\mathbf{l}}\,\hat{a}_{\mathbf{m}}\,,$$

is the Green's function defined by the tight-binding Hamiltonian $\hat{H}_0$, which is evaluated keeping the molecule "frozen" in its minimum-energy configuration Q_0.

2.5.2 Quantum Transport Field Theory

A major simplification which follows from the small oscillation approximations is that the integral over the small displacement of the molecular coordinates from their equilibrium position δr can be performed analytically. The result is an QTFT with non-instantaneous interactions between quantum excitations:

$$\rho_{\mathbf{ij}}(t) = \frac{1}{\mathrm{Tr}\,[\hat{\rho}(0)]}\int \mathcal{D}\phi^{'}\mathcal{D}\phi^{'*}\phi^{'}_{\mathbf{i}}(t)\phi^{'*}_{\mathbf{k}_i}(0)\; e^{-\phi^{'*}_{\mathbf{m}}(0)\phi^{'}_{\mathbf{m}}(0)} \int \mathcal{D}\phi^{''}\mathcal{D}\phi^{''*}\phi^{''}_{\mathbf{k}_i}(0)\phi^{''*}_{\mathbf{j}}(t)\; e^{-\phi^{''*}_{\mathbf{m}}(t)\phi^{''}_{\mathbf{m}}(t)}$$
$$\times\, e^{\frac{i}{\hbar}S_{\mathbf{0}}[\phi^{'},\phi^{'*}]-\frac{i}{\hbar}S_{\mathbf{0}}[\phi^{''},\phi^{''*}]}\; e^{\frac{i}{\hbar}S_{\mathbf{I}}[\phi^{'*},\phi^{'},\phi^{''*},\phi^{''}]}, \tag{2.26}$$

where unperturbed $\mathcal{S}_{\mathbf{0}}$ and interaction $\mathcal{S}_{\mathbf{I}}$ action read

$$\mathcal{S}_{\mathbf{0}}[\phi,\phi^*] = \int_0^t dt'\phi^*_{\mathbf{n}}(t')\left[i\hbar\,\frac{\partial}{\partial t'}\delta_{\mathbf{nm}} - f^0_{\mathbf{nm}}\right]\phi_{\mathbf{m}}(t')\,, \tag{2.27}$$

$$\mathcal{S}_{\mathbf{I}}[\phi',\phi^{'*},\phi'',\phi^{''*}] = \frac{1}{4}\int_0^t dt'dt''\left(\phi^{'*}_{\mathbf{k}}\phi^{'}_{\mathbf{l}}+\phi^{''*}_{\mathbf{k}}\phi^{''}_{\mathbf{l}}\right)(t')\; f^i_{\mathbf{kl}}\mathcal{V}_{ij}(t'-t'')f^j_{\mathbf{mn}}\;\left(\phi^{'*}_{\mathbf{m}}\phi^{'}_{\mathbf{n}}-\phi^{''*}_{\mathbf{m}}\phi^{''}_{\mathbf{n}}\right)(t'')$$
$$+\frac{i\;M\gamma}{\beta\hbar}\int_0^t dt'dt''\left(\phi^{'*}_{\mathbf{k}}\phi^{'}_{\mathbf{l}}-\phi^{''*}_{\mathbf{k}}\phi^{''}_{\mathbf{l}}\right)(t')\; f^i_{\mathbf{kl}}\Delta_{ij}(t'-t'')f^j_{\mathbf{mn}}\;\left(\phi^{'*}_{\mathbf{m}}\phi^{'}_{\mathbf{n}}-\phi^{''*}_{\mathbf{m}}\phi^{''}_{\mathbf{n}}\right)(t'') \tag{2.28}$$

Let us point out that, performing the Gaussian integral over δr in Eq. (2.22) we consider the mean-field value of the surface term $\delta r(0)$ in the Boltzmann average. In this way, we can neglect the average over the Boltzmann distribution in our calculated. [6].

In Eq. (2.28), $\Delta_{ij}(t'-t'')$, and $\mathcal{V}_{ij}(t-t')$ are respectively the Green's functions of the $[\hat{L}^\dagger\hat{L}]$ operator and the sum of the Green's functions of the $\hat{L}$ and $\hat{L}^\dagger$ operators. In order to explicitly compute them, it is convenient to transform to the normal mode basis, in which the Hessian of the potential energy at the minimum energy configuration Q_0 is diagonal:

$$U^\dagger_{ks}\;\mathcal{H}_{sj}U_{ji} = \delta_{ki}\;M\;\Omega^2_k\,.$$

[6] An exact calculation that take in account also the Boltzmann average over the initial condition δr is not straightforward, since it needs to switch to discrete path integral representation [93, 96], or to average over differente initial conditions.

In this equation, Ω_k denotes the frequency of the k-th normal mode. In this basis, the expressions of the vibron propagators $\Delta_{ij}(t'-t'')$ and $\mathcal{V}_{ij}(t-t')$ read (see the derivation in the Appendix A.4)

$$\Delta_{ij}(t) = \frac{e^{-\frac{1}{2}\gamma\ |t|}}{2\ M^2\ \Omega_k^2}\ U_{ik}^\dagger\ U_{kj}\ a_k(t)\,, \tag{2.29}$$

$$\mathcal{V}_{ij}(t) = \frac{2\ e^{-\frac{1}{2}\gamma\ |t|}}{M\ \omega_0^k}\ U_{ik}^\dagger\ U_{kj}\ b_k(t)\,, \tag{2.30}$$

where $\omega_0^k = \sqrt{|4\Omega_k^2 - \gamma^2|}$ and

$$a_k(t) = \begin{cases} \dfrac{\sin\left(\frac{1}{2}\omega_0^k\ |t|\right)}{\omega_0^k} + \dfrac{\cos\left(\frac{1}{2}\omega_0^k\ |t|\right)}{\gamma} & \text{if } 2\Omega_k \geq \gamma\,, \\ \dfrac{\sinh\left(\frac{1}{2}\omega_0^k\ |t|\right)}{\omega_0^k} + \dfrac{\cosh\left(\frac{1}{2}\omega_0^k\ |t|\right)}{\gamma} & \text{if } 2\Omega_k < \gamma\,, \end{cases} \tag{2.31}$$

$$b_k(t) = \begin{cases} \sin\left(\frac{1}{2}\omega_0^k\ |t|\right) & \text{if } 2\Omega_k \geq \gamma\,, \\ \sinh\left(\frac{1}{2}\omega_0^k\ |t|\right) & \text{if } 2\Omega_k < \gamma\,. \end{cases} \tag{2.32}$$

It is useful to consider the asymptotic expressions for the Green's functions in the limit $\gamma \gg 2\Omega_k$, which corresponds to the over-damping regime:

$$\Delta_{ij}(t) = \frac{e^{-\frac{\Omega_k^2}{\gamma}\ |t|}}{2\ M^2\ \gamma\ \Omega_k^2}\ U_{ik}^\dagger\ U_{kj}\,,$$

$$\mathcal{V}_{ij}(t) = \frac{1}{M\ \gamma}\left(1 + 2\frac{\Omega_k^2}{\gamma}\right)\left(e^{-\frac{2\Omega_k^2}{\gamma}|t|} - e^{-\gamma|t|}\, e^{\frac{2\Omega_k^2}{\gamma^2}|t|}\right)\ U_{ik}^\dagger\ U_{kj}\,.$$

In the opposite under-damped regime ($\gamma \ll \Omega_k$) the asymptotic expression for the propagators is:

$$\Delta_{ij}(t) = \frac{e^{-\frac{\gamma}{2}\ |t|}}{2\ M^2\ \gamma\ \Omega_k^2}\ \cos\left(\Omega_k|t|\right)\ U_{ik}^\dagger\ U_{kj}\,,$$

$$\mathcal{V}_{ij}(t) = \frac{e^{-\frac{\gamma}{2}\ |t|}}{2\ M\ \Omega_k}\ \sin\left(\Omega_k|t|\right)\ U_{ik}^\dagger\ U_{kj}\,.$$

Eq. (2.26) is one of the central results of this work. It shows that the reduced density matrix $\rho_{\mathbf{ij}}(t)$ for the dissipative dynamics of a quantum excitation can be written in a form which is *formally* analogue to a 4-point correlation function, in an effective zero-temperature quantum field theory. This analogy is quite remarkable, since our theory describes an open system and is fully consistent with the fluctuation-dissipation relation. Therefore, we can adopt several quantum field theory techniques developed to evaluate directly the reduced density matrix and the expectation values of operators.

In the next chapter we show that, for a sufficiently short time interval, the evolution of the reduced density matrix can be obtained even analytically, by relying on a simple diagrammatic perturbative technique. In section 4, we analyze the opposite long-time and long-distance regime using the renormalization group formalism. Finally, in section 5 we adopt the resummation technique in order to formalize a non-perturbative scheme, obtaining a Bethe-Salpether equation for the time-evolution of the density matrix.

Chapter 3

Quantum Propagation at Short-Distance and Short-Time

Phenomena of quantum transport along short-distance and for short-time can be studied analytically by means of the field theory derived in the previous chapter, adopting the perturbation diagrammatic scheme. In this chapter we illustrate this approach computing the relevant leading-order Feynman diagrams of our QTFT, and presenting a simple application to the charge transport along a conjugate polymer [1].

3.1 Perturbation Theory and Feynman Diagrams

3.1.1 Dirac-Like Notation

The symmetric structure of the exponent in the path integral representation of the reduced density matrix $\rho_{\mathbf{ij}}(t)$ between forward, $\phi^{'}$, and backward field, $\phi^{''}$, suggests the collection of all coherent field degrees of freedom into a single 2-component Grassmann field ψ defined as:

$$\psi_{\mathbf{n}} \equiv \begin{pmatrix} \phi^{'}_{\mathbf{n}} \\ \phi^{''}_{\mathbf{n}} \end{pmatrix}. \tag{3.1}$$

Similarly, we collect all conjugate fields into $\psi^{\dagger}_{\mathbf{n}} \equiv \left(\phi^{'*}_{\mathbf{n}}, \phi^{''*}_{\mathbf{n}}\right)$. In view of the formal analogy with a Dirac theory in two-dimension, it is convenient to introduce also the following 2×2 matrices, which define the projection onto the upper and lower component of the doublet and the interchange between them:

$$\begin{aligned} \gamma_0 &= \begin{pmatrix} 1 & 0 \\ 0 & -1 \end{pmatrix}, & \gamma_+ &= \begin{pmatrix} 1 & 0 \\ 0 & 0 \end{pmatrix}, \\ \gamma_- &= \begin{pmatrix} 0 & 0 \\ 0 & 1 \end{pmatrix}, & \gamma_5 &= \begin{pmatrix} 0 & 1 \\ 1 & 0 \end{pmatrix}. \end{aligned} \tag{3.2}$$

In addition, we change variables in the integration over the $\psi^{\dagger}$ field by means of the substitution

$$\bar{\psi}_{\mathbf{n}}(t) \equiv \psi^{\dagger}_{\mathbf{n}}(t)\ \gamma_0\,. \tag{3.3}$$

Using the notation defined in Eq.s (3.1), (3.2) and (3.3), the reduced density matrix in Eq. (2.26) is written as:

$$\begin{aligned} \rho_{\mathbf{ij}}(t) \;=\; \frac{-1}{\mathrm{Tr}\left[\hat{\rho}(0)\right]} \int \mathcal{D}\bar{\psi}\ \mathcal{D}\psi\ e^{-\mathcal{L}_1(t,0)} \left(\bar{\psi}_{\mathbf{j}}(t)\ \gamma_-\gamma_5\ \psi_{\mathbf{i}}(t)\ \bar{\psi}_{\mathbf{k}_i}(0)\ \gamma_+\gamma_5\ \psi_{\mathbf{k}_i}(0)\right) \\ \times\ e^{\frac{i}{\hbar}S_{\mathbf{0}}[\bar{\psi},\psi]}\ e^{\frac{i}{\hbar}S_{\mathbf{I}}[\bar{\psi},\psi]}, \end{aligned} \tag{3.4}$$

where the term[1]

$$S_{\mathbf{0}}[\bar{\psi},\psi] \;=\; \int_0^t dt'\; \bar{\psi}_{\mathbf{m}}\; \left(i\hbar\,\partial_{t'}\delta_{\mathbf{mn}} - f^0_{\mathbf{mn}}\right)\; \psi_{\mathbf{n}}\,, \tag{3.5}$$

corresponds to Eq. (2.27) in the new variables, and it describes the quantum propagation of the charge in the absence of any coupling with the molecular dynamics. In this Dirac-like notation, the interaction action in Eq. (2.28) reads

$$\begin{aligned} S_{\mathbf{I}}[\bar{\psi},\psi] \;&=\; \frac{1}{4}\int_0^t dt'dt''\; \left(\bar{\psi}_{\mathbf{k}}(t')\;\gamma_0\; f^i_{\mathbf{kl}}\;\psi_{\mathbf{l}}(t')\right)\;\mathcal{V}_{ij}(t'-t'')\;\left(\bar{\psi}_{\mathbf{m}}(t'')\;f^j_{\mathbf{mn}}\;\psi_{\mathbf{n}}(t'')\right) \\ &+\; \frac{i\;M\gamma}{\beta\hbar}\int_0^t dt'dt''\; \left(\bar{\psi}_{\mathbf{k}}(t')\;f^i_{\mathbf{kl}}\;\psi_{\mathbf{l}}(t')\right)\;\Delta_{ij}(t'-t'')\;\left(\bar{\psi}_{\mathbf{m}}(t'')\;f^j_{\mathbf{mn}}\;\psi_{\mathbf{n}}(t'')\right)\,, \end{aligned} \tag{3.6}$$

where Δ and $\mathcal{V}$ are the non-local interaction terms derived in the previous chapter. The surface term $\mathcal{L}_1(t,0)$ follows from the over completeness of the coherent-field basis, and reads

$$\mathcal{L}_1(t,0) \;=\; \left(\bar{\psi}_{\mathbf{m}}(0)\;\gamma_0\;\gamma_+\;\psi_{\mathbf{m}}(0) + \bar{\psi}_{\mathbf{m}}(t)\;\;\gamma_0\;\gamma_-\;\psi_{\mathbf{m}}(t)\right)\,, \tag{3.7}$$

Some comments on Eq. (3.4) are in order. Firstly, we note that the overall minus sign appearing in front of the integral is a consequence of the Fermi statistics and ensures the overall positivity of the probability density. Secondly, we observe that, while the path integral (2.22) is defined over forward- and backward- propagating fields, the path integral Eq. (3.4) contains only the integration in the forward time direction. Indeed, the backward-propagating fields have been replaced by lower-components of the doublet field, hence they can be *formally* interpreted as anti-matter degrees of freedom propagating forward in time. This analogy can be useful to derive perturbative calculation and to adopt non-perturbative quantum field theory technique.

3.1.2 Short-time Regime

Let us now evaluate the reduced density matrix $\rho_{\mathbf{ij}}(t)$ in the short-time regime by means of perturbation theory. This method derives by performing a Taylor expansion of the exponents in Eq. (3.4) in powers of the interaction terms

$$\begin{aligned} V_1 \;&=\; \frac{-M\gamma}{\beta\hbar^2}\int_0^t dt'\int_0^t dt''\;\bar{\psi}_{\mathbf{m}}(t')\;f^i_{\mathbf{mn}}\;\psi_{\mathbf{n}}(t')\;\Delta_{ij}(t'-t'')\;\bar{\psi}_{\mathbf{k}}(t'')\;f^j_{\mathbf{kl}}\;\psi_{\mathbf{l}}(t'')\,, \\ V_2 \;&=\; \frac{i}{4\hbar}\;\int_0^t dt'\int_0^t dt''\;\bar{\psi}_{\mathbf{m}}(t')\;\gamma_0 f^i_{\mathbf{mn}}\;\psi_{\mathbf{n}}(t')\;\mathcal{V}_{ij}(t'-t'')\;\bar{\psi}_{\mathbf{k}}(t'')\;f^j_{\mathbf{kl}}\;\psi_{\mathbf{l}}(t'')\,. \end{aligned}$$

The reduced density matrix is then written as

$$\rho_{\mathbf{ij}}(t) = \sum_i^{\infty}\rho^{(i)}_{\mathbf{ij}}\,(t)\;, \tag{3.8}$$

where $\rho^{(0)}_{\mathbf{ij}}\,(t)$ corresponds to the unperturbed reduced density matrix, which neglects all the couplings between the quantum excitation, the heat bath and the vibronic modes,

$$\rho^{(0)}_{\mathbf{ij}}\,(t) = \frac{-1}{Z^{(0)}}\int \mathcal{D}\bar{\psi}\;\mathcal{D}\psi\;e^{-\mathcal{L}_1(t,0)}\left(\bar{\psi}_{\mathbf{j}}(t)\;\gamma_-\gamma_5\;\psi_{\mathbf{i}}(t)\;\bar{\psi}_{\mathbf{k}_i}(0)\;\gamma_+\gamma_5\;\psi_{\mathbf{k}_i}(0)\right)\;e^{\frac{i}{\hbar}S_{\mathbf{0}}[\bar{\psi},\psi]}\,. \tag{3.9}$$

Its normalization factor $Z^{(0)}$ can be written in path integral form as:

$$Z^{(0)} = \int \mathcal{D}\bar{\psi}\;\mathcal{D}\psi\;e^{-\mathcal{L}_1(t,0)}\;\sum_{\mathbf{n}}\left(\bar{\psi}_{\mathbf{n}}(t)\;\gamma_-\gamma_5\;\psi_{\mathbf{n}}(t)\;\bar{\psi}_{\mathbf{k}_i}(0)\;\gamma_+\gamma_5\;\psi_{\mathbf{k}_i}(0)\right)\;e^{\frac{i}{\hbar}S_{\mathbf{0}}[\bar{\psi},\psi]}\,. \tag{3.10}$$

[1] Throughout this thesis we shall adopt Einstein's notation and implicitly assume the summation over all bold repeated indexes, except for the initial exciton position $\mathbf{k}_i$ which is held fixed.

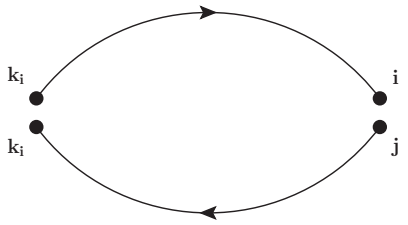

Figure 3.1: The diagram corresponding to the unperturbed contribution to reduced density matrix evolution $\rho_{\mathbf{ij}}(t)$, with initial condition $\rho(0) = |\mathbf{k}_i\rangle\langle\mathbf{k}_i|$.

The leading-order perturbative correction in the series (3.8) reads

$$\rho^{(1)}_{\mathbf{ij}}(t) \;=\; \frac{-1}{Z^{(0)}+Z^{(1)}} \int \mathcal{D}\bar{\psi}\;\mathcal{D}\psi\; e^{-\mathcal{L}_1(t,0)} \left(\bar{\psi}_{\mathbf{j}}(t)\;\gamma_-\gamma_5\;\psi_{\mathbf{i}}(t)\;\bar{\psi}_{\mathbf{k}_i}(0)\;\gamma_+\gamma_5\;\psi_{\mathbf{k}_i}(0)\right) \times\; (V_1+V_2)\;\; e^{\frac{i}{\hbar}S_0[\bar{\psi},\psi]}\,, \tag{3.11}$$

where the corresponding leading-order correction to the normalization factor is

$$Z^{(1)} \;=\; \int \mathcal{D}\bar{\psi}\;\mathcal{D}\psi\; e^{-\mathcal{L}_1(t,0)} \sum_{\mathbf{n}} \left(\bar{\psi}_{\mathbf{n}}(t)\;\gamma_-\gamma_5\;\psi_{\mathbf{n}}(t)\;\bar{\psi}_{\mathbf{k}_i}(0)\;\gamma_+\gamma_5\;\psi_{\mathbf{k}_i}(0)\right) \times\; (V_1+V_2)\;\; e^{\frac{i}{\hbar}S_0[\bar{\psi},\psi]}\,. \tag{3.12}$$

Eq.s (3.9), (3.10), (3.11) and (3.12) correspond to correlation functions in the free limit for the effective Dirac-like quantum field theory. According to Wick's theorem, these Green's functions can be evaluated by considering the sum of all possible contractions between the ψ and $\bar{\psi}$ fields and replacing each contraction with time-ordered Feynman propagator:

$$\overbrace{\psi_{\mathbf{i}}(t'')\;\bar{\psi}_{\mathbf{j}}}(t') \to G^0_{\mathbf{ij}}(t''-t') = \;V^\dagger_{\mathbf{is}}\; e^{-\frac{i}{\hbar}f^0_{\mathbf{s}}(t''-t')}\;V_{\mathbf{sj}}\;\left[\;\gamma_+\theta(t''-t')-\gamma_-\theta(t'-t'')\;\right], \tag{3.13}$$

where the matrix elements $V_{\mathbf{ij}}$ define the unitary transformation which diagonalizes the hopping matrix $f^0_{\mathbf{ij}}$, while $f^0_{\mathbf{s}}$ are the corresponding eigenvalues[2].

From the zero-th order diagram shown in Fig. 3.1 we readily re-obtain the unperturbed reduced density matrix $\rho^{(0)}_{\mathbf{ij}}(t)$ described in Eq. (2.25)

$$\rho^{(0)}_{\mathbf{ij}}(t) = -G^0_{\mathbf{ik_i}}(t)\,G^0_{\mathbf{k_i j}}(-t) = \;V^\dagger_{\mathbf{in}}\,e^{-\frac{i}{\hbar}f^0_{\mathbf{n}}t}\,V_{\mathbf{nk_i}}\,V^\dagger_{\mathbf{k_i s}}\,e^{\frac{i}{\hbar}f^0_{\mathbf{s}}t}\,V_{\mathbf{sj}} \;=\; \left[G^>_0(\mathbf{i},t|\mathbf{k}_i)\cdot G^{>\dagger}_0(\mathbf{j},t|\mathbf{k}_i)\right].$$

The Wick contractions are most conveniently defined and computed using a diagrammatic technique, i.e. by applying the Feynman rules shown in Fig. 3.2. Just like in the standard quantum field theory, we can prove that the corrections to the normalization factor $Z^{(1)}$ exactly cancel out with the contribution of disconnected diagrams, order-by-order in perturbation theory.

The different types of diagrams which contribute to $\rho^{(1)}_{\mathbf{ij}}(t)$ are shown in Fig. 3.3. We note that the first two of such diagrams contain a *self-energy*-type correction to one of the propagators. The third diagram contains the interaction of forward and backward propagating quantum excitations and we called it *crossing*-type diagram. Finally, the last diagram is a *tad-pole*. After collecting all terms, we obtain the following expression for the first-oder correction to the reduced density

[2] The corresponding propagators for the fields $\phi^{'}$ and $\phi^{''}$ are

$$\overbrace{\phi^{'}_{\mathbf{i}}(t'')\;\phi^{'*}_{\mathbf{j}}}(t') \;=\; \theta(t''-t')\;V^\dagger_{\mathbf{is}}\,e^{-\frac{i}{\hbar}f^0_{\mathbf{s}}(t''-t')}\,V_{\mathbf{sj}}\,, \qquad \overbrace{\phi^{''}_{\mathbf{i}}(t'')\;\phi^{''*}_{\mathbf{j}}}(t') \;=\; \theta(t'-t'')\;V^\dagger_{\mathbf{is}}\,e^{-\frac{i}{\hbar}f^0_{\mathbf{s}}(t''-t')}\,V_{\mathbf{sj}}\,.$$

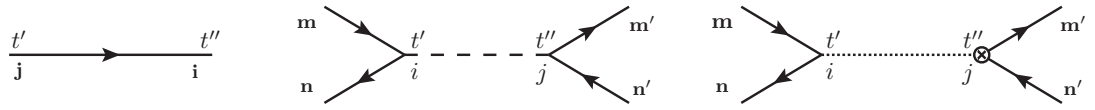

$G^0_{\mathbf{ij}}(t''-t')$ $\quad -\frac{M\gamma}{\beta\hbar^2}\ f^i_{\mathbf{mn}}\ \Delta_{ij}(t'-t'')\ f^j_{\mathbf{m'n'}}$ $\quad \frac{i}{2\hbar}\ f^j_{\mathbf{m'n'}}\ \gamma_0\ \mathcal{V}_{ji}(t''-t')\ f^i_{\mathbf{mn}}$

Figure 3.2: Feynman rules for the QTFT for charge propagation in the macromolecule. On the left panel, we show the quantum excitation Feynman propagator, on the center panel the effective interaction V_1, and on the right panel the effective interaction V_2.

matrix evolution:

$$\begin{aligned}
\rho^{(1)}_{\mathbf{ij}}(t) &= \frac{4M\gamma}{\beta\hbar^2}\mathrm{Re}\Big[\int_0^t d\tau d\tau' G^0_{\mathbf{iq'}}(t-\tau')f^j_{\mathbf{q's'}}\Delta_{ji}(\tau'-\tau)G^0_{\mathbf{s's}}(\tau'-\tau)f^i_{\mathbf{sq}}G^0_{\mathbf{qk_i}}(\tau)G^0_{\mathbf{k_ij}}(-t)\Big] \\
&+ \frac{2}{\hbar}\ \mathrm{Im}\Big[\int_0^t d\tau d\tau' G^0_{\mathbf{iq'}}(t-\tau')f^j_{\mathbf{q's'}}\mathcal{V}_{ji}(\tau'-\tau)G^0_{\mathbf{s's}}(\tau'-\tau)f^i_{\mathbf{sq}}G^0_{\mathbf{qk_i}}(\tau)G^0_{\mathbf{k_ij}}(-t)\Big] \\
&+ \frac{2}{\hbar}\ \mathrm{Im}\Big[\int_0^t d\tau d\tau' G^0_{\mathbf{iq}}(t-\tau)f^i_{\mathbf{s's'}}\mathcal{V}_{ij}(\tau'-\tau)f^j_{\mathbf{qs}}G^0_{\mathbf{sk_i}}(\tau)G^0_{\mathbf{k_ij}}(-t)\Big] \\
&+ \frac{2M\gamma}{\beta\hbar^2}\int_0^t d\tau d\tau'\ G^0_{\mathbf{is}}(t-\tau)f^i_{\mathbf{sq}}G^0_{\mathbf{qk_i}}(\tau)\Delta_{ji}\,(\tau'-\tau)\,G^0_{\mathbf{k_is'}}(-\tau')f^j_{\mathbf{s'q'}}G^0_{\mathbf{q'j}}(\tau'-t)\,. \quad (3.14)
\end{aligned}$$

The first two lines are the contributions due to the *self-energy*-type diagrams, the third is derived from the *tad-pole* diagram, and the last line is derived from the *crossing*-type diagram. Further details of this calculation are provided in Appendix B.1.

We conclude this section by discussing the regimes in which we expect the perturbative expansion to be applicable. To this end, we introduce the explicit expressions for $G^0_{\mathbf{ij}}$, Δ_{ij}, and $\mathcal{V}_{ij}$ into Eq. (3.14), take the short time limit $t \ll 1/\Omega_k$, $t \ll 1/\gamma$, and consider for simplicity only the over-damped and under-damped asymptotic expressions for the Green's functions.

In the in the over-damped regime, we find the conditions of validity

$$\begin{aligned}
\frac{2\ f^{i\,2}_{\mathbf{qs}}\ t^2}{\beta\ M\ \Omega_k^2\ \hbar^2} &\ll 1 \qquad \text{(from the } V_1\text{-type interaction)}\,, \\
\frac{4\ f^{i\,2}_{\mathbf{qs}}\ t^2}{M\ \gamma\ \hbar} &\ll 1 \qquad \text{(from the } V_2\text{-type interaction)}\,.
\end{aligned}$$

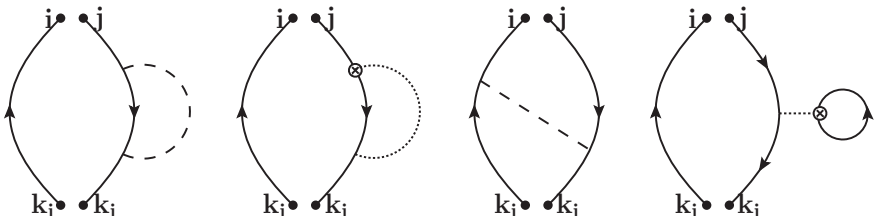

Figure 3.3: The diagrams involved in the leading-order correction to the reduced density matrix. The first two diagrams from the left-hand-side are called *self-energy*-type. The third diagram is called *crossing*-type and the last is a *tad-pole* diagram. Similar diagrams exist for *self-energy* and *tad-pole* diagrams, in which the vibron propagators are coupled with the quantum excitation propagator on the left.

In the under-damped regime, the conditions of validity of the perturbative expansion are

$$\frac{2\ f_{\mathbf{qs}}^{i\,2}\ t^2}{\beta\ M\ \Omega_k^2\ \hbar^2} \ll 1 \qquad \text{(from the } V_1\text{-type interaction)}\,,$$

$$\frac{2\ f_{\mathbf{qs}}^{i\,2}\ t^2}{M\ \Omega_k\ \hbar} \ll 1 \qquad \text{(from the } V_2\text{-type interaction)}\,.$$

We note that in both the under-damped and over-damped regimes the perturbative approach is only valid at short times. This is completely expected, because the long-time and long-distance propagation necessarily involves multiple scattering of the quantum excitation with the heat bath and molecular vibrations, hence require a non-perturbative treatment. By plugging order of magnitude estimates of the normal-mode frequencies ($\Omega_k \sim 10^{-3}$ fs^{-1}), the gradient of the hopping matrix elements ($f^i \sim 10^{-2}$ eV Å^{-1}), and the viscosity ($\gamma = 0.1$ fs^{-1}) we find that, at room temperature and in the over-damped limit, the V_1-type interaction is several orders of magnitude larger than the V_2-type, hence determines the range of validity of the perturbative expansion. On the other hand, in the opposite under-damped limit, the driving interaction is V_2-type.

3.2 Charge Propagation through a Conjugate Polymer

Let us now illustrate the perturbative approach developed in the previous sections by investigating the intra-chain propagation of electron holes through the backbone of a poly(3-alkylthiophene) (P3HT) polymer. Quasi-crystalline materials made of inter-digited PH3T polymers have received much attention, in connection with the possibility of realizing nanoscale organic transistors [66, 97, 98]. The atomistic three-dimensional structure of a PH3T molecule is shown in the upper panel of Fig. 3.4.

Here, we are only interested in providing a qualitative description of the charge propagation in such systems, leaving a more sophisticated quantitative description to future works. Our main goal is to estimate the order of magnitude of the range of times and distances over which the perturbative approach is applicable. Secondly, for validation purposes we are interested in comparing the reduced quantum density matrix evolution obtained by analytic perturbative expansion in Eq. (3.14) and by the integration of the quantum and stochastic equations of motion (2.21). Finally, we investigate how the different effective interactions which appear in Eq. (3.4) affect the dynamics and in particular quantum decoherence and recoherence phenomena.

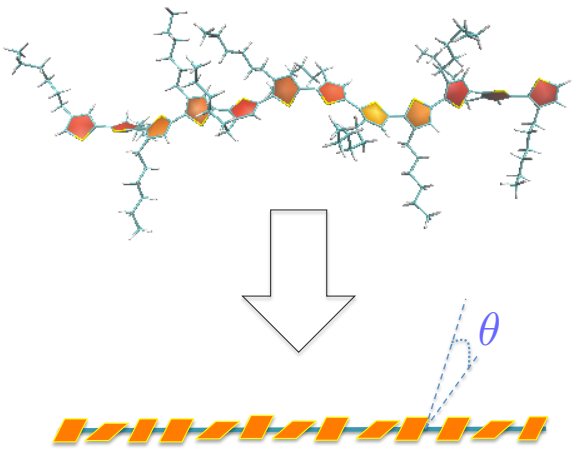

Figure 3.4: **Upper panel**: three-dimensional structure of a P3HT polymer. **Lower panel**: the coarse-grained representation corresponding to our effective model.

3.2.1 Coarse-Grained Model for P3HT Dynamics

In order to address these points, we adopt a simple coarse-grained representation of the molecule in which side-chain degrees of freedom are not taken explicitly into account. Furthermore, the molecular potential energy function is assumed to effectively depend only on the dihedral angles formed by neighboring aromatic rings. Hence, the molecular configuration is specified by the set of dihedral angles $\Theta = (\theta_1, \ldots, \theta_N)$, and the chain is mapped into an effective one-dimensional system consisting of N plaquettes which can rotate around their symmetry axis, as sketched in the lower-right panel of Fig. 3.4.

The potential energy of a molecular configuration is approximated with sum of only neighbors interaction terms, each of which depends on the relative dihedral angle of two consecutive monomers,

$$U(\Theta) = \sum_i u(\theta_i - \theta_{i+1}) \, .$$

We have obtained the pair-wise interaction energy $u(\theta_i - \theta_{i+1})$ as a function of the relative angle $\theta = \theta_i - \theta_{i+1}$ from DFT-TB electronic structure calculations, using the *DFTB+* package [99]. The results are shown in the left panel of Fig. 3.5. We point out that the mechanical equilibrium configuration is achieved when aromatic rings in different residues form a relative dihedral angle of $(-1)^i \ \theta_0$, where $\theta_0 = 20^o$ and i is the monomer index.

The conformational dynamics is therefore described by the Hamiltonian:

$$H_M = \frac{1}{2I} \ \sum_{i=1}^{N} p_i^2 + U(\Theta) \, ,$$

where I is the momentum of inertia of the monomers (including the contribution from the atoms in the side-chain) and $p_i = I\dot{\theta}_i$ is the canonical momentum conjugated to the θ_i generalized coordinate.

At room temperature, this system performs only small thermal oscillations around the minimum energy configuration. Hence, we can perform a small-angle expansion, leading to the simple harmonic form:

$$H_M \simeq \frac{1}{2I} \ \sum_{i=1}^{N} p_i^2 + \sum_{i=1}^{N-1} \frac{\kappa}{2} (\theta_{i+1} - \theta_i + (-1)^i \theta_0)^2 + \frac{\kappa}{2} \theta_1^2 + \frac{\kappa}{2} \theta_N^2 \, . \tag{3.15}$$

The last two terms follow from assuming that the first and last monomers in the chain are bond to external non-conducting leads which tend to align them horizontally.

The momentum of inertia I can be calculated directly from the three-dimensional structure of the chain and affects the frequencies of the chain's normal modes of oscillations,

$$\omega^2 \sim \frac{\kappa}{I} \, .$$

In the systems which are of technological and experimental interest, P3HT polymers are embedded in organic frameworks. In such a configuration, the chain exchanges energy with neighboring molecules, which play the role of a heat bath. In addition, the steric interaction with neighbors generates strong constraints on the chain dynamics and in particular affects the amplitude and frequencies of thermal oscillations. In order to account for this effect, we consider an effective model in which the spring constant κ which appears in the molecular potential energy function $U(\Theta)$ is artificially rescaled in such a way that the typical square fluctuations of the dihedral angles around their equilibrium values, $\langle \Delta\theta^2 \rangle_{MD} = \frac{1}{N} \sum_i \langle ((\theta_{i+1} - \theta_i + (-1)^i \ \theta_0)^2 \rangle_{MD}$ matches the value obtained from classical molecular dynamics simulations for a system of inter-digited PH3T polymers [100]:

$$\kappa \to \kappa_{eff} \, , \qquad \text{and} \qquad \langle \Delta\theta^2 \rangle_{MD} \simeq \frac{k_B \ T}{\kappa_{eff}} \, .$$

$e_0\,[eV]$	$T_0\,[eV]$	$T_1\,[eV]$	$\theta_0\,[deg]$	$\gamma\,[fs^{-1}]$	$\kappa\,[eV]$	$\kappa_{eff}\,[eV]$	$T\,[^oK]$	$I\,[uma\ \text{Å}^2]$
5.4	0.4	0.06	20	0.1	0.13	0.20	300	3400

Table 3.1: Parameters of the coarse-grained model which describes intra-chain hole propagation in P3HT polymers. The PH3T chain investigated in the simulations consists of 9 monomers.

The hopping matrix elements T_{ii+1} between neighboring monomers and the on-site energies e_i as a function of the chain's configurations have also been obtained by DFT-TB calculations. In analogy with molecular energy calculations, the transition matrix elements T_{ii+1} have been computed assuming that they effectively depend only on the relative angles, $|\theta_{i+1} - \theta_i|$. For sake of simplicity, we have taken the on-site energies ϵ_i to be constant and equal to the value at the mechanical equilibrium configuration. This choice can be motivated by the observation made by different groups (see e.g. Ref. [81]) that fluctuations of the on-site energies have a much smaller effect on the electric conduction than fluctuations of the transfer matrix elements. The results for $T_{ii+1}(\theta_{i+1} - \theta_i)$, in the vicinity of the equilibrium configuration θ_0 are reported in the right panel of Fig. 3.5. By assuming a linear approximation, Eq. (2.3) takes the form

$$f_{mn}\,(\theta_i) \;\; = \;\; f^0_{mn} + f^1_{mn}\;\; (\,|\theta_m - \theta_n| - \theta_0)\;,$$

where

$$\begin{aligned} f^0_{mn} &= T_0\;\;(1-\delta_{mn}) - e_0\;\delta_{mn} \\ f^1_{mn} &= T_1\;\;(1-\delta_{mn})\;. \end{aligned}$$

Finally, the viscosity parameter γ may be determined from MD simulations by computing the velocity autocorrelation function. On the other hand, we have observed that the results of the perturbative calculation depend very weakly on the this parameter. Hence, for sake of simplicity, here we assume a reasonable value $\gamma = 0.1$ fs^{-1}.

The numerical values of the parameters of this coarse grained model are summarized in Table 3.1. The equilibrium configuration can be chosen to be:

$$\theta_i = \begin{cases} 0 & \text{if } i \text{ odd}, \\ \theta_0 & \text{if } i \text{ even}. \end{cases}$$

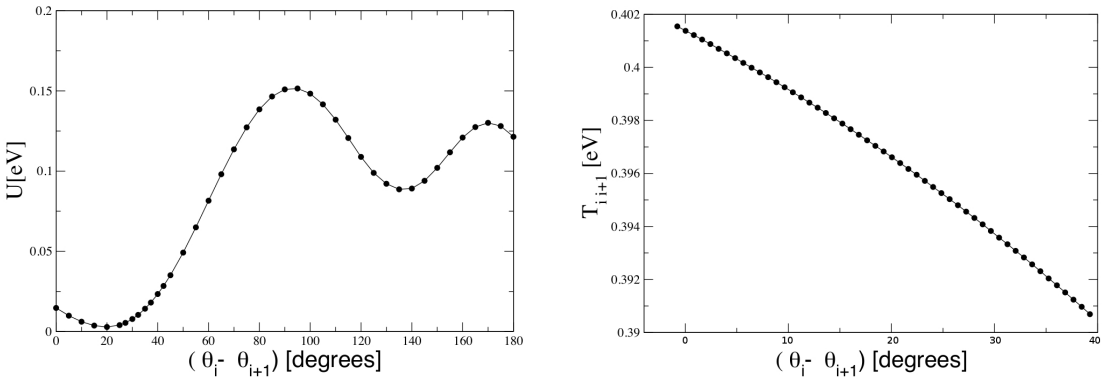

Figure 3.5: **Left panel**: DTP-B calculation of the molecular potential energy of two consecutive monomers as a function of the difference of dihedral angles. The mechanical equilibrium is retained at an angle s^i, which in this case is $\simeq 20^o$. In general $s^i = \pm\theta_0$ for i odd (even), with $\theta_0 = 20^o$. **Right panel**: DFT-TB calculation of the transfer integrals $T_{i+1,i}$ as a function of the difference in the dihedral angles $(\theta_{i+1} - \theta_i)$, in the proximity of the mechanical equilibrium configuration θ_0.

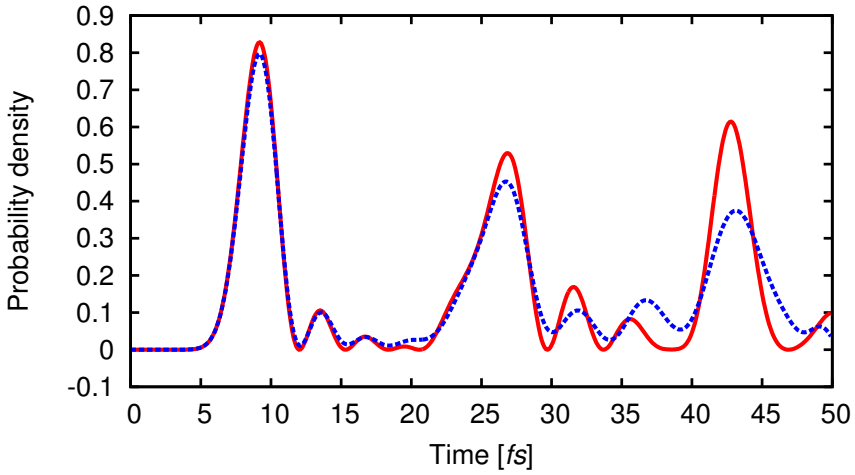

Figure 3.6: Time evolution of the charge density at the right endpoint of the chain, assuming that a hole is initially created at the left end of the chain. The solid line represents the unperturbed prediction, the dashed line includes the effects of the coupling with the molecular vibration and the heat bath to leading-order in perturbation theory.

The hole propagator $G^0_{lm}(t)$ is constructed by diagonalizing the $\hat{f}^0$ matrix, defined in Eq. (3.16). Its n-th eigenvector reads

$$\phi_n(j) = \sqrt{\frac{2}{N+1}}\ \sin\left[\frac{n\ \pi}{(N+1)}\ j\right]\ .$$

The corresponding eigenvalue is

$$E_n = -e_0 - 2T_0\ \cos(k_n)\,,$$

where k_n is the wave-vector

$$k_n = \frac{\pi n}{(N+1)}, \quad n = 1, 2, \ldots, N\,.$$

Hence, the hole Feynman propagator is given by

$$G^0_{k_f,k_i}(t) \quad = \quad \sum_{n=1}^{2(N+1)} \phi^*_n(k_f)\ \phi_n(k_i)\ e^{-iE_nt}\ \left(\gamma_+\theta(t) - \gamma_-\theta(-t)\right).$$

With the present set of model parameters, we find that the friction coefficient γ is significantly larger than the typical frequencies of normal models, i.e. $\gamma \gg \Omega_k$. Hence, we can use the over-damped limit for the vibronic propagators.

3.2.2 Time Evolution of the Conditional Probability

We assume that the hole is initially created at the left end of the chain, i.e. the initial reduced density matrix is $\hat{\rho}(0) = |1\rangle\langle 1|$. The first quantity that we study is the hole density at the opposite end of the chain, i.e. last the diagonal element of the reduced density matrix

$$P_t(N|1) = \rho_{NN}(t)\,, \qquad \text{where } N = 9.$$

In Fig. 3.6 we show the results of our leading-order perturbative calculation based on Eq. (3.14) of the conditional probability to observe the quantum excitation at the end of the chain as a function of the time interval t.

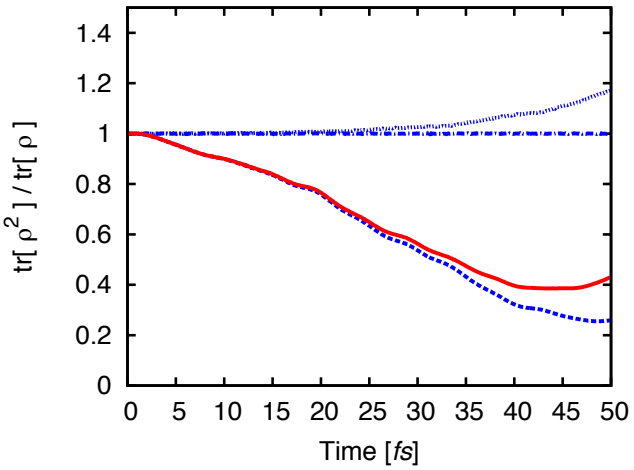

Figure 3.7: Perturbative calculation of the different contribution to the ratio $R(t)$ which quantifies the decoherence effects in hole propagation. The dot-dashed line is the unperturbed result, which remains coherent at all times. The solid line is the result including the leading order correction. Dotted and dashed lines correspond to the contribution of *self-energy*-type and *crossing*-type, respectively. For this model, the *tad-pole*-type contribution is identically zero.

Some comments on these results are in order. First of all, we notice the existence of three peaks in the charge density, at times $t \sim 10, 20, 40$ ps. These corresponds to integer multiples of the time interval it takes the hole to run along the entire chain. Next, we note that the scattering of the holes with the molecular normal modes and with the heat bath slows down the charge propagation, as expected. This is evident from the fact that the probability of observing the hole at the right end-point of the chain as a function of time is reduced once the perturbative corrections are included. Correspondingly, the times at which the hole rebounds to the right end-point of the chain are delayed by the interactions. We recall that the norm of the conditional probability is conserved even after perturbative corrections. Hence, the reduction of the charge density at the end-point of the chain implies that the scattering distributes the charge density in the central region of the chain.

We observe that the correction to the conditional probability starts to be of the same order of the unperturbed prediction starting from time intervals of the order of ~ 40 fs. Beyond this time scale, the perturbative approach breaks down and we have to resort to non-perturbative approaches in which many Feynman diagrams are resummed.

3.2.3 Quantifying the Loss of Quantum Coherence

We have seen that analytic perturbative calculations break down beyond a few tens of fs, hence do not represent a useful tool to investigate the long-time long-distance dynamics of hole propagation. On the other hand, they provide a valuable tool to gain analytic insight into the physical mechanisms which drive decoherence and re-coherence during hole propagation across the chain.

As measure of the degree of quantum coherence in the dynamics of an open system, we consider the ratio [101, 102]:

$$R(t) = \frac{\mathrm{Tr}\rho^2(t)}{\mathrm{Tr}\rho(t)} \,.$$

In Appendix B.2 we show that this ratio is identically equal 1 for pure states (corresponding to fully coherent propagation), and that it is smaller than 1 for mixed states.

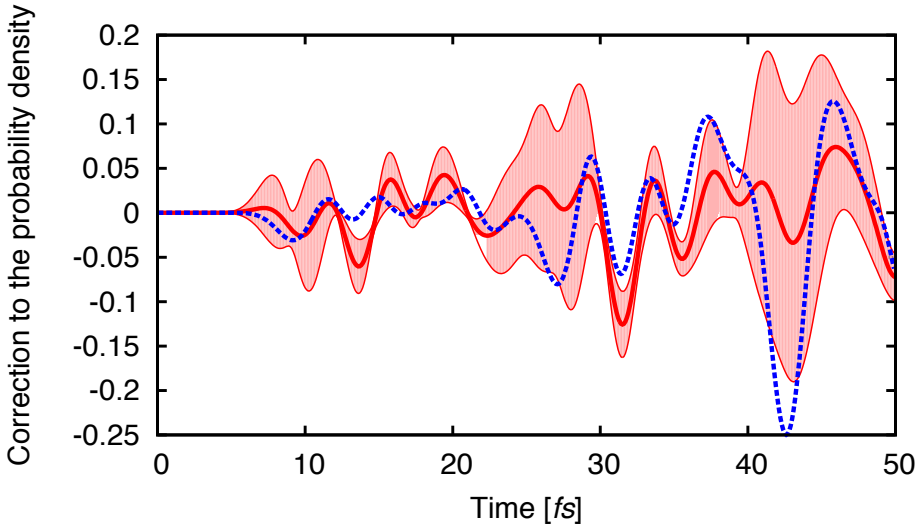

Figure 3.8: Time evolution of the charge probability density at the right end-point of the chain assuming that the hole is initially created at the left-end of the chain. We compare non-perturbative numerical calculation obtained by integrating the Eq.s (2.21) (solid line) and the analytic perturbative calculations (dotted line). The shaded area represents the statistical uncertainty on the non-perturbative calculation.

In Fig. 3.7 we compare this ratio for the model under consideration in the limit of unperturbed propagation and including the leading-order scattering with the molecular vibrations and with the heat bath. We see that the interaction with the environment suppresses the quantum coherence on time scales which are of the order of 10 fs.

It is interesting to compare the contribution to $R(t)$ coming from the different Feynman diagrams shown in Fig. 3.3. We find that the quantum decoherence is driven by the *crossing*-type diagram shown in figure 3.3, which tends to correlate the field components associated to propagation forward and backwards in time. On the other hand, the so-called *self*-type diagrams act in the opposite direction, slowing down the overall rate of quantum decoherence.

The identification on the diagram which drives the quenching of $R(t)$ with time offers a scheme to study how the chemical and mechanical properties of the macromolecule affect the quantum decoherence of the propagating excitation. Indeed, by varying the parameters of the QTFT (namely the spectrum of normal modes ω_k entering in the vibron propagators and unperturbed tight-binding matrix elements $f^0_{\mathbf{lm}}$ and their gradient $f^i_{\mathbf{lm}}$, which enter the effective interaction vertexes) and computing the corresponding relative weight of the *cross*-type diagram, we may in principle identify what properties of the macromolecular system are most effective in suppressing (or enhancing) the quantum coherent transport. This information may be useful e.g. in the context of the study of exciton propagation in photosynthetic complexes, which have been found to display quantum coherent dynamics over surprisingly long time intervals [33, 34].

3.2.4 Comparison between the Perturbative Estimate and the Result of Integrating the Quantum/Stochastic Equations of Motion

The perturbative approach developed in the previous sections allows to analytically compute the charge density, in the range of time intervals $0 < t \lesssim 50$ fs. It is interesting to compare the perturbative calculation with the results of non-perturbative numerical simulations, obtained by averaging over many independent solutions of the set of quantum/stochastic equations of motion defined in Eq. (2.21) and derived in Ref. [78]. On the one hand, this provides a non-trivial test for

the perturbative scheme developed in this work. On the other hand, it offers an estimate of the statistical accuracy which is needed in order to resolve the effects of the interactions on the charge propagation dynamics in non-perturbative numerical simulations.

In Fig. 3.8 we present the difference between the interacting and the free conditional probabilities $P_t(N|1) - P_t^{(0)}(N|1)$, evaluated in the perturbative and non-perturbative methods (we recall that $N = 9$). The shaded area represents the statistical error in numerical simulations, which is estimated from the variance calculated from 10000 independent trajectories. Accumulating this statistics required about 6 Central Processor Units (CPU) hours of simulation on a regular desktop. By contrast, the perturbative estimates took about a minute on the same machine.

We find that the two approaches are quantitatively consistent with one another, even at time scales of the order of 50 fs. Beyond such a time scale the perturbative approach becomes unreliable and the comparison is meaningless.

It is important to emphasize that these two methods are based on different approximations. In particular, the algorithm defined by Eq.s (2.21) was obtained by neglecting the fluctuations of the coherent fields around their functional saddle-point solution. At such a saddle-point, the forward- and backward- propagating fields are identical, $\phi'(t) = \phi''(t)$ (see Appendix A.2). The leading-order perturbative estimate goes beyond such a saddle-point condition and accounts for independent quadratic fluctuations on $\phi'(t)$ and on $\phi''(t)$. The relatively good agreement between the two calculation schemes at short times can be used as an argument in favor of the accuracy of the saddle-point approximation used in the non-perturbative approach.

Chapter 4

Quantum Propagation at Long-Distance and Long-Time

In the previous chapter we observed that perturbative approach breaks down in long-time regime, and typically becomes inapplicable after 50-100 fs. Therefore, to investigate quantum transport over larger distance and longer time intervals in this formalism we need to apply a fully non-perturbative approach.
In this chapter, we investigate the quantum propagation through a macromolecule in the limit in which the quantum excitation travels for a long time and covers distances which are large compared to its de Broglie's thermal wavelength λ_B. To this aim, we use the Renormalization Group (RG) formalism to systematically coarse-grain the dynamics. The final result is a rigorous "low-resolution" approximation of our original microscopic QTFT which is much simpler and it admits an analytic solution [2].

This chapter is organized as follows. In the first section we review the Effective Field Theory (EFT) formalism and the RG scheme, which allows us to construct rigorous low-energy approximations to physical theories. In section 4.2, we apply the EFT framework to derive our systematic approximation of the microscopic QTFT, yielding the same dynamics in the large-distance and long-time regimes. In section 4.3 we derive the analytic expression for the probability density, while we discuss the renormalization of the EFT. Finally section 4.4 is devoted to an illustrative application of this framework, investigating the hole propagation in a homo-DNA chain.

4.1 Effective Field Theory Formalism and Renormalization Group Scheme

The internal dynamics of macromolecules is characterized by a multitude of time-scales, which are spread over many orders of magnitude. Conformational transitions typically occur beyond the ns time scale, hence are clearly decoupled from the local thermal vibrations and the solvent-induced dissipative relaxation times, which occur at the ps scale. The hopping of quantum excitations across nearby molecular orbitals and the loss of quantum coherence crucially depend on the specific chemical structure of the molecule, but typically range from a few fs to fractions of ps.

The existence of relatively large gaps between the different characteristic time scales in macromolecules naturally suggests we should apply RG methods to device rigorous "low-energy" descriptions of the dynamics. In particular, the EFT formalism (for a pedagogical introduction see e.g. Ref.s [103, 104]) provides a very practical implementation of the RG scheme, which is both rigorous and systematically improvable. Despite these features, to date there have been only a few applications of this framework to quantum transport problems [105, 106] and to conformational dynamics in macromolecules [107, 108, 109].

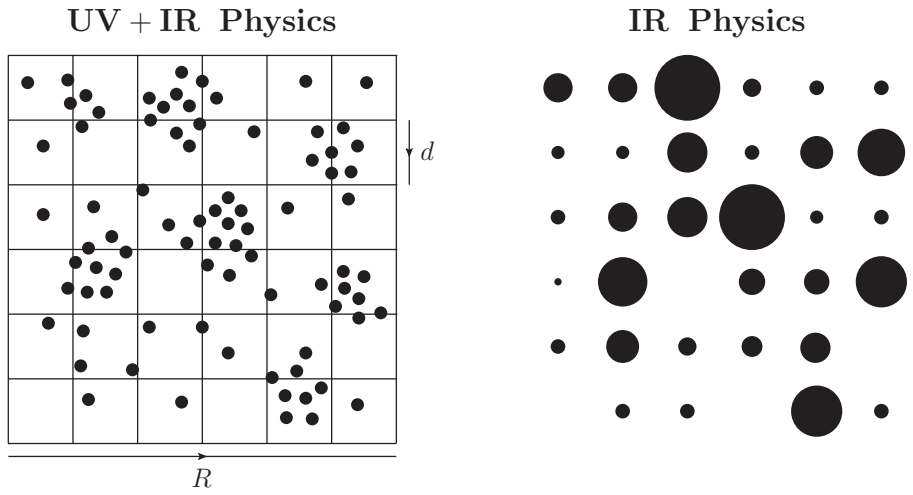

Figure 4.1: A schematic representation of scale separation between UV and IR Physics. On the **left panel** we represent a microscopic description, for example any dot can symbolize a charge point. On the **right panel**, we coarse grain the left configuration assuming $R \gg d$. The length d is the characteristic size of the agglomerate and R is the IR physics scale which we are interested. Any microscopic details smaller than d is incorporate in the multi-pole coefficient.

The main idea underlying the EFT approach is the familiar observation that an experimental probe with a given wave-length λ is insensitive to the *details* of the physics associated to length scales $\ll \lambda$ and time intervals $\ll \lambda/v$ (where v is the velocity of propagation of the probe). This fact can be exploited to build in a rigorous way predictive physical theories in which only the degrees of freedom that can be resolved by the probe's wavelength are treated explicitly, while all the ultraviolet (UV) effects (i.e. the physics which is not resolved by the probe) are treated at the implicit level, through a set of local interactions and effective parameters.

A familiar example of this type of approach is the multi-pole expansion in classical electrodynamics: the soft components of the classical radiation generated by an arbitrarily complicated current source $\mathbf{J}(\mathbf{r}, t)$ of size d and characteristic time τ can be replaced by the radiation generated by a sum of point-like multipole currents d_i, m_i, D_{ij}, ... Thus, to compute the vector field $\mathbf{A}$ at long-distance $R \gg d$, and averaging the signal over long-time ($T \gg \tau$, i.e for low frequency $\nu \ll 1/\tau$), we have the following multi-pole expansion [110]

$$\mathbf{A}(R,t) = \frac{1}{c}\int d^3\mathbf{r}\frac{\mathbf{J}(\mathbf{r}, t - R/c)}{R} \quad \rightarrow \quad \mathbf{A}(R,t) \simeq \frac{\dot{\mathbf{d}}}{cR} + \frac{\dot{\mathbf{m}} \times \mathbf{n}}{cR} + \frac{\ddot{D}_{ij} n_j}{6c^2 R} + o\left(\frac{d}{R}\right) + o\left(\nu\tau\right) ,$$

where $\mathbf{n}$ is the normal vector between the source and the space point where we compute $\mathbf{A}$. In such an expansion, the multipole coefficients implicitly account for the UV physics, which is associated to short distances, of the order of d, and high frequency, of the order of $1/\tau$. The result is that we need only a finite number of multipole terms to reproduce to any arbitrary (but *finite*) level of accuracy the electro-magnetic radiation at distances $\gg d$, and frequency $\ll 1/\tau$.
In the following, we shall refer to the physics at length scales much larger than the UV cutoff length-scale as the IR sector of the dynamics. In Fig. 4.1, we show a schematic representation of separation of scales between UV and IR physics.

In the context of quantum theories, the EFT scheme is implemented in four steps:

1. We introduce the cut-off scale λ, which defines the separation between the IR physics one is interested in, and the UV physics to be treated implicitly.

2. The most general possible description of the IR dynamics is derived by analyzing the structure and symmetries of the underlying (more) microscopic theory.

3. A so-called power-counting scheme is introduced in order to identify which coupling terms in the effective field theory dominate in the IR limit. Typically, in the field theory formalism, the last step leads to retaining only operators with the lowest number of time and space derivatives of the fields or of the wave-function.

4. Through the renormalization procedure, the effective coefficients are determined by matching against experiments or more microscopic calculations, and the dependence on the cut-off is replaced by a (typically much weaker) dependence on the renormalization scale.

It is important to emphasize that in EFTs there are no UV divergences, because the cut-off specifies the level of resolution of the theory. Hence the theory is kept finite at all times. However, the short-distance physics which is excluded by the finite cut-off is not simply neglected. Instead, it is accounted for by means of local effective vertexes, called the counter-terms, which enter in the low-energy effective action. These vertexes parametrize the effects of very short-distance interactions on the long-distance dynamics.

The effectiveness of the EFT scheme depends crucially on the size of the gap separating the IR and the UV physics. The smaller the gap, the larger the number of effective interactions and parameters that have to be introduced in the EFT to reach the desired accuracy. In the absence of a decoupling between IR and UV scales, the dynamics of the EFT depends on infinitely many effective interactions and parameters, hence loses its predictive power.

In this chapter, we exploit the separations in the length and time scales characterizing the internal dynamics of macromolecular systems to build an EFT for dissipative quantum transport in the large-distance and long-time regime. In particular, we restrict our attention to systems in which quantum excitations can propagate over distances much larger than the size of the individual molecular orbitals and we consider time intervals much longer than those characterizing the damping of local thermal conformational oscillations of the macromolecule. Hence, our typical UV cutoff length scale is of the order of the nm and the typical UV time scale is of the order of a few fractions of ps.

In the next section, we apply the EFT framework to construct a rigorous low-energy approximation of this theory, and then discuss its implications in different time regimes.

4.2 Effective Field Theory for Dissipative Quantum Transport

We are interested in constructing an EFT which describes the same IR dynamics of the microscopic theory defined in the previous chapter, at a much lower level of spatial and temporal resolution. In particular, we focus on macromolecular systems for which the quantum excitation can cover distances which are long compared to those at which the molecular three-dimensional structure is resolved. In Fourier space, this implies that the corresponding coherent fields have only soft momentum components. Consequently, the effective interaction terms with a larger and larger number of spatial derivatives are increasingly irrelevant. Similarly, since thermal oscillations are damped by the coupling with the heat-bath, in order to investigate the long-time regime, the terms with higher number of time derivatives can be dropped.

4.2.1 Long-time and Long-distance Limit

Let us now define the action functional of the effective field theory. We begin by analyzing the kinetic term and we first consider the case in which the hopping of the excitations between molecular orbitals which are spatially neighboring. In this case, the hopping matrix in the microscopic theory

defined in Eq. (2.27) takes the simple form

$$f_{\mathbf{nm}}(Q) \;=\; \sum_{\hat{i}} \tau_{\mathbf{nm}}(Q)(\delta_{\mathbf{m}(\mathbf{n}+\hat{i})} + \delta_{\mathbf{m}(\mathbf{n}-\hat{i})}) - e^0_{\mathbf{n}}(Q)\;\delta_{\mathbf{nm}}\,.$$

where the sum runs over the unit vectors $\hat{i}$ pointing to the nearest neighbor sites from the site $\mathbf{m}$. Due to the low spatial resolution, in the corresponding effective field theory we can replace the discrete site indexes $\mathbf{m}, \mathbf{n}$ with continuous variables $\mathbf{x}, \mathbf{y}$, i.e. to introduce continuous complex fields

$$\phi_{\mathbf{n}}(t) \to \phi(\mathbf{x}, t), \quad \phi^*_{\mathbf{n}}(t) \to \phi^*(\mathbf{x}, t)\,,$$

or in the more compact dirac-like notation introduced in section 3.1.1

$$\psi_{\mathbf{n}}(t) \to \psi(\mathbf{x}, t), \quad \bar{\psi}_{\mathbf{n}}(t) \to \psi^*(\mathbf{x}, t)\,.$$

In the continuum limit, the matrices $f^0_{\mathbf{mn}}$ and $f^i_{\mathbf{nm}}$ become differential operators[1]

$$\begin{aligned} f^0_{\mathbf{mn}} \quad &\to \quad f^0(\mathbf{x},\mathbf{y}) \equiv \delta(\mathbf{x}-\mathbf{y})\left[\epsilon(\mathbf{x}) - \frac{\hbar^2\;\mu^{-1}_{ij}(\mathbf{x})}{2}\partial_i\partial_j\right]\,, \\ f^a_{\mathbf{nm}} \quad &\to \quad f^a(\mathbf{x},\mathbf{y}) \equiv \delta(\mathbf{x}-\mathbf{y})\left[\epsilon^a(\mathbf{x}) - \frac{\hbar^2\mu^{a\,-1}_{ij}(\mathbf{x})}{2}\partial_i\partial_j\right]\,. \end{aligned}$$

Notice that $\mu_{ij}(\mathbf{x})$ can be interpreted as a position dependent effective mass tensor. With the notation defined above, the free component of the action functional $S_{\mathbf{0}}$ in Eq. (3.5) is written as

$$S_{\mathbf{0}}[\bar{\psi},\psi] \;\simeq\; \int_0^t dt' \int d\mathbf{x}\;\bar{\psi}(\mathbf{x},t')\;\left(i\hbar\partial_t - \epsilon(\mathbf{x}) + \frac{\hbar^2}{2}\mu^{-1}_{ij}(\mathbf{x})\partial_i\partial_j\right)\;\psi(\mathbf{x},t'). \tag{4.1}$$

It is immediate to verify that accounting for non-nearest neighbor hopping leads to higher derivative terms. According to our power-counting scheme, such terms are irrelevant in the IR limit and can be ignored.

Let us now analyze the interaction terms in Eq. (2.28). The Green's functions $\Delta_{ab}(t-t')$ and $\mathcal{V}_{ab}(t-t')$ are evaluated explicity in Eq.s (2.29) and (2.30), where they are shown to decay exponentially at time-scales of the order of the inverse collision rate $t \sim 1/\gamma$. Since we are focusing in time intervals $t \gg 1/\gamma$, they can be replaced by

$$\Delta_{ab}(t-t') \;\simeq\; d^{(0)}_{ab}\delta(t-t') + d^{(1)}_{ab}\;i\hbar\;\frac{d}{dt}\delta(t-t') + \dots\,, \tag{4.2}$$

$$\mathcal{V}_{ab}(t-t') \;\simeq\; v^{(0)}_{ab}\delta(t-t') + v^{(1)}_{ab}\;i\hbar\frac{d}{dt}\delta(t-t') + \dots \tag{4.3}$$

Corrections to these terms are irrelevant, as they involve higher time-derivatives. The effective interaction in Eq. (3.6) becomes

$$\begin{aligned} \mathcal{S}_{\mathbf{I}}[\bar{\psi},\psi] \;\simeq\; & \frac{1}{4}\int_0^t dt'\;dt''\int d\mathbf{x}\;d\mathbf{y} \\ & \left\{\bar{\psi}(\mathbf{x},t')\gamma_0 f^a(\mathbf{x},\mathbf{y})\psi(\mathbf{y},t')\left[\left(v^{(0)}_{ab} - iv^{(1)}_{ab}\frac{d}{dt'}\right)\delta(t'-t'')\right]\bar{\psi}(\mathbf{x},t'')f^b(\mathbf{x},\mathbf{y})\psi(\mathbf{y},t'')\right\} \\ & + \frac{iM\gamma}{\beta\hbar}\int dt'\;dt''\int d\mathbf{x}\;d\mathbf{y} \\ & \left\{\bar{\psi}(\mathbf{x},t')f^a(\mathbf{x},\mathbf{y})\psi(\mathbf{y},t')\left[\left(d^{(0)}_{ab} - id^{(1)}_{ab}\frac{d}{dt'}\right)\;\delta(t't'')\right]\bar{\psi}(\mathbf{x},t'')f^b(\mathbf{x},\mathbf{y})\psi(\mathbf{y},t'')\right\}\,. \end{aligned} \tag{4.4}$$

[1] The discrete second order derivative can be represent as $\partial^2_x f(x) = \frac{f(x+h)-2f(x)+f(x-h)}{h^2}$

The combination $D = 1/(\beta M \gamma)$ yields the diffusion coefficient of the atoms in their surrounding heat-bath.

The scalar and tensor fields $\epsilon(\mathbf{x}), \mu_{ij}(\mathbf{x})$ appearing in Eq. (4.1) encode the information about the conformational and electronic structure of the molecule in the neighborhood of point $\mathbf{x}$, while the uniform tensors $v_{ab}^{(k)}$ and $d_{ab}^{(k)}$ (with $k = 0, 1$) in Eq. (4.4) parametrize the fluctuation-dissipation effects arising from the coupling of the molecule with its heat-bath.

The effective action (4.4) does not yet define our EFT. Indeed, so far, we have only performed a continuous formulation of the original microscopic theory. On the other hand, we have not yet exploited the decoupling of UV and IR length-scales and taken the large-distance limit.

To derive the effective couplings in the EFT, let us consider the Fourier transformation of the space-dependent scalar and tensor parameters in Eq. (4.4) (in the following we focus on $\epsilon(\mathbf{x})$ for sake of definiteness):

$$\epsilon(\mathbf{p}) = \epsilon_0 \; \delta(\mathbf{p}) + \delta\epsilon(\mathbf{p}) \, . \tag{4.5}$$

We notice that ϵ_0 is the Fourier component which corresponds to a uniform field[2]. We recall that the parameter fields are assumed to vary over length scales which are much shorter than those over which the quantum excitation's density changes. In Fourier space, this implies that $\epsilon(\mathbf{p})$ has only hard components

$$\delta\epsilon(\mathbf{p}) \simeq 0, \qquad \text{for} \quad |\mathbf{p}| \lesssim 1/\lambda \, , \tag{4.6}$$

while the field $\psi(\mathbf{p})$ has only soft Fourier components,

$$\psi(\mathbf{p}) \simeq 0, \qquad \text{for} \quad |\mathbf{p}| \gtrsim 1/\lambda \, . \tag{4.7}$$

Due to such a decoupling, all the short-distance local fluctuations of the parameter fields average away:

$$\int d\mathbf{x} \; \epsilon(\mathbf{x}) \bar{\psi}(\mathbf{x}, t) \psi(\mathbf{x}, t) \quad \simeq \quad \epsilon_0 \int d\mathbf{x} \; \bar{\psi}(\mathbf{x}, t) \psi(\mathbf{x}, t) \, ,$$

since

$$\int d\mathbf{x} \; \delta\epsilon(\mathbf{x}) \bar{\psi}(\mathbf{x}, t) \psi(\mathbf{x}, t) \; = \; \int \frac{d\mathbf{p}}{2\pi} \int \frac{d\mathbf{q}}{2\pi} \; \bar{\psi}(\mathbf{p}) \delta\epsilon(\mathbf{q}) \psi(-(\mathbf{p}+\mathbf{q}), t) \; \simeq \; 0 \, .$$

In addition, all coupling terms in Eq. (4.4) which include spatial derivatives of the fields are irrelevant in the large distance limit, hence can be neglected. Similarly, for the effective mass tensor field, one has

$$\mu_{ij}(\mathbf{x}) \simeq m_{ij} \, . \tag{4.8}$$

In conclusion, to the lowest-order in our power-counting scheme, the path integral which represents the conditional probability for a quantum excitation to be created in a point $\mathbf{x}$ and to be found in $\mathbf{y}$, after a time interval t, reduces to

$$P(\mathbf{y}, t|\mathbf{x}, 0) \quad = \quad \frac{-1}{\mathcal{N}} \int \mathcal{D}\bar{\psi} \mathcal{D}\psi \; n(\mathbf{y}, t) \; n(\mathbf{x}, 0) \; e^{-\mathcal{L}_1 + \frac{i}{\hbar} S_{\mathbf{0}}^{eff}[\bar{\psi}, \psi] + \frac{i}{\hbar} S_{\mathbf{int}}^{eff}[\bar{\psi}, \psi]} \, , \tag{4.9}$$

where

$$n(\mathbf{x}, \tau) \; = \; \bar{\psi}(\mathbf{x}, \tau) \, \gamma_0 \gamma_5 \, \psi(\mathbf{x}, \tau) \; = \; \Big(\phi^{'*}(\mathbf{x}, \tau) \phi^{''}(\mathbf{x}, \tau) + \phi^{''*}(\mathbf{x}, \tau) \phi^{'}(\mathbf{x}, \tau) \Big) \, , \tag{4.10}$$

which specifies the initial or the final position of the quantum excitation in the path integral (4.9). This term contains both creation and annihilation of a quantum excitation, hence in quantum field it corresponds to the density operators.

[2] In order to go beyond the uniform parameter approximation, we can add derivative terms to Eq. (4.5), i.e. $\epsilon_n \; \mathbf{p}^n$.

In Eq. (4.9), the normalization of the probability, the surface term which arise from the over completeness of the coherent states, and the effective actions read, respectively,

$$\mathcal{N} \simeq \int \mathcal{D}\bar{\psi}\mathcal{D}\psi \; n(\mathbf{x},0) \; e^{-\mathcal{L}_1 + \frac{i}{\hbar} S_{\mathbf{0}}^{eff}[\bar{\psi},\psi]} \; e^{\frac{i}{\hbar} S_{\mathbf{int}}^{eff}[\bar{\psi},\psi]} , \tag{4.11}$$

$$\mathcal{L}_1[\bar{\psi},\psi] = \int d\mathbf{x} \; \bar{\psi}(\mathbf{x},0)\gamma_0\gamma_-\psi(\mathbf{x},0) + \bar{\psi}(\mathbf{x},t)\gamma_0\gamma_+\psi(\mathbf{x},t) , \tag{4.12}$$

$$S_{\mathbf{0}}^{eff}[\bar{\psi},\psi] = \int_0^t dt' \int d\mathbf{x} \; \bar{\psi}(\mathbf{x},t')\big[i\hbar\partial_{t'} - \epsilon_0 + \frac{\hbar^2}{2} m_{ij}^{-1}\partial_i\partial_j\big]\psi(\mathbf{x},t') , \tag{4.13}$$

and

$$S_{\mathbf{int}}^{eff}[\bar{\psi},\psi] = \int_0^t dt' \int d\mathbf{x} \; \Big[\bar{\psi}\psi\left(A_v^0 - \hbar A_v^1 i\partial_{t'}\right)\bar{\psi}\gamma_0\psi + \frac{i}{D\hbar\beta^2}\bar{\psi}\psi\left(A_d^0 - \hbar A_d^1 i\partial_{t'}\right)\bar{\psi}\psi\Big] . \tag{4.14}$$

A_v^0, A_v^1, A_d^0 and A_d^1 are real effective coupling constants. It is important to emphasize that the couplings of low-energy effective field theories may depend in general on the heat-bath temperature [111].

It is important to emphasize that the effective action defined so far only describes the long-time and large-distance dynamics of the excitations. Indeed, the short-distance and short-time physics has been quenched, by introducing the cut-offs on the length and time scales and by neglecting the high derivative terms in the effective action.

In general, completely neglecting the high-frequency modes represents a very crude approximation, since the short-distance physics does have an influence on the long-distance dynamics. The crucial point to make is that, at a low-resolution power, the long-distance dynamics becomes insensitive to the *details* of the short-distance physics, which can be therefore encoded by means of local effective interactions.

These physical ideas are implemented by the renormalization procedure. In practice, one adds to the effective action in Eq. (4.9) the *most general* set of *local* effective vertexes compatible with the symmetry of the underlying microscopic theory and in retains only the terms among them which display the least number of derivatives and fields (see e.g. the discussion in [103]).

However, in our specific case, the inclusion of additional terms is in fact redundant. Indeed, we observe that the effective Lagrangian in Eq. (4.9) already contains all possible local effective couplings with the least number of derivatives and fields. Hence, to lowest-order, the renormalization procedure simply amounts to rescaling the corresponding effective parameters A_v^0, A_v^1, A_d^0 and A_d^1.

We observe that Eq. (4.9) corresponds to the time evolution of the diagonal elements of the reduced density matrix defined in Eq. (2.9). Let us point out that in this chapter we ignore the off-diagonal elements in the density matrix. This choice is motivated by the long-time regime, which assure us that the system is decorrelated in this limit.

Let us summarize what we have obtained so far. We have shown that, in the large-distance and long-time limit, the probability density for the quantum excitations can be *formally* mapped into a vacuum-to-vacuum two-point function in a relativistic-like quantum field theory with local 4-field interactions. Note that our theory contains an imaginary coupling constant, which breaks unitarity and describes the dissipation generated by the coupling with the damped molecular oscillations.

4.2.2 Effective Stochastic Description

In the asymptotic long-time regime, the large number of collisions with the molecular vibrations and with the environment depletes the quantum coherence. As a result, the emergent dynamics of the quantum excitation is diffusive and quasi-classical. In order to investigate the quasi-classical limit it is convenient to switch to the first-quantization formalism and represent the time-dependent probability (4.9) using the coordinate representation path integral.

To this end, it is important to recall that the position eigenstates of the EFT do not coincide with those of a microscopic theory. Indeed, in the EFT, each point $\mathbf{X}$ is indistinguishable from

those which lie in a neighborhood of the size of the probe's resolution power, λ. Most generally, the position eigenstates in the EFT, $|\mathbf{R}\rangle_\lambda$ are defined as

$$|\mathbf{R}\rangle_\lambda \equiv \int d\mathbf{X}\ \Psi_\lambda(\mathbf{X}-\mathbf{R})\ |\mathbf{X}\rangle\,,$$

where $|\mathbf{X}\rangle$ denote the position eigenstates of the microscopic theory. The wave function $\Psi_\lambda(\mathbf{X}-\mathbf{R})$ is determined by the normalization condition,

$$_\lambda\langle\mathbf{R}'|\mathbf{R}\rangle_\lambda \;=\; \int d\mathbf{X}\Psi_\lambda(\mathbf{X}-\mathbf{R})\ \Psi^*_\lambda(\mathbf{X}-\mathbf{R}') \;=\; \delta_\lambda(\mathbf{R}'-\mathbf{R})\,,$$

where $\delta_\lambda(\mathbf{R}'-\mathbf{R})$ is some smeared representation of the δ-function, of width λ. In particular, in the following, we adopt a Gaussian smearing (in three dimensions)

$$\delta_\lambda(\mathbf{R}-\mathbf{R}') \;\equiv\; \sqrt{\det[m]}\left(\frac{1}{2\pi\ \lambda^2\ \mathrm{Tr}[m]}\right)^{3/2}\ e^{-\frac{(R_i-R'_i)m_{ij}(R_j-R'_j)}{2\ \lambda^2\ \mathrm{Tr}[m]}}\,. \tag{4.15}$$

With this choice, the effective wave-function $\Psi_\lambda(\mathbf{X})$ reads:

$$\Psi_\lambda(\mathbf{X}) = \sqrt{\det[m]}\left(\frac{1}{\pi\ \lambda^2\ \mathrm{Tr}[m]}\right)^{3/2}\ e^{-\frac{X_i m_{ij} X_j}{\lambda^2\ \mathrm{Tr}[m]}}\,.$$

Notice that this regularization choice corresponds to approximating the local delocalization with an harmonic oscillator wave-function and takes into account for the tensor structure of the effective mass. However, the specific short-distance structure of this wave function is irrelevant for the long-distance dynamics.

Denoting with $\mathbf{X}[\tau]$ and $\mathbf{Y}[\tau]$ the paths in coordinate space of quantum excitation described by the coherent fields $\phi^{'}$ and $\phi^{''}$, respectively, the probability density in Eq. (4.9) can be written as

$$P(\mathbf{y},t|\mathbf{x},0) \;=\; \int_{\mathbf{x}}^{\mathbf{y}}\mathcal{D}\mathbf{X}\int_{\mathbf{x}}^{\mathbf{y}}\mathcal{D}\mathbf{Y}\ e^{\frac{i}{\hbar}S_0[\mathbf{X}]}\ e^{-\frac{i}{\hbar}S_0[\mathbf{Y}]}\ e^{\frac{i}{\hbar}(I[\mathbf{X},\mathbf{Y}]+J[\mathbf{X},\mathbf{Y}])}\,, \tag{4.16}$$

where the quantum propagation in absence of interaction is described by the free action

$$S_{\mathbf{0}}\,[\mathbf{X}] = \int_0^t d\tau\ \frac{1}{2}\,\dot{X}_i\,m_{ij}\,\dot{X}_j\,.$$

The action $S_{\mathbf{0}}$ corresponds to kinetic terms.
Furthermore, the functionals $I[\mathbf{X},\mathbf{Y}]$ and $J[\mathbf{X},\mathbf{Y}]$ originate from translating into the first quantized representation the field-theoretic functional $S^{eff}_{\mathbf{int}}$ appearing in Eq. (4.14). In Appendix C.1.1, we derive them explicitly and we obtain $J=0$ and $I = I_1+I_2+I_3$, with

$$\begin{aligned}
I_1 \;&=\; I_2 = \frac{it}{\beta^2 D\hbar}\frac{\sqrt{\det m}}{(4\mathrm{Tr}\,m\ \lambda^2\pi)^{3/2}}\ A^0_d\,,\\
I_3 \;&=\; \frac{-\sqrt{\det[m]}}{\beta^2 D\hbar\,(4\pi\,\mathrm{Tr}[m]\,\lambda^2)^{3/2}}\int_0^t dT\left(i2A^0_d - \frac{\hbar A^1_d\ m_{ij}}{2\mathrm{Tr}[m]\lambda^2}(Y-X)_i(\dot{Y}+\dot{X})_j\right)e^{\frac{-(X-Y)_i m_{ij}(X-Y)_j}{4\,\mathrm{Tr}[m]\,\lambda^2}}\,.
\end{aligned}$$

Similarly to the transformation apply in section 2.3.2, we perform the following change of variables in the path integral:

$$\mathbf{R}(\tau) \;=\; \frac{1}{2}\Big(\mathbf{X}(\tau)+\mathbf{Y}(\tau)\Big)\,,\qquad \mathbf{Q}(\tau) \;=\; \mathbf{X}(\tau)-\mathbf{Y}(\tau)\,.$$

In addition, for reasons which will become clear soon, it is convenient to introduce the following tensor combination:

$$\Gamma^0_{ij} \;=\; \frac{A^1_d\sqrt{\det[m]}}{16D\beta^2(\mathrm{Tr}[m])^{5/2}\,\lambda^5\sqrt{\pi^3}}\ m_{ij}\,.$$

After these replacements, the path integral in Eq. (4.16) reads

$$P(\mathbf{y},t|\mathbf{x},0) = e^{-4t\frac{\lambda^2\,\mathrm{Tr}[\Gamma^0]\,A^0_d}{\hbar^2\beta A^1_d}} \int_{\mathbf{x}}^{\mathbf{y}} \mathcal{D}\mathbf{R} \int_{\mathbf{0}}^{\mathbf{0}} \mathcal{D}\mathbf{Q}\; e^{\int_0^t dT\left\{ \frac{i}{\hbar} m_{ij}\dot{R}_i\dot{Q}_j + \left(\frac{4\,\lambda^2\mathrm{Tr}[\Gamma_0]A^0_d}{\hbar^2\beta A^1_d} - \frac{i\Gamma^0_{ij}}{\hbar} Q_i\dot{R}_j \right) e^{-\frac{m_{ij}Q_jQ_i}{4\mathrm{Tr}[m]\;\lambda^2}} \right\}} . \tag{4.17}$$

We now observe that, by expanding the exponent in the last equation to $\mathcal{O}(\mathbf{Q^2})$ we obtain:

$$P(\mathbf{y},t|\mathbf{x},0) = \int_{\mathbf{x}}^{\mathbf{y}} \mathcal{D}\mathbf{R} \int_{\mathbf{0}}^{\mathbf{0}} \mathcal{D}\mathbf{Q}\; e^{\int_0^t dT\left\{ \frac{i}{\hbar}\; m_{ij}\dot{R}_i\dot{Q}_j - \frac{\Gamma_{ij}A^0_d}{\hbar^2\beta A^1_d} Q_jQ_i - \frac{i\Gamma^0_{ij}}{\hbar} Q_i\dot{R}_j \right\}} .$$

Performing the Gaussian functional integration over $\mathbf{Q}$ one obtains (neglecting as usual any overall multiplication constant)

$$P_{cl.}(\mathbf{y},t|\mathbf{x},0) = \int_{\mathbf{x}}^{\mathbf{y}} \mathcal{D}\mathbf{R}\; e^{-\frac{\beta^2}{4}\int_0^t dT\left(m_{il}\ddot{R}_l + \Gamma^0_{il}\dot{R}_l\right) D^0_{ij}\;\left(m_{jk}\ddot{R}_k + \Gamma^0_{jk}\dot{R}_k\right)} . \tag{4.18}$$

where we have introduced the tensor

$$D^0_{ij} \equiv \frac{1}{\beta}\;\left(\frac{A^1_d}{\beta A^0_d}\right)\;\Gamma^{0\,-1}_{ij} . \tag{4.19}$$

We now recognize that Eq. (4.18) has the same structure of the Onsager-Machlup functional integral representation [91] of the solution of a Fokker-Planck equation with an anisotropic viscosity tensor Γ^0_{ij} and diffusion tensor D^0_{ij}. The request that the system should ultimately reach a thermal equilibrium with the surrounding heat-bath implies the fluctuation-dissipation relationship,

$$D^0_{ij} = \frac{1}{\beta}\Gamma^{0-1}_{ij} . \tag{4.20}$$

This condition determines a relationship between the effective parameters, $A^1_d = \beta\; A^0_d$. The friction tensor Γ^0_{ij} has to be determined by matching of the predictions of our EFT against the quantum excitation's, either measured experimentally [112] or computed theoretically using a (more) microscopic model [113]. This renormalization procedure will be illustrated in detail in section 4.3.

Let us now return to the full path integral (4.17) in order to determine the quantum corrections to Eq. (4.18). For sake of simplicity, in the rest of this chapter we focus in the high-friction limit, in which the dynamics is over-damped. In addition, without loss of generality, we can assume that the friction tensor Γ^0_{ij} is diagonal, and we introduce the inner product notation

$$\mathbf{A}\cdot\mathbf{B} \equiv g^0_{ij}\; A_iB_j ,$$

where g^0_{ij} is a diagonal metric tensor defined as

$$\Gamma^0_{ij} = \frac{1}{\beta D_0}\; g^0_{ij} ,$$

and D_0 has the dimension of a diffusion constant. Dropping the inertial term, the path integral (4.17) reduces to

$$P(\mathbf{y},t|\mathbf{x},0) = \int_{\mathbf{x}}^{\mathbf{y}} \mathcal{D}\mathbf{R} \int_{\mathbf{0}}^{\mathbf{0}} \mathcal{D}\mathbf{Q}\; e^{-\int_0^t dT\left\{ \frac{\mathbf{Q}^2}{\hbar^2 D_0\beta^2} + \frac{i\mathbf{Q}\cdot\dot{\mathbf{R}}}{\hbar\beta D_0} \right\}}\; e^{\int_0^t dT\left\{ \left(\frac{4\lambda^2}{\hbar^2 D_0\beta^2} - \frac{i\mathbf{Q}\cdot\dot{\mathbf{R}}}{\hbar\beta D_0} \right) V(\mathbf{Q}) + \frac{i\mathbf{Q}\cdot\dot{\mathbf{R}}}{\hbar\beta D_0}\,\frac{\mathbf{Q^2}}{4\lambda^2} \right\}} . \tag{4.21}$$

where

$$V(\mathbf{Q}) = e^{-\frac{\mathbf{Q^2}}{4\lambda^2}} - 1 + \frac{\mathbf{Q^2}}{4\lambda^2} . \tag{4.22}$$

The probability distribution (4.21) can be cast in the following convenient form,

$$P(\mathbf{y},t|\mathbf{x},0)=\int_{\mathbf{x}}^{\mathbf{y}}\mathcal{D}\mathbf{R}\,e^{-S_{eff}[\dot{\mathbf{R}}]}\,, \tag{4.23}$$

where the effective "action" functional S_{eff} is defined as

$$e^{-S_{eff}[\dot{\mathbf{R}}]}\equiv\int_{\mathbf{0}}^{\mathbf{0}}\mathcal{D}\mathbf{Q}\;e^{-\int_0^t dT\left\{\frac{\mathbf{Q}^2}{\hbar^2 D_0\beta^2}+\frac{i\mathbf{Q}\cdot\dot{\mathbf{R}}}{\hbar\beta D_0}\right\}}\;e^{\int_0^t dT\left(\frac{4\lambda^2}{\hbar^2 D_0\beta^2}-\frac{i\mathbf{Q}\cdot\dot{\mathbf{R}}}{\hbar\beta D_0}\right)V(\mathbf{Q})+\frac{i\mathbf{Q}\cdot\dot{\mathbf{R}}}{\hbar\beta D_0}\frac{\mathbf{Q}^2}{4\lambda^2}}\,. \tag{4.24}$$

We emphasize that, at this level, no approximation has been made on the path integral (4.9), we have only switch it to the first quantization formalism. Hence, Eq. (4.23) represents the full real-time dynamics of the quantum excitation in our EFT, to leading-order in the momentum-frequency power counting scheme.

4.2.3 Computing the Quantum Effective Functional

In general, the effective action $S_{eff}[\dot{\mathbf{R}}]$ which enters Eq. (4.24) is a non-local functional of the path $\mathbf{R}(\tau)$ and such a non-locality reflects the quantum delocalization of the excitation's wave-function. However, we shall now show that, in the limit of low-spatial resolution, the effective action S_{eff} can be systematically represented as an expansion in local functionals. In this regime, the quantum dynamics of our EFT can be described as a modified diffusion process.

To derive this result, we begin by recalling that in a thermal heat-bath the amplitude of quantum fluctuations are of the order of the De Broglie's thermal wave-length

$$\lambda_B\equiv\hbar\sqrt{\frac{\beta}{2\pi\mu_0}}\,, \tag{4.25}$$

where $\mu_0=\frac{1}{3}\mathrm{Tr}\,[m_{ij}]$ is an effective mass scale for the quantum excitation.

If the cut-off scale λ is chosen in such a way that $\lambda\gg\lambda_B$, we have

$$\xi=\frac{\lambda_B}{\lambda}\ll 1\quad\text{and}\quad\frac{|\mathbf{Q}|}{\lambda}\sim\xi\,. \tag{4.26}$$

Hence, ξ provides a small expansion parameter which enables us to evaluate the effective action S_{eff} within a systematic perturbation theory. We note that, in order to obtain the $\mathcal{O}(\xi^2)$ expression, it is sufficient to expand the exponent in the second line of Eq. (4.24) to order in $\mathbf{Q}^4$, since all higher-order terms lead to corrections which are of order $\mathcal{O}(\xi^4)$. After discretization of the time interval t in N_t steps, the path integral factorizes as a product of N_t moments of Gaussian distribution, in the form:

$$\begin{aligned}\int d\mathbf{Q}_k\;\exp&\left[i\frac{(\mathbf{R}_{k+1}-\mathbf{R}_k)}{D_0\sqrt{2\pi\beta\mu_0}}\cdot\frac{\mathbf{Q}_k}{\lambda_B}-\frac{\Delta t}{2\beta D_0\mu_0\pi}\,\frac{\mathbf{Q}_k^2}{\lambda_B^2}\right]\\&\times\left(1-\frac{i(\mathbf{R}_{k+1}-\mathbf{R}_k)\cdot\mathbf{Q}_k}{4\beta D_0\sqrt{2\pi\mu_0\beta}\,\lambda_B}\,\frac{\mathbf{Q}_k^2}{\lambda^2}+\frac{\Delta t\;\mathbf{Q}^2}{16\beta D_0\mu_0\pi\,\lambda_B^2}\,\frac{\mathbf{Q}^2}{\lambda^2}\right)\,,\end{aligned} \tag{4.27}$$

where $\mathbf{Q}_k\equiv\mathbf{Q}(t_k)$. The incremental time interval $\Delta t\equiv t/N_t$ plays the role of a regularization cut-off and is the time analog of the distance regularization cut-off λ. We recall that, in the EFT framework, both Δt and λ are kept finite at all stages of the calculation. The result of the Gaussian integral (4.27) can be written in the form

$$\mathcal{N}e^{-\frac{(\mathbf{R}_{k+1}-\mathbf{R}_k)^2}{4D_0\Delta t}}\;e^{\frac{\beta\mu_0\pi}{16\Delta t^3}\xi^2\left(5\Delta t(\mathbf{R}_{k+1}-\mathbf{R}_k)^2-3\frac{(\mathbf{R}_{k+1}-\mathbf{R}_k)^4}{4D_0}\right)}\,,$$

where $\mathcal{N}$ is an irrelevant constant factor. Multiplying all the N_t terms and restoring the continuum notation, we obtain

$$S_{eff}\simeq\int_0^t dT\left[\frac{\dot{\mathbf{R}}^2}{4D_0^b}-\xi^2\left(C_2^b\;\dot{\mathbf{R}}^2-C_4^b\;\dot{\mathbf{R}}^4\right)\right]\,, \tag{4.28}$$

where the coefficients of the correction terms order $\mathcal{O}(\xi^2)$ are

$$C_2^b \equiv \frac{5\beta\mu_0\pi}{16\,\Delta t}\,, \qquad C_4^b \equiv \frac{3\beta\mu_0\pi}{64\,D_0^b}\,. \tag{4.29}$$

In Eq.s (4.28) and (4.29), we have added the superscript "b" to emphasize that D_0^b, C_2^b and C_4^b are *bare* effective constants.

Summarizing, up to corrections of order $\mathcal{O}\left(\frac{\lambda_B}{\lambda}\right)^4$, the quantum excitotion's probability density can be approximated as

$$P(\mathbf{y},t|\mathbf{x},0) \simeq \int_{\mathbf{x}}^{\mathbf{y}} \mathcal{D}\mathbf{R}\; e^{-\int_0^t dT\left[\frac{1}{4D_0^b}\dot{\mathbf{R}}^2-\xi^2\left(C_2^b\;\dot{\mathbf{R}}^2-C_4^b\;\dot{\mathbf{R}}^4\right)\right]}\,. \tag{4.30}$$

The path integral (4.30) describes the propagation of the quantum excitation as a modified diffusion process, where the quantum effects are approximated with an accuracy of order ξ^2, and represents one of the main results of this thesis.

We emphasize that, in deriving our long-distance expression for the path integral, we have truncated two independent expansions: (i) we have retained only the lowest terms in the spatial- and time- derivative expansion of all the fields in section 4.2.1 and (ii) we have kept only the leading-order terms in the expansion in ξ^2 of the first quantized path integral (4.21). Furthermore, unlike in relativistic EFT, the cut-offs defining the time and spatial resolutions are not directly related. Clearly, the existence of multiple expansions and cut-offs offers several alternatives for the power-counting schemes. A systematic analysis of all these possibilities is quite involved and goes beyond the scope of this thesis. Here, we limit ourselves to note that by simply retaining the next order in $\mathbf{Q^2}$ in the expansion of the function $V(\mathbf{Q})$ in Eq. (4.22) and then truncating the resulting effective action to order ξ^4 one may miss some important contributions, if the fields vary sufficiently rapidly in time and space. Indeed, additional first-quantized operators at order in ξ^4 may generated by expanding the field operators in Eq.s (4.2) through (4.8) to include terms with higher number of space and time derivatives.

In section 4.4, we present an application of this framework to investigate hole transport in a long DNA molecule. We find that the lowest-order analytic effective theory gives results which are essentially indistinguishable from those obtained from numerical simulations in a more microscopic model. This finding suggests that, in practice, the inclusion of ξ^4 terms may not be crucial in order to achieve an accurate description of the long-distance long-time physics in realistic macromolecular systems.

Finally, we observe that, even though the expansion in ξ^2 generates terms with increasing powers of $\hbar^2$, the EFT expansion is not conceptually equivalent to the semi-classical approximation [114, 115, 116, 117]. Indeed, the EFT approach is defined in terms of external cut-off scales, which set the resolution power of the theory and are chosen *a priori*.

4.3 Solution of the Path Integral and Renormalization

The effective theory defined in Eq. (4.30) explicitly depends on the cut-off scales Δt and λ and needs to be renormalized. This can be done by introducing appropriate counter-terms into the effective action and matching the prediction of the effective theory against experiment or more microscopic calculations, at some time-scale t^*. Through such a renormalization procedure, the power-law dependence of the effective coefficients on the cut-offs Δt and λ is removed and is replaced by a much weaker dependence on the renormalization scale t^*.

To implement this program, let us consider for sake of simplicity the simple case of isotropic diffusion (i.e. $g_{ij}^0 = \delta_{ij}$). The same procedure can be straightforwardly applied to the general case of anisotropic diffusion, by repeating the same analysis component-by-component.

After introducing the renormalizing counter-terms, the path integral (4.30) is modified as follows:

$$P(\mathbf{y},t|\mathbf{x},0) \;\simeq\; \int_{\mathbf{x}}^{\mathbf{y}} \mathcal{D}\mathbf{R}\; e^{-\mathcal{S}_{eff}\left[\dot{\mathbf{R}}\right]+\xi^2\left(Q_2\;\dot{\mathbf{R}}^2+Q_4\;\dot{\mathbf{R}}^4\right)}\,, \tag{4.31}$$

where Q_2 and Q_4 are insofar unknown coefficients. To order ξ^2 the renormalized expression for the effective action then reads

$$\bar{\mathcal{S}}_{eff} = \int_0^t dT\left[\frac{\dot{\mathbf{R}}^2}{4D_{ren}} + C_{ren}\dot{\mathbf{R}}^4\right],$$

where D_{ren}, and C_{ren} are the renormalized coefficients. In the following, we show how they can be determined up to $\mathcal{O}\left(\xi^2\right)$ accuracy.

To this end, we first analytically compute the path integral given in Eq. (4.31) to leading-order in a perturbative expansion in ξ^2 (see derivation in Appendix C.2). We obtain

$$\begin{aligned} P(\mathbf{y},t|\mathbf{x},0) \simeq P_0(\mathbf{y},t|\mathbf{x},0;D_0^b)\;\Bigg[1+\xi^2(C_2^b+Q_2)\cdot\left(\frac{(\mathbf{x}-\mathbf{y})^2}{t}-6D_0^b\right) \\ -\xi^2(C_4^b-Q_4)\left(\frac{(\mathbf{x}-\mathbf{y})^4}{t^3}-\frac{\Delta t-t}{\Delta t}\;\frac{20D_0^b(\mathbf{x}-\mathbf{y})^2}{t^2}+\frac{\Delta t-2t}{\Delta t}\;\frac{60{D_0^b}^2}{t}\right)\Bigg], \end{aligned} \tag{4.32}$$

where

$$P_0(\mathbf{y},t|\mathbf{x},0;D_0^b) = \frac{e^{\frac{-1}{4tD_0^b}(\mathbf{y}-\mathbf{x})^2}}{2\sqrt{tD_0^b\pi}}\,, \tag{4.33}$$

is the unperturbed expression. To implement the renormalization, we choose to match the prediction of the two lowest moments of this distribution, against the results of experiment or microscopic simulations at some time-scale t^*:

$$\langle\Delta\mathbf{R}^2(t^*)\rangle_{exp} \;\equiv\; \langle\Delta\bar{\mathbf{R}}^2(t^*)\rangle = 6D_{ren}t^*\,, \tag{4.34}$$

$$\langle\Delta\mathbf{R}^4(t^*)\rangle_{exp} \;\equiv\; \langle\Delta\bar{\mathbf{R}}^4(t^*)\rangle = 60D_{ren}^2t^{*2} - C_{ren}t^*\,, \tag{4.35}$$

where $\Delta\mathbf{R} = (\mathbf{y}-\mathbf{x})$ and

$$D_{ren} \;=\; D_0\left[1+4\xi^2D_0\Big(C_2^b+Q_2-\frac{20D_0}{\Delta t}\left(C_4^b-Q_4\right)\Big)\right]+o\left(\xi^4\right)\,, \tag{4.36}$$

$$C_{ren} \;=\; 1920\xi^2D_0^4\left(C_4^b-Q_4\right)+o\left(\xi^4\right)\,, \tag{4.37}$$

are the renormalized constants, which are finite combinations of bare effective coefficients and counter-terms. Their numerical value is expected to run weakly with the matching time scale t^*.

An important observation to make is that the mean-square displacement $\langle\Delta\mathbf{R}^2(t)\rangle$ retains its linear dependence on time t (Einstein's law), even when quantum corrections are taken into account. In contrast, quantum corrections do affect the time dependence of $\langle\Delta\mathbf{R}^4(t)\rangle$, by introducing a linear term, which is absent in the classical diffusion limit.

Thus, the renormalized probability density including the leading-order quantum corrections reads:

$$\bar{P}(\mathbf{y},t|\mathbf{x},0) \;\simeq\; P_0(\mathbf{y},t|\mathbf{x},0;D_{ren})\left[1-C_{ren}\;\left(\frac{(\mathbf{y}-\mathbf{x})^4}{t^3D_{ren}}-20\frac{(\mathbf{y}-\mathbf{x})^2}{t^2}+\frac{60D_{ren}}{t}\right)\right]. \tag{4.38}$$

We emphasize that the ξ^2 expansion does not break down in the long-time limit. This can been seen directly from the expression (4.38), which shows that the perturbative corrections decay with time faster than the unperturbed term. In particular, the quantum excitation's dynamics reduces to the (unperturbed) classical over-damped diffusion, in the asymptotic long-time limit, implying that the stochastic collisions contribute to quench the quantum effects.

As a final remark of this section, we stress that effective theories are non-renormalizable. This means that, in order to compute the transition probability $P(\mathbf{y}, t|\mathbf{x}, 0)$, and any observables, at $\mathcal{O}(\xi^4)$ accuracy, one needs to define a next-to-leading order effective action which includes additional operators and related counter-terms.

4.4 Hole transport in a Long Homo-DNA Molecular Wire

For illustration purposes, in this section we apply the effective theory developed above to investigate the dynamics of inelastic hole propagation along a long homo-DNA molecule, which is regarded as an infinite molecular wire. To this end we first define a microscopic theory and then match the corresponding effective theory at a given time scale t^* to define the renormalized parameters and finally use the effective theory to study the long-time and large-distance dynamics.

We consider a very simple discrete model for the DNA conformational dynamics introduced in Ref. [118], in which the molecules vibration are effectively represented by the one-dimensional harmonic chain:

$$V(Q) = \sum_{n=1}^{N} \frac{\kappa}{2} \left(x_i - x_{i-1} - a_0\right)^2 .$$

In this equation x_i denotes the position of the $i-$th base pair, while κ=0.85 eV/Å^2 is the spring constant, while $a_0 = 3.4$ Å is the equilibrium distance between two neighboring bases. In natural units (in which $\hbar = c = 1$) the mass of each base pare is $M = 2.44\ 10^{11}$ eV.

The transfer integrals at the equilibrium position $f_{\mathbf{lm}}(Q_0)$ and its derivatives $f^a_{\mathbf{lm}}(Q_0)$, entering Eq. (2.3), have been fixed in order to match the main features of the statistical distribution of transfer matrix elements for a homo-base DNA, computed microscopically in Ref. [25] from DFT-B electronic-structure calculations performed on snapshot of atomistic MD trajectories. Namely, we have set

$$\begin{aligned} f^0_{\mathbf{lm}} = &\quad \langle t_{\mathbf{lm}} \rangle &&\equiv t_0 \left(\delta_{\mathbf{l(m-1)}} + \delta_{\mathbf{l(m+1)}}\right) - e_0 \delta_{\mathbf{lm}} , \\ f^a_{\mathbf{lm}} = &\quad \sigma_{\mathbf{lm}} \sqrt{\beta\kappa} &&\equiv t' \left(\delta_{\mathbf{l(m-1)}} + \delta_{\mathbf{l(m+1)}}\right) , \end{aligned}$$

where $\langle t_{\mathbf{lm}} \rangle$ and $\sigma_{\mathbf{lm}}$ denote the average and the variance of the distribution reported in Ref. [25], leading to

$$e_0 = 4.5 \text{ eV}, \qquad t_0 = 0.03 \text{ eV}, \qquad t' = 0.15 \text{ eV/Å}.$$

The system's temperature was set to $T = 300K$ and numerical simulations were performed on a 200-base pair molecule.

We have studied the time-evolution of the probability density of an electronic hole, initially prepared at the center of the molecule, using the algorithm introduced in section 2.4, in which the stochastic conformational dynamics of the molecular wire is coupled to the quantum dynamics of the electronic hole.

The formalism presented in the previous sections can be used to define a low-resolution perturbative effective theory for this molecular wire. In Fig. 4.2, we show the matching between the numerical simulations and analytic calculations in such an effective theory for the observables $\langle \Delta R^2(t) \rangle$ and $\langle \Delta R^4(t) \rangle$, fitted at the time scale $t^* = 10$ ps (represented by a dot on the simulation curves). We note that the two approaches give consistent results. In particular, the inclusion of order ξ^2 corrections is necessary to reproduce the time-evolution of the $\langle R^4(t) \rangle$ moment. At times

t^* $[ps]$	1	5	7.5	10	12.5	15
$D_{ren}[\text{Å}^2/ps] \times 10^2$	3,6 ± 0.2	3.0 ± 0.1	2.95 ± 0.05	2,90 ± 0.04	2.87 ± 0.04	2.85 ± 0.03
$C_{ren}[\text{Å}^4/ps] \times 10^6$	-1.3 ± 0.1	-2.7 ± 0.3	-3.1 ± 0.3	-3.2 ± 0.4	-3.2 ± 0.4	-3.1 ± 0.4

Table 4.1: Renormalized coefficient in Eq.s (4.34) and (4.35) fitted at different time scales t^*.

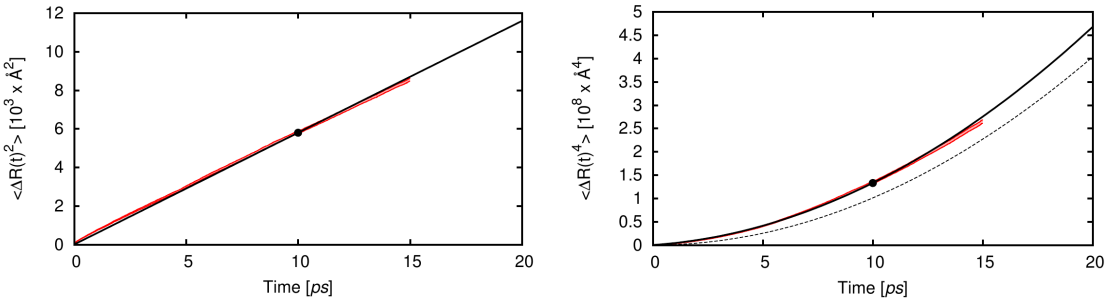

Figure 4.2: Time dependence of $\langle \Delta R^2(t) \rangle$ (left panel) and $\langle \Delta R^4(t) \rangle$ (right panel), in the microscopic model (red line) and in our effective theory (solid black line). The dashed line in the right panel represents the prediction of a purely diffusive model (zero-th order contribution in ξ^2 expansion) and the black circles represent the matching point (i.e. the renormalization time scale is $t^* = 10$ ps). The predictions in the microscopic model have been obtained in 200-base pair long molecule, by averaging over 800 different trajectories generated using the algorithm discussed in section. 2.4. Beyond 15 fs these result become affected by fine-size effects.

larger than 15 ps finite size effects begin to affect the numerical simulations, and the microscopic model cannot be used to investigate the long distance propagation.

In Table 4.1 we compare different values of the renormalized coefficient D_{ren} and C_{ren} corresponding to different renormalization time scales t^*. We observe that the effective parameters run only weakly with the renormalization scale t^*, as expected.

Chapter 5

Quantum Propagation at Intermediate time and distance

In this section we are concerned with quantum transport over time intervals too long for the perturbative approach to be applicable, yet too short for the diffusive approximation to hold. This regime is the most relevant for the analysis of several experiments on quantum transport through macromolecules, in particular for 2DPE experiments.

In this chapter we develop a non-perturbative method based on a resummation scheme which provides the time evolution of the density matrix We show that in the Markovian limit we recover a Lindblad quantum master equation. In order to deal with the non-Markovian case we introduce a series of approximations, thanks to which we are able to analytically solve the quantum transport dynamics. Then, we apply this result to evaluate the exciton energy transfer in a simple model of a molecular dimer. Finally, we briefly review the theoretical framework to investigate the 2DPE experiments, applying it to the dimer model as an illustrative example.

5.1 Resummation of Diagrams

In quantum field theory, a common way to go beyond perturbative approaches consists in resumming only specific subclasses of diagrams. This technique consists in expressing a sum of infinite correction terms in a compact way. The basic idea is the resumattion of the geometric series:

$$S = \sum_{i=0}^{\infty} x^i = 1 + x \sum_{i=0}^{\infty} x^i = 1 + xS \qquad \Rightarrow \qquad S = \frac{1}{1-x} \ .$$

In our study, the identity corresponds to a known propagator G_0 and the variable x is replaced by one-particle irreducible diagrams Σ, representing the interactions with the environment. This approach is general, given that it can be applied both to the dressing of exciton propagator forward or backward in time, and to the non-perturbative evoluation of the time evolution of the density matrix. Using the resummation of the geometric series we obtain,

$$G = G_0 \sum_{i=0}^{\infty} (\Sigma G_0)^i = G_0 + G_0 \ \Sigma \ G_0 \sum_{i=0}^{\infty} (\Sigma G_0)^i = G_0 + G_0 \ \Sigma \ G \quad \Rightarrow \quad G = \frac{G_0}{1 - G_0 \ \Sigma} \ .$$

In the next section, we show how to use this method to study the evolution of our open quantum system. In order to compute the density matrix evolution, we need to perform two resummations. The first step consists in the non-perturbative evoluation of the forward, G^f, and backward propagators, G^b, separately. These calculations are presented in subsection 5.1.1. Next, we used such dressed propagators in the resummation of the so-called ladder diagrams, in which

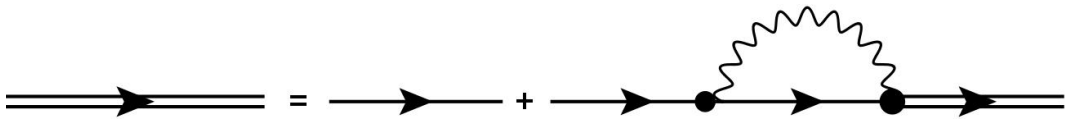

Figure 5.1: Diagramatic representation of Dyson's Equation (5.2) for the forward Green's function. The single line is the unperturbed Green's function $G^{f0}_{\mathbf{ij}}$, instead the double line represents the corrected propagator $G^{f}_{\mathbf{ij}}$. Difference between forward and backward resummation consist in opposite sign in the imaginary corrections .

forward-and backward-propagaging excitations exchange vibrons. These calculations are shown in subsection 5.1.2.

5.1.1 Dressing the Exciton Propagator

As we derived in Chapter 3, effective interaction terms in Eq. (2.28) describe an exchange of *vibrons* along the forward (or backward) evolution. At the perturbative level, this kind of corrections are included in the so called *self*-diagrams. In order to include non-perturbative corrections, we consider the infinite sum[1]

$$\begin{aligned} G_{\mathbf{k_f k_i}}(t) \;=\; & G^0_{\mathbf{k_f k_i}}(t) + \int d\tau d\tau' G^0_{\mathbf{k_i q}}(t-\tau)\Sigma_{\mathbf{qq'}}(\tau-\tau')G^0_{\mathbf{q'k_i}}(\tau') \\ & + \int d\tau d\tau' d\tau'' d\tau''' G^0_{\mathbf{k_i q}}(t-\tau)\Sigma_{\mathbf{qq'}}(\tau-\tau')G^0_{\mathbf{q's}}(\tau'-\tau'')\Sigma^0_{\mathbf{ss'}}(\tau''-\tau''')G^0_{\mathbf{s'k_i}}(\tau''') + \dots \end{aligned}$$

where Σ is the self-energy which follows from a single-vibron excange (see details in Appendix D.1). A considerable disadvantage of working in time representation (as opposed to frequency representation) is the presence of several convolution integrals. Upon moving to frequency space by means of the Fourier transformation, all convolutions are replaced by products. Thus, the previous series reads

$$\begin{aligned} G_{\mathbf{k_f k_i}}(\omega) \;=\; & G^0_{\mathbf{k_f k_i}}(\omega) + G^0_{\mathbf{k_i q}}(\omega)\;\Sigma_{\mathbf{qq'}}(\omega)\;G^0_{\mathbf{q'k_i}}(\omega) + \\ & + G^0_{\mathbf{k_i q}}(\omega)\;\Sigma_{\mathbf{qq'}}(\omega)\;G^0_{\mathbf{q's}}(\omega)\;\Sigma_{\mathbf{ss'}}(\omega)\;G^0_{\mathbf{s'k_i}}(\omega) + \dots \end{aligned} \tag{5.1}$$

As showed above, we collect one interaction term and we recognize the same infinite series. The results are the following Dyson's equations for the full forward and backward propagators

$$G^f_{\mathbf{k_f k_i}}(\omega) \;=\; G^{f0}_{\mathbf{k_f k_i}}(\omega) \;+\; G^{f0}_{\mathbf{k_f q'}}(\omega)\;\Sigma^f_{\mathbf{q'q}}(\omega)\;G^f_{\mathbf{qk_i}}(\omega)\,, \tag{5.2}$$

$$G^b_{\mathbf{k_i k_f}}(\omega) \;=\; G^{b0}_{\mathbf{k_i k_f}}(\omega) \;+\; G^{b0}_{\mathbf{k_i q'}}(\omega)\;\Sigma^b_{\mathbf{q'q}}(\omega)\;G^b_{\mathbf{qk_f}}(\omega)\,, \tag{5.3}$$

where $G^{f(b)}_{\mathbf{nm}}$ represents the non-perturbative forward (backward) Green's function. In Fig. 5.1 we diagrammatically represent the two previous equations. Eq.s (5.2) and (5.3) can be solved, and the solutions read

$$G^f_{\mathbf{k_f k_i}}(\omega) \;=\; iV^\dagger_{\mathbf{k_f n}}\left[\delta_{\mathbf{nm}}\left(\omega-\epsilon^0_{\mathbf{n}}+i0^+\right)+i\;\tilde{\Sigma}^f_{\mathbf{nm}}(\omega)\right]^{-1}V_{\mathbf{mk_i}}\,, \tag{5.4}$$

$$G^b_{\mathbf{k_i k_f}}(\omega) \;=\; -\,iV^\dagger_{\mathbf{k_i n}}\left[\delta_{\mathbf{nm}}\left(\omega-\epsilon^0_{\mathbf{n}}-i0^+\right)+i\;\tilde{\Sigma}^b_{\mathbf{nm}}(\omega)\right]^{-1}V_{\mathbf{mk_f}}\,, \tag{5.5}$$

where the matrix elements $V_{\mathbf{in}}$ define the unitary transformation which diagonalize the tight-binding Hamiltonian H_0, i.e. they represent the change of basis between the base of sites and the base of eigestates of the tight-binding hamiltonian, $\epsilon^0_{\mathbf{n}}$ are the corresponding eigenvalues (energy levels of H_0), and $\tilde{\Sigma}$ is the self-energy expressed in the basis of the eigenstates of H_0.

[1] Let us point out that, throughout this thesis we shall adopt Einstein's notation and implicitly assume the summation over all bold repeated indexes, except for the initial and final exciton position $\mathbf{k}_i$ and $\mathbf{k}_f$ which is held fixed.

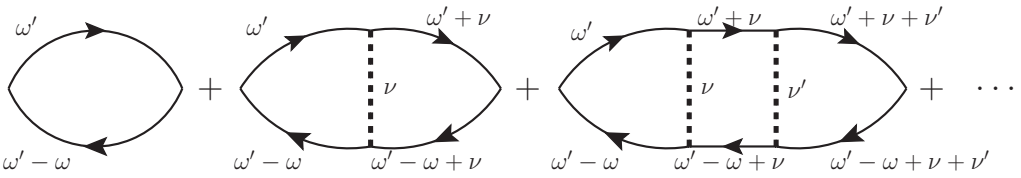

Figure 5.2: Diagramatic representation of the Ladder expansion in Eq. (5.7) for the dynamical map $\mathcal{G}$.

5.1.2 Ladder Expansion for the Density Matrix Evolution

To predict any physical observable in an open quantum system we need to know the density matrix. In Chapter 3, we demonstrate that without any interaction between the forward and backward propagators, the density matrix at time t starting from the initial $\rho^0_{\mathbf{kl}}$ reads

$$\rho_{\mathbf{ij}}(t) \;=\; G^f_{\mathbf{ik}}(t)\;\rho^0_{\mathbf{kl}}\;G^b_{\mathbf{lj}}(-t)\,,$$

thus the quantum Liouvillian operator, or dynamical map $\mathcal{G}^0_{\mathbf{ij\ kl}}(t)$,[2] describing the density matrix time evolution is the product of them,

$$\mathcal{G}^0_{\mathbf{ij\ kl}}(t) \;=\; G^f_{\mathbf{ik}}(t)\;G^b_{\mathbf{lj}}(-t)\;.$$

We notice that in $\mathcal{G}^0_{\mathbf{ij\ kl}}$ the first pair of indices corresponds to the final indices of the density matrix $\rho_{\mathbf{ij}}(t)$, whereas the second pair corresponds to the initial of ones, $\rho^0_{\mathbf{kl}}$. In frequency space, the product between the forward and backward propagators becomes a convolution,

$$\mathcal{G}^0_{\mathbf{ij\ kl}}(\omega) \equiv \int \frac{d\omega'}{2\pi}\, G^f_{\mathbf{ik}}(\omega')\;G^b_{\mathbf{lj}}(\omega'-\omega)\,. \tag{5.6}$$

In order to include fluctuation-dissipation effects in the dynamical map $\mathcal{G}$, we apply the *ladder expansion*, which consists in resumming only contributions due to the exchange of a single vibron between the forward and backward propagators (*cross*-interaction diagrams introduced in Chapter 3). In Fig. 5.2 we diagrammatically represent the infinite series that we need to compute, which reads

$$\begin{aligned}\mathcal{G}(\omega) = \int \frac{d\omega'}{2\pi}\Bigg\{ & G^f_{\mathbf{ik}}(\omega')\;G^b_{\mathbf{lj}}(\omega'-\omega) + \int \frac{d\nu}{2\pi}\; G^f_{\mathbf{ik}}(\omega')G^b_{\mathbf{lj}}(\omega'-\omega)\Delta(\nu)G^f_{\mathbf{ik}}(\omega'+\nu)G^b_{\mathbf{lj}}(\omega'-\omega+\nu) + \\ & + \int \frac{d\nu d\nu'}{(2\pi)^2} G^f_{\mathbf{ik}}(\omega')G^b_{\mathbf{lj}}(\omega'-\omega)\Delta(\nu)G^f_{\mathbf{ik}}(\omega'+\nu)G^b_{\mathbf{lj}}(\omega'-\omega+\nu)\Delta(\nu')\times \\ & \qquad \times\; G^f_{\mathbf{ik}}(\omega'+\nu+\nu')G^b_{\mathbf{lj}}(\omega'-\omega+\nu+\nu') + \ldots\Bigg\}\,.\end{aligned} \tag{5.7}$$

The main difference with the previous series in Eq. (5.1) is the impossibility to perform a direct resummation. The reason is that it is not possible identify the non-perturbative quantum Liouvillian operator $\mathcal{G}$ on the right side of Eq. (5.7). In order to work around this problem, we introduce the quantity Γ related to the quantum Liouvillian operator by the following definition

$$\mathcal{G}_{\mathbf{ij\ kl}}(\omega) \equiv \int \frac{d\omega_1}{2\pi} \int \frac{d\omega_2}{2\pi}\; \Gamma_{\mathbf{ij\ kl}}(\omega_1, \omega_1-\omega; \omega_2, \omega_2-\omega)\;. \tag{5.8}$$

[2] The quantum Liouvillian operator has been introduced in eq (1.1).

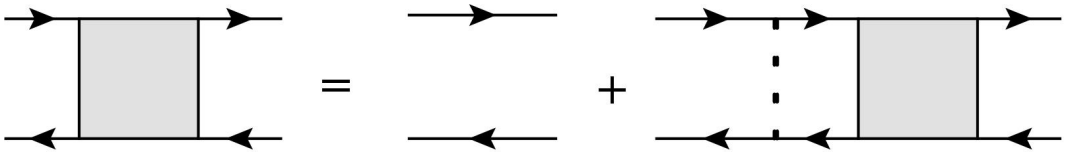

Figure 5.3: Diagramatic representation of Bethe Salpeter Equation (5.9) for the Γ function.

Replacing this definition in Eq. (5.7) and after some manipulation, we can follow the same resummation procedure used above (see Appendix D.2). Hence, we can write down the following equation, similar to the Bethe-Salpeter equation, for the quantities Γ:

$$\begin{aligned}\Gamma_{\mathbf{ij\ kl}}(\omega_1,\ \omega_1-\omega;\ \omega_2,\ \omega_2-\omega) \ &= \ G^f_{\mathbf{ik}}(\omega_1)\ G^b_{\mathbf{lj}}(\omega_1-\omega)\delta\left(\omega_1-\omega_2\right) \\ &+ \int \frac{d\nu}{2\pi}\, G^f_{\mathbf{in}}(\omega_1)\ G^b_{\mathbf{mj}}(\omega_1-\omega)\ \Delta_{\mathbf{nm\ qs}}(\nu)\ \Gamma_{\mathbf{qs\ kl}}(\omega_1+\nu,\omega_1+\nu-\omega;\omega_2,\omega_2-\omega)\end{aligned} \tag{5.9}$$

In Fig. 5.3, we diagramatically show the resummation of the *cross*-interaction. Due to the presence of the integral convolution, the resolution of this equation is only possible numerically, hence additional approximations are needed in order to obtain a simpler equation.

In the following, we introduce the Markovian approximation for the $\Delta(\nu)$ interaction recovering a Lindblad equation, and we discuss its limitation. Then, we relax the Markovian approximation and we find a simpler formulation of Eq. (5.9).

5.1.3 Markovian Limit: *Lindblad Equation*

The dynamics of quantum excitations propagating in macromolecules is shaped by three main characteristic time scales: τ_S is the time scale at which the quantum excitations propagate through the system, τ_v is the time scale associated to the periods of the important conformational oscillations (i.e. the inverse of the most relevant normal mode frequencies Ω) and τ_E is the time scale at which such vibrations are damped by dissipation.

Suppose we are interested in studying quantum energy transport over very long time scales so that: $\tau_S \gg \tau_E, \tau_v$. In this case we can adopt the so called Markovian limit, which consists in neglecting all memory effects. It is well known that, in this limit, we expect the density matrix to obey a Lindblad equation. In the QTFT framework, the Markovian condition is implemented by taking the small frequency expansion of the vibron propagator, which is equivalent to reduce the QTFT to a Fermi-like theory with only contact interactions:

$$\Delta_{\mathbf{nm\ qs}}(t) \simeq d_{\mathbf{nm\ qs}}\,\delta(t) \qquad \Rightarrow \qquad \Delta_{\mathbf{nm\ qs}}(\nu) \simeq 2\pi\, d_{\mathbf{nm\ qs}}\,.$$

In frequency space this approximation corresponds to replace vibronic Green's function Δ whit the constant $d_{\mathbf{nm\,qs}}$ in Eq. (5.9), obtaining

$$\begin{aligned}\Gamma_{\mathbf{ij\ kl}}(\omega_1,\ \omega_1-\omega;\ \omega_2,\ \omega_2-\omega) \ &= \ G^f_{\mathbf{ik}}(\omega_1)\ G^b_{\mathbf{lj}}(\omega_1-\omega)\delta\left(\omega_1-\omega_2\right) \\ &+ \int \frac{d\nu}{2\pi}\, G^f_{\mathbf{in}}(\omega_1)\ G^b_{\mathbf{mj}}(\omega_1-\omega)\ d_{\mathbf{nm\ qs}}\ \Gamma_{\mathbf{qs\ kl}}(\omega_1+\nu,\omega_1+\nu-\omega;\omega_2,\omega_2-\omega)\ ,\end{aligned}$$

In order to compute the quantum Liouvillian operators $\mathcal{G}(\omega)$, we integrate the last formula over the variables ω_1 and ω_2[3]:

$$\mathcal{G}_{\mathbf{ij\ kl}}(\omega) \ = \ \mathcal{G}^0_{\mathbf{ij\ kl}}(\omega) \ + \ \mathcal{G}^0_{\mathbf{ij\ nm}}(\omega)\ d_{\mathbf{nm\ qs}}\ \mathcal{G}_{\mathbf{qs\ kl}}(\omega)\ , \tag{5.10}$$

[3] Shifting the integral variable $\nu \to \nu' = \nu + \omega_1$, we can factorize the unperturbed $\mathcal{G}^0$ and the non-perturbative $\mathcal{G}$ dynamical maps

where $\mathcal{G}^0$ is the unperturbed dynamical map defined in Eq. (5.6). Expressing the last equation for $\mathcal{G}$ in the energy level basis and neglecting the matrices Σ, we find the following analytic solution for the dynamical map:

$$\mathcal{G}_{\mathbf{ij\ kl}}(t) \;=\; \int \frac{d\omega}{2\pi} e^{-i\omega t}\; i\left[(\omega - \epsilon_{\mathbf{i}} + \epsilon_{\mathbf{j}})\,\delta_{\mathbf{ik}}\;\delta_{\mathbf{lj}} \;+\; i\,d_{\mathbf{ij\,kl}}\right]^{-1}. \tag{5.11}$$

In Appendix D.3 we show that this is precisely the expression for the quantum liuvillian operator which corresponds to the Lindblad equation, which is the most general type of Markovian and time-homogeneous master equation describing non-unitarity time evolution of the density matrix. This approximation confirm that our resummation describes the correct quantum transport dynamics in the limit of long time, i.e. for time longer than $\tau_E \sim 1$ ps.

We emphasize, however, that the Markovian approximation may not provide a very accurate description of the quantum transport dynamics, since typically the time scales associated to quantum transport are comparable or even smaller than those associated to the vibrations and damping. Consequenlty, in the following we proposed a way to compute dynamical maps beyond the Markovian limit.

5.1.4 Beyond Markovian Limit: *Resonant Approximation*

In order to go beyond the Markovian limit showed above, we analyze the *vibron* Green's function $\Delta(\nu)$, showing its resonant behavior around a frequency. The exchange of *vibrons* is described by the non-instantaneous interaction $\Delta(\nu)$, that reads

$$\Delta_{\mathbf{nm\ qs}}(\nu) = f^i_{\mathbf{nq}} U_{in} \Delta^n(\nu) U^\dagger_{nj} f^j_{\mathbf{sm}}\,, \tag{5.12}$$

where the U and $U^\dagger$ are the unitary matrix that diagonalize the Hessian of the molecular potetial energy $V(Q)$ at mechanical equilibrium, and Δ^n is the vibronic two-point function related to the normal frequencies Ω_n (see Appendix A.4)

$$\Delta^n(\nu) = \frac{4\gamma}{M\beta}\;\frac{1}{(\nu^2 - \Omega_n^2)^2 + \gamma^2\nu^2}\,. \tag{5.13}$$

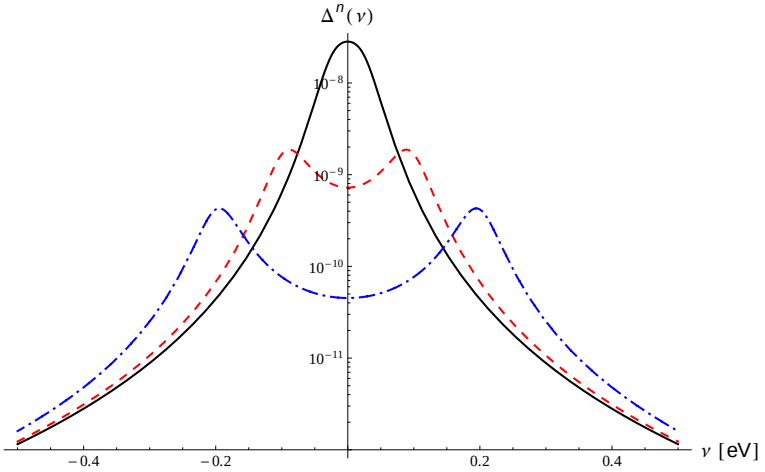

Figure 5.4: Two point correlation function for a vibron exchange, $\Delta^n(\nu)$, for different normal frequencies. The full line correspond to the case $2\Omega_n^2 < \gamma^2$ ($\Omega_n = 0.04$ eV), the dashed line show the case $(1+\sqrt{2})\gamma^2 > 2\Omega_n^2 \geq \gamma^2$ ($\Omega_n = 0.1$ eV), and the dash-dot line represent the case $2\Omega_n^2 \geq (1+\sqrt{2})\gamma^2$ ($\Omega_n = 0.2$ eV). In the plot we used $\gamma = 0.1$ eV, $M = 100$ uma, $T = 300$ K.

In Fig. 5.4, we point out the resonant behaviour of Δ^n. We observe that this function is peaked around a value $\bar{\nu}$, which depends on the ratio between γ and Ω_n. Due to this property we apply the following approximation:

$$\Delta^n(\nu) \;\simeq\; \Delta^n(\bar{\nu}_n)\;\delta(\nu-\bar{\nu}_n)\;\Delta\nu_n\,,$$

that we call *resonant approximation*, which consist in imposing that only the resonant frequency $\bar{\nu}$ is exchanged. The quantity $\Delta\nu$ in the last equation is the full width at half maximum.
Studying Eq. (5.13), we can identify three characteristic behaviors:

- CASE I: there is only one peak in $\bar{\nu}_n = 0$, when
$$2\Omega_n^2 < \gamma^2$$
- CASE II: there are two peaks in $\bar{\nu}_n = \pm\sqrt{\frac{2\Omega_n^2-\gamma^2}{2}}$, and the minimum in $\nu = 0$ is higher than the half maximum, when
$$(1+\sqrt{2})\gamma^2 > 2\Omega_n^2 \geq \gamma^2$$
- CASE III: there are two well separate peaks in $\bar{\nu}_n = \pm\sqrt{\frac{2\Omega_n^2-\gamma^2}{2}}$, when
$$2\Omega_n^2 \geq (1+\sqrt{2})\gamma^2$$

In the three different cases we have a different formulation for the full width at half maximum of the peaks

$$\Delta\nu_n = \begin{cases} \sqrt{2}\sqrt{-\gamma^2+2\Omega_n^2+\sqrt{\gamma^4-4\gamma^2\Omega_n^2+8\Omega_n^4}} \;\simeq\; \sqrt{8}\dfrac{\Omega_n^2}{\gamma} & \text{CASE } I \\ 2\sqrt{-(\gamma^2/2)+\Omega_n^2+1/2\sqrt{-\gamma^4+4\gamma^2\Omega_n^2}} \;\simeq\; 2\Omega_n & \text{CASE } II \\ 2\sqrt{-\gamma^2+2\Omega_n^2-\sqrt{2\gamma^4-8\gamma^2\Omega_n^2+4\Omega_n^4}} \;\simeq\; \gamma & \text{CASE } III \end{cases}$$

and three different maximum

$$\Delta^n(\bar{\nu}_n) = \begin{cases} \dfrac{4\gamma}{M\beta}\,\dfrac{1}{\Omega_n^4} & \text{CASE } I \\ \dfrac{4}{M\beta}\,\dfrac{1}{\gamma\,(4\Omega_n^2-\gamma^2)} & \text{CASE } II \\ \dfrac{4}{M\beta}\,\dfrac{1}{\gamma\,(4\Omega_n^2-\gamma^2)} & \text{CASE } III \end{cases}$$

Adopting the *resonant approximation* for the Δ interaction in Eq. (5.9), and performing the integral over ν, we obtain

$$\begin{aligned}\Gamma_{\mathbf{ij\;kl}}(\omega_1,\;\omega_1-\omega;\;\omega_2,\;\omega_2-\omega) \;&=\; G^f_{\mathbf{i\;k}}(\omega_1)\;G^b_{\mathbf{j\;l}}(\omega_1-\omega)\delta(\omega_1-\omega_2) \\ &+\;\sum_n G^f_{\mathbf{i\;n}}(\omega_1)\;G^b_{\mathbf{j\;m}}(\omega_1-\omega)\;\bar{\Delta}^n_{\mathbf{nm\;qs}}\;\Gamma_{\mathbf{qs\;kl}}(\omega_1+\bar{\nu}_n,\omega_1-\omega+\bar{\nu}_n;\omega_2,\omega_2-\omega)\end{aligned} \tag{5.14}$$

where $\bar{\Delta}^n$ represents the resonant contribution due to exchanges between the forward and backward propagation of the *vibron* at frequency Ω_n, and it reads

$$\bar{\Delta}^n_{\mathbf{nm\;qs}} = f^i_{\mathbf{nq}}U_{in}\;\left[\Delta\nu_n\;\Delta^n(\bar{\nu}_n)\right]U^\dagger_{nj}f^j_{\mathbf{ms}}\,. \tag{5.15}$$

Let us point out that on the right-side in Eq. (5.14) every Γ function is multiplied by forward G^f, and backward G^b, exciton propagators. From Eq.s (5.4) and (5.5), we observe that these quantities are peaked around the energy level $\epsilon_{\mathbf{n}}$, which is order of magnitude bigger than any frequency shift ($\epsilon_{\mathbf{i}} \gg \bar{\nu}_n$). Accordingly, we neglect the small frequency shift in the Γ functions

in Eq. (5.14), because both arguments are the same of the peaked Green's functions G^f and G^b. Therefore Eq. (5.14) after some manipulation becomes

$$\begin{aligned}\Big[\delta_{\mathbf{ij\ qs}} - G^f_{\mathbf{i\ n}}(\omega_1)\ G^b_{\mathbf{j\ m}}(\omega_1-\omega)\bar{\Delta}_{\mathbf{nm\ qs}}\Big]\ \Gamma_{\mathbf{qs\ kl}}(\omega_1,\ \omega_1-\omega;\ \omega_2,\ \omega_2-\omega) = \\ = G^f_{\mathbf{i\ k}}(\omega_1)\ G^b_{\mathbf{j\ l}}(\omega_1-\omega)\delta(\omega_1-\omega_2)\ ,\end{aligned} \tag{5.16}$$

where the matrix $\bar{\Delta}$ collects all the *cross*-interaction effects, $\bar{\Delta} = \sum_n \bar{\Delta}^n$. After some manipulation[4], we find the following solution for the Γ function

$$\begin{aligned}&\Gamma_{\mathbf{qs\ kl}}(\omega_1,\ \omega_1-\omega;\ \omega_2,\ \omega_2-\omega) = \\ &= \big[\mathbb{1} - G^f(\omega_1)\ G^b(\omega_1-\omega)\ \bar{\Delta}\big]^{-1}_{\mathbf{qs\ ij}}\ G^f_{\mathbf{i\ k}}(\omega_1)\ G^b_{\mathbf{j\ l}}(\omega_1-\omega)\delta(\omega_1-\omega_2)\ .\end{aligned}$$

By replacing it in Eq. (5.8), we obtain a final formula for the quantum Liouvillian operator

$$\mathcal{G}_{\mathbf{nm\ kl}}(\omega) = \int \frac{d\omega'}{2\pi}\left[G^{f\ -1}(\omega')\ G^{b\ -1}(\omega'-\omega)\ -\ \bar{\Delta}\right]^{-1}_{\mathbf{nm\ kl}}\ . \tag{5.17}$$

Hence, the density matrix at time t reads

$$\rho_{\mathbf{ij}}(t) = \int \frac{d\omega}{2\pi}\ e^{-i\omega t}\ \int \frac{d\omega'}{2\pi}\left[G^{f\ -1}(\omega')\ G^{b\ -1}(\omega'-\omega)\ -\ \bar{\Delta}\right]^{-1}_{\mathbf{nm\ kl}}\rho^0_{\mathbf{kl}}\,. \tag{5.18}$$

The expression (5.18) is quite general, but the integral is not analytically solvable. Even numerical integration is challenging due to the strongly oscillatory behavior of the integrand, consequently the numerical computation of the dynamical map in Eq. (5.18) is beyond the objective of this thesis. However, in order to gain some partial insight, we discuss two physical limits: first we recover the dephasing behaviour of Eq. (5.18) imposing the Δ-matrix to zero and assuming constant the self-energy, $\Sigma(\omega) \simeq \Sigma^0$; then, we neglect the off-diagonal terms of the Δ-matrix diagonals and the self-energy obtaining dissipation effects.

We begin, by introducing explicitly the forward and backward Green's functions in Eq. (5.17) and expressing the quantum Liouvillian in the energy level basis:

$$\begin{aligned}&\tilde{\mathcal{G}}_{\mathbf{ns\ mt}}(\omega) = \int \frac{d\omega'}{2\pi}\ V_{\mathbf{sl}}V_{\mathbf{ni}}\left[G^{f\ -1}(\omega')\ G^{b\ -1}(\omega'-\omega)\ -\ \bar{\Delta}\right]^{-1}_{\mathbf{ij\ kl}}V^\dagger_{\mathbf{km}}V^\dagger_{\mathbf{jt}} = \\ &\int \frac{d\omega'}{2\pi}\ \Big[\left(\delta_{\mathbf{nm}}\left(\omega' - \epsilon^0_{\mathbf{n}} + i0^+\right) + i\tilde{\Sigma}^f_{\mathbf{nm}}(\omega')\right)\left(\delta_{\mathbf{st}}\left(\omega' - \omega - \epsilon^0_{\mathbf{s}} - i0^+\right) + i\tilde{\Sigma}^b_{\mathbf{st}}(\omega'-\omega)\right) - \tilde{\bar{\Delta}}_{\mathbf{nt\,ms}}\Big]^{-1}\ ,\end{aligned} \tag{5.19}$$

where the *cross*-interaction matrix is expressed in the energy levels basis and reads

$$\tilde{\bar{\Delta}}_{\mathbf{nt\ ms}} = \ V_{\mathbf{np}}f^i_{\mathbf{pq}}V^\dagger_{\mathbf{qm}}\ \Big[U_{in}\Delta\nu_n\Delta^n(\bar{\nu}^n)U^\dagger_{nj}\Big]\ V_{\mathbf{sv}}f^j_{\mathbf{vw}}V^\dagger_{\mathbf{wt}}\,. \tag{5.20}$$

Imposing $\tilde{\bar{\Delta}} = 0$ is equivalent to ignore the interaction between forward and backward propagators, while assuming that the self-energy is approximated to a constant means adopting the Markovian limit, namely ignoring memory effects during quantum transports. In order to perform analytically the integral in Eq. (5.19), we consider only diagonal terms of Σ obtaining the following dynamical map

$$\tilde{\mathcal{G}}_{\mathbf{ns\ mt}}(t) = \int \frac{d\omega}{2\pi}e^{-i\omega t}\ i\left[\left(\omega - \epsilon^0_{\mathbf{n}} + \epsilon^0_{\mathbf{s}}\right) + i\tilde{\Sigma}^{(0)f}_{\mathbf{n}} + i\tilde{\Sigma}^{(0)b}_{\mathbf{s}}\right]^{-1}\delta_{\mathbf{nm}}\delta_{\mathbf{st}}\,, \tag{5.21}$$

[4] In particular, we use the property of the inverse of a matrix product $[A\ B]^{-1} = B^{-1}A^{-1}$. We exploit this rules in Eq. (5.16) in this way:

$$\begin{aligned}\big[\mathbb{1} - G^f(\omega')\ G^b(\omega'-\omega)\ \bar{\Delta}\big]^{-1}_{\mathbf{nm\ ij}} &= \big[G^f(\omega')\ G^b(\omega'-\omega)\left(G^{f\ -1}(\omega')\ G^{b\ -1}(\omega'-\omega) - \bar{\Delta}\right)\big]^{-1}_{\mathbf{nm\ ij}} \\ &= \big[G^{f\ -1}(\omega')\ G^{b\ -1}(\omega'-\omega) - \bar{\Delta}\big]^{-1}_{\mathbf{nm\ kl}}\big[G^f(\omega')\ G^b(\omega'-\omega)\big]^{-1}_{\mathbf{kl\ ij}}\ .\end{aligned}$$

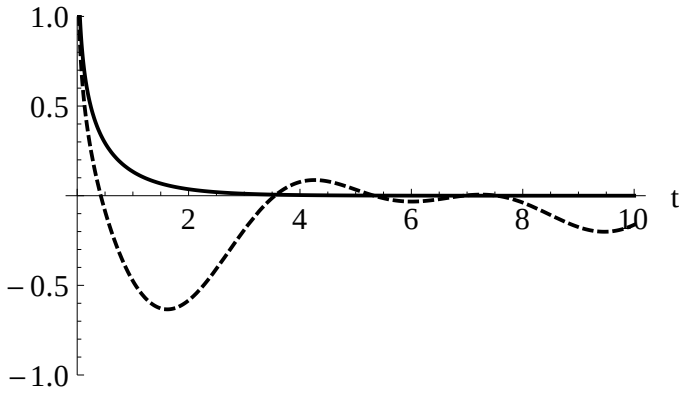

Figure 5.5: The full line represent the Bessel function $K_0(t)$ and the dashed line the difference between Bessel function and Struvel function $Y_0(t) - \mathbf{H}_0(t)$) in Eq. (5.23).

where the self-energy plays the role of the dephasing terms. Indeed, the last equation corresponds to a Lindblad equation with only dephasing terms $D_{\mathbf{ij\,ij}}$ (see Appendix D.3). In this physical limit we have recovered the dephasing behaviour of our dynamical map (5.18), derived in the *resonant approximation*.

The second physical limit consists in a strong approximation which allows us to solve analytically the dynamical map and to show dissipative effects included in Eq. (5.18). In the next section, we will discuss the limitation of this approximation in an illustrative example.
We prove that we are able to analytically derive the quantum Liouvillian operator $\mathcal{G}_{\mathbf{nm\ kl}}(\omega)$ whenever it is possible to neglect the off-diagonal terms of the matrix $\bar{\Delta}$ in Eq. (5.15) in the energy level basis. This condition is equivalent to suppose that the gradients of the hopping matrix elements is almost diagonal in the energy level basis, namely

$$\tilde{f}^n_{\mathbf{nm}} \equiv V_{\mathbf{np}} f^i_{\mathbf{pq}} V^\dagger_{\mathbf{qm}} U_{in} \approx \delta_{\mathbf{nm}}\ f^n_{\mathbf{m}}\,. \tag{5.22}$$

In order to interpret this strong approximation, we write down the hopping matrix in the energy level basis $\tilde{f}_{\mathbf{nm}}(Q)$, depending on the molecular configuration Q:

$$\tilde{f}_{\mathbf{nm}}(Q) \;=\; \epsilon_{\mathbf{n}}\,\delta_{\mathbf{nm}}\,\delta(Q-Q_0) + \tilde{f}^n_{\mathbf{nm}}\,(Q-Q_0)_n + \dots\,,$$

where Q_0 is the mechanical equilibrium configuration and $\epsilon_{\mathbf{n}}$ is the $\mathbf{n}$th-energy level. The diagonal values of $\tilde{f}^n_{\mathbf{nm}}$ represent the variation of the energy levels, while the off-diagonal terms the coupling between them due to the nth-vibrational mode around Q_0. Hence, the approximation in Eq. (5.22) means that the relevant vibrational modes are coupled strongly to the energy levels and weakly to the coupling between different energy levels[5].

In this diagonal limit it is convenient to get rid of unnecessary indexes[6], by introducing the notation

$$g_{\mathbf{ns}}(\omega) \equiv \tilde{\mathcal{G}}_{\mathbf{ns\ ns}}(\omega)\,.$$

As shown in Appendix D.1 the elements of the self-energy are peaked functions, and the maxim is smaller in comparison to the molecular energy levels, $|\Sigma| \ll \epsilon^0$. Hence, a second approximation

[5] Another interpretation of this approximation is that the molecular eigenfunctions are insensible on the interaction with the environment, i.e. the matrices which diagonalize the hopping matrix $V_{\mathbf{nm}}$ weakly depend on the configuration:

$$\epsilon_{\mathbf{n}}(Q)\delta_{\mathbf{nm}} \;=\; V_{\mathbf{np}}(Q) f^i_{\mathbf{pq}}(Q) V^\dagger_{\mathbf{qm}}(Q) \simeq V_{\mathbf{np}}(Q_0) f^i_{\mathbf{pq}}(Q) V^\dagger_{\mathbf{qm}}(Q_0)\,.$$

Thus the main effect of the fluctuation is the variation of the energy levels $\epsilon_{\mathbf{n}}$.

[6] We consider only the diagonal elements, namely the elements where $\mathbf{n} = \mathbf{m}$ and $\mathbf{s} = \mathbf{t}$ in Eq. (5.19).

consists in neglecting the self-energy corrections in Eq. (5.19). In absence of these contributions the quantum Liouvillian operator becomes

$$g_{\mathbf{ns}}(\omega)=\int\frac{d\omega'}{2\pi}\left[\omega'-\frac{1}{2}(1-\Gamma_{\mathbf{ns}}(\omega)\theta^{\Gamma}(\omega))\ (\epsilon^0_{\mathbf{n}}+\omega)-\frac{1}{2}(1+\Gamma_{\mathbf{ns}}(\omega)\theta^{\Gamma}(\omega))\ \epsilon^0_{\mathbf{s}}+i0^+\Gamma_{\mathbf{ns}}(\omega)\theta^{\Gamma}(\omega)\right]^{-1}$$
$$\left[\omega'-\frac{1}{2}(1+\Gamma_{\mathbf{ns}}(\omega)\theta^{\Gamma}(\omega))\ (\epsilon^0_{\mathbf{n}}+\omega)-\frac{1}{2}(1-\Gamma_{\mathbf{ns}}(\omega)\theta^{\Gamma}(\omega))\ \epsilon^0_{\mathbf{s}}-i0^+\Gamma_{\mathbf{ns}}(\omega)\theta^{\Gamma}(\omega)\right]^{-1}.$$

where we have introduced the following quantities

$$\begin{aligned}\Gamma(\omega) &= \sqrt{\left|1+\frac{4\tilde{\tilde{\Delta}}_{\mathbf{ns\ ns}}}{(\epsilon^0_{\mathbf{s}}-\epsilon^0_{\mathbf{n}}+\omega)^2}\right|}\\ \theta^{\Gamma}(\omega) &= \begin{cases} i & \text{if } \ 4\tilde{\tilde{\Delta}}_{\mathbf{ns\ ns}}+(\epsilon^0_{\mathbf{s}}-\epsilon^0_{\mathbf{n}}+\omega)^2<0\\ 1 & \text{elsewhere}\end{cases}\end{aligned}$$

After integration over ω' the full propagator for diagonal elements reads

$$g_{\mathbf{ns}}(\omega)=\frac{1}{\Gamma(\omega)\,(\omega-\epsilon^0_{\mathbf{s}}+\epsilon^0_{\mathbf{n}}+2i0^+)}\times\begin{cases}\text{sign}(\epsilon^0_{\mathbf{s}}-\epsilon^0_{\mathbf{n}}+\omega) & \text{if } \ 4\tilde{\tilde{\Delta}}_{\mathbf{ns\ ns}}+(\epsilon^0_{\mathbf{s}}-\epsilon^0_{\mathbf{n}}+\omega)^2<0\,,\\ i & \text{elsewhere.}\end{cases}$$

In this particular case we are able to come back in time domain by means of the inverse Fourier transformation. Thus, the quantum Liouvillian time operator reads

$$g_{\mathbf{ns}}(t)=e^{-i(\epsilon^0_{\mathbf{s}}-\epsilon^0_{\mathbf{n}})t}\begin{cases}\frac{1}{\pi}K_0\left(t\ 2\tilde{\tilde{\Delta}}^{1/2}_{\mathbf{ns\ ns}}\right) & \text{if } \ 4\tilde{\tilde{\Delta}}_{\mathbf{ns\ ns}}>0\,,\\ \frac{-1}{2}Y_0\left(t\ 2|\tilde{\tilde{\Delta}}_{\mathbf{ns\ ns}}|^{1/2}\right)-\frac{1}{2}\mathbf{H}_0\left(t\ 2|\tilde{\tilde{\Delta}}_{\mathbf{ns\ ns}}|^{1/2}\right) & \text{elsewhere.}\end{cases}\tag{5.23}$$

where K_0 and Y_0 are Bessel functions of the first kind (modified and non-modified), and $\mathbf{H}_0$ is the modified Struvel function. These functions are represented in Fig. 5.5. Therefore, the density matrix in the energy level basis at time t reads[7]

$$\rho_{\mathbf{ns}}(t)\ =\ \frac{g_{\mathbf{ns}}(t)}{\text{Tr}[\rho(t)]}\,\rho^0_{\mathbf{ns}}\,.\tag{5.24}$$

In the next section, we briefly show an application of these equations in studying the excitation energy transport in a dimer, showing that this physical limit include dissipative effects. Furthermore, we prove *a posteriori* that this approximation consists in an effective low temperature limit.

5.2 Excitation Energy Transfer in a Dimer Model

In order assess the validity of our approximations, we apply the analytic quantum Liouvillian operator computed above to a dimer model. In the study of quantum transport, the two-site system is the simplest model representing the energy transfer process from a donor to an acceptor. To this end, we first introduce a simple model of two chromophores, and then predict the density matrix evolution. Finally, we discuss the goodness of our approximations.

5.2.1 Dimer Model

Inspired by recent theoretical papers [46, 47, 49] aimed to study the long-lived coherence in 2DPE spectroscopy experiments (see Section 1.2), we consider an exitonically coupled dimer, consisting

[7] The normalization factor on the denominator derives from Eq. (2.9), and it guarantees the trace conservation along the time evolution.

$e^0\,[eV]$	$\Delta e\,[eV]$	$t^0\,[eV]$	$\Omega\,[eV]$	$\gamma\,[fs^{-1}]$	$r_0\,[\text{Å}]$	$T\,[^oK]$	$M\,[uma]$
1.4	0.2	0.1	0.01	0.1	7	300	100

Table 5.1: Parameters of the two-states model which describes exciton energy transport between two chromophores.

of two sites (chromophore 1 and 2), interacting via an electrostatic dipole-dipole interaction. The excitonic dimer Hamiltonian can be expressed as

$$H_{\mathbf{S}} = e_1[r]\; a_1^\dagger a_1 + e_2[r]\; a_2^\dagger a_2 + t[r]\left(a_1^\dagger a_2 + a_2^\dagger a_1\right) \tag{5.25}$$

where $e_1[r]$ and $e_2[r]$ are the on-site energies defined in Eq. (2.5), $t[r]$ is the hopping coefficient introduced in Eq. (2.4), and r is the distance between the two sites. We model the molecular vibrations with an harmonic oscillator between the two sites. Therefore, the molecular dynamics is described by the following Hamiltonian:

$$H_M = \frac{1}{2M}p_r^2 + \frac{1}{2}M\Omega^2(r-r_0)^2\,,$$

where M is the effective mass of the system, p_r the canonical momentum conjugated to the r coordinate, and r_0 correspond to the equilibrium distance [119]. In the case of neutral molecules, the interaction between different chromophores is dominated by their dipole-dipole interaction

$$V_{12} \sim \frac{1}{r^3}\left(\boldsymbol{\mu}_1\cdot\boldsymbol{\mu}_2 - 3/r^2\,\boldsymbol{\mu}_1\cdot\mathbf{r}\;\boldsymbol{\mu}_2\cdot\mathbf{r}\right)\,,$$

where $\boldsymbol{\mu}_i$ is the transition dipole moment of chromophore i. As a consequence, we assume the following dependence by the distance r of the tight-binding parameters:

$$\begin{aligned} e_n[r] &= \left(e^0 \pm \frac{\Delta e}{2}\right)\frac{r_0^3}{r^3} \qquad \rightarrow\; e^1[r_0] = -3\,e^0\;(1+n\Delta e)\;\frac{1}{r_0}\,,\\ t[r] &= t^0\;\frac{r_0^3}{r^3} \qquad\qquad\qquad \rightarrow\; t^1[r_0] = -3\,t^0\;\frac{1}{r_0}\,, \end{aligned}$$

where Δe is the energy gap between the site, and e^0 t^0 are the values of the parameters entering the tight-binding Hamiltonian, at the equilibrium configuration. The numerical values of the parameters of this dimer model are summarized in Table 5.1.

5.2.2 Time Evolution of the Density Matrix

In order to compute the dynamics of an exciton in the dimer by means of the quantum Liouvillian operator in Eq. (5.23), we need to evaluate the diagonal elements of the Δ-matrix defined in Eq. (5.20). Replacing the expressions for the full width at half maximum $\Delta\nu$, and the maximum $\Delta(\bar{\nu})$, Eq. (5.20) becomes

$$\tilde{\tilde{\Delta}}_{\mathbf{ns\;ns}} = \;\frac{4\sqrt{8}}{M\beta\Omega^2}\;\tilde{f}^i_{\mathbf{nn}}\;\tilde{f}^j_{\mathbf{ss}}\,.$$

The mean square displacement for an harmonic oscillator is $\langle(r-r_0)^2\rangle = 1/(M\beta\Omega^2)$. Replacing it into the previous equation, we find the following relation

$$\tilde{\tilde{\Delta}}_{\mathbf{ns\;ns}} \;\propto\; \langle(r-r_0)^2\rangle\,.$$

Hence, a wide thermal fluctuations in the distance $(r-r_0)$ induces large dissipation effects in the energy-transfer dynamics

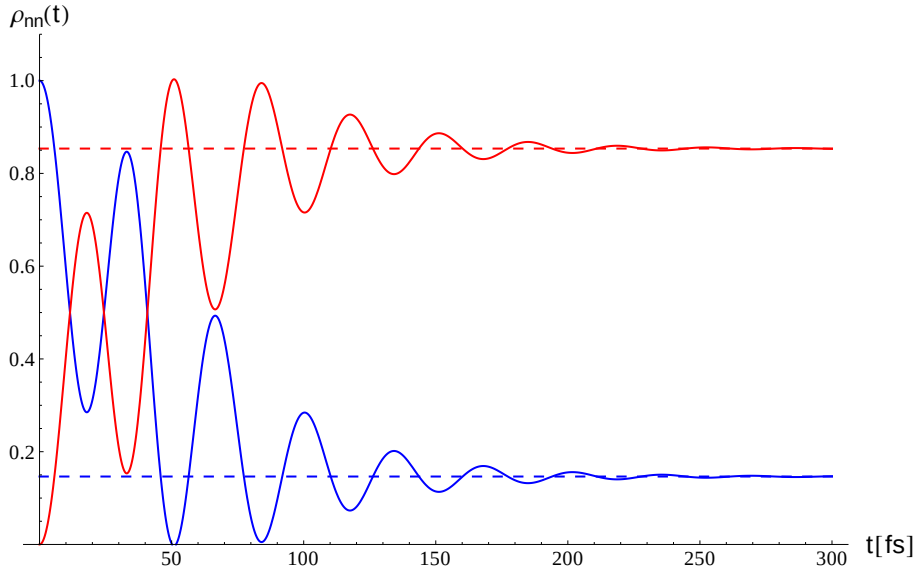

Figure 5.6: Time evolution of the probability to find the excitation at site 1 (line blue), and site 2 (line red). We notice that this probability reach the thermal equilibrium, the dashed line represent the probability calculated from the Boltzmann distribution.

We assume that at time $t = 0$ the exciton is localized on the site with greater on-site energy, in our model is the chromophore 1, $\rho(0) = |1\rangle\langle 1|$. In Fig. 5.6 we show the time evolution of the probability to find the exciton at the different sites.

Some comments on this result are in order. First of all, we notice the transfer between the site with greater on-site energy to the site with lower energy, as expected. We explain this transport phenomena as a energy dissipation effect, proving that the quantum Liouvillian operator described by Eq. (5.18) include also dissipative effects. Next, we note that the oscillator behavior is damped at 200 fs, when the population ratio reaches an equilibrium value [120]. Finally we observe that the density matrix for this dimer model reaches the thermal equilibrium. In Fig. (5.6), we find an agreement between the long-time equilibrium described by the dynamical map computed in the previous section and value computed from the Boltzmann distribution, $\langle \mathbf{i}|e^{-\beta H_0}|\mathbf{i}\rangle$.

However, we realized that in case $\beta\Delta e \lesssim 1$ this agreement is lost. To find the origin of this discrepancy we study the asymptotic behavior of the density matrix evolution in the energy basis. The Bessel function $K_0(t)$ for large time t has the following exponential decaying behavior,

$$K_0(x) \sim \sqrt{\frac{\pi}{2x}}\, e^{-x}\,.$$

Replacing it in Eq. (5.24), the density matrix in the localized site basis for longer time reads

$$\rho_{ij}(t) \;=\; \frac{e^{-1/2\sqrt{\Delta}_{ij}t}}{e^{-1/2\sqrt{\Delta}_1 t} + e^{-1/2\sqrt{\Delta}_2 t}} \;\xrightarrow{t\to\infty}\; \begin{cases} 1 & \text{if } \Delta_{ij} = \Delta_2 \\ 0 & \text{elsewhere} \end{cases} \quad ,$$

where $\Delta_1 > \Delta_2$ are the diagonal elements of the Δ-matrix. In other words, the final state of the dynamics is the pure eigenstate with the lowest energy level (and the lowest Δ elements), where the whole dynamics condensate. This behavior is physical only in the low temperature regime $\beta\Delta e \gg 1$, when the gap energy is big enough to force the exciton to migrate in the lower energy.

5.3 Two-Dimensional Photon Echo Spectroscopy

In this section we describe how to compute the 2DPE Spectroscopy signal in the joint perturbative and impulsive limit [121, 122, 123], in order to establish a more direct connection between theoretical predictions and experimental observations. Furthermore, we show an illustrative example based on the dimer model presented above.

The 2DPE Spectroscopy is a non-linear optical spectroscopy technique, consisting in the illumination of the sample by three consecutive ultrashort laser pulses, and in the reception of a four photon. The first τ_1 and third τ_3 time intervals are related to the absorption and emission spectra by means of Fourier transformation, while the delay time between the second and the third impulse corresponds to the *population time* τ_2, corresponding to the evolution time t of the density matrix. Therefore varying τ_2 we can experimentally investigate the time evolution of our system. Indeed, the result of 2DPE spectroscopy experiments is usually presented as a series of 2DPE maps for different τ_2, where on the axis we find the frequencies dependency obtained by means of a Fourier transformation with respect to the time delays τ_1 and τ_3 (see Fig. 5.7).

In the following we introduce the semiclassical treatment, which is often used to described non-linear spectroscopic experiments.

5.3.1 Semiclassical Theory in 2D-Photon Echo Experiments

This methodology has been developed primarily by Mukamel and coworkers [121], while in order to review it we follow the Ref. [123].

In the semiclassical method, the light is treated classically, while the sample under investigation is treated quantum mechanically. In this contest, the interaction between the laser pulses and the system is described by a dipolar coupling of the form

$$H_{\text{int}} = E(\mathbf{r}, t) \cdot \boldsymbol{\mu} \,,$$

where the operator $\boldsymbol{\mu}$ denotes the transition dipole moment operator of the system, and E is the total electric field describing the three incoming pulses. The total electric field is described by the superpositions of three classical wave packets,

$$E(\mathbf{r}, t) = \sum_{i=1}^{3} \boldsymbol{\varepsilon}_i E_i^0(t - t_i^0) \;\; \sin\left(\omega(t - t_i^0) + \mathbf{k}_i \mathbf{r}\right) \,,$$

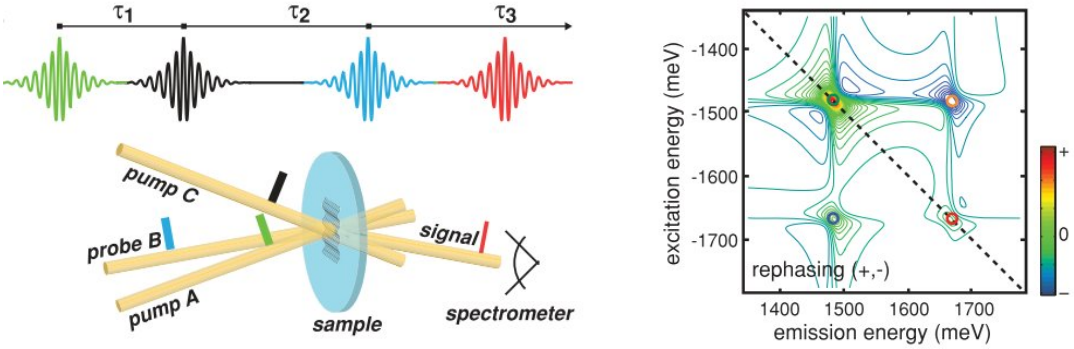

Figure 5.7: **Left panel**: schematic representation of the 2D-Photon Echo experiment, and the pulse-timing sequence. **Right panel**: example of a 2D Echo map for a dimer. Figure taken from Ref. [123]

where i denotes the ith-laser pulse, $\boldsymbol{\varepsilon}_i$ is the respective polarization vector, and $E_i^0(t)$ represents the i-th pulse shape. The time variables t_i^0 indicate the moment when each pulse interacts with the sample.

The fourth electric signal measured is proportional to the non-linear polarization $P(t)$, which is a macroscopic collective dipole moment per unit volume and can be written as the expectation value of the transition dipole moment operator

$$P(t) = \langle \boldsymbol{\mu} \rangle = \mathrm{tr}\left[\boldsymbol{\mu}\rho(t)\right] , \tag{5.26}$$

where $\rho(t)$ is the density matrix of the sample system at time t. When this polarization is measured under low laser intensity, the light-matter interaction can be evaluated perturbatively and the dominant term comes from the third order contribution, which can be formally expressed as

$$P^{(3)}(t) = \int_0^\infty dt_3 \int_0^\infty dt_2 \int_0^\infty dt_1 \; R^{(3)}\left(t, t_3, t_2, t_1\right) E(t_3)E(t_2)E(t_1) , \tag{5.27}$$

where $R^{(3)}$ is the third-order response function, which in the theoretical framework introduced in this thesis reads

$$\begin{aligned} R^{(3)}\left(t, t_3, t_2, t_1\right) \; &= \; \left(\frac{-i}{\hbar}\right)^3 \; \langle \boldsymbol{\mu}(t)\boldsymbol{\mu}(t_3)\boldsymbol{\mu}(t_2)\boldsymbol{\mu}(t_1)\rangle \; = \\ &= \int d\phi_t' d\phi_t^{'*} \, d\phi_t'' d\phi_t^{''*} e^{-\phi_t^{'*}\phi_t' - \phi_t^{''*}\phi_t''} \int d\phi_0' d\phi_0^{'*} \, d\phi_0'' d\phi_0^{''*} e^{-\phi_0^{'*}\phi_0' - \phi_0^{''*}\phi_0''} \langle \phi_0' | \rho_0 | \phi_0'' \rangle \\ &\quad \left(\frac{-i}{\hbar}\right)^3 \int \mathcal{D}[\phi', \phi^{'*}, \phi'', \phi^{''*}] \; \boldsymbol{\mu}(t)\boldsymbol{\mu}(t_3)\boldsymbol{\mu}(t_2)\boldsymbol{\mu}(t_1) \; e^{\phi_t^{'*}\phi_t' + \phi_0^{''*}\phi_0''} \; e^{\frac{i}{\hbar} \; \mathcal{S}[\phi', \phi^{'*}, \phi'', \phi^{''*}]} . \end{aligned} \tag{5.28}$$

In the previous equation, the quantum field $\phi_{\mathbf{n}}'$ and $\phi_{\mathbf{n}}''$ corresponds to the coherent states propagating forward and backward in time respectively, which have been introduced in Chapter 2. The integrals over $d\phi_0$ represent the basis change from site basis $|\mathbf{i}\rangle$, to coherence state basis $|\phi\rangle$ for the initial density matrix ρ_0, while the integrals over ϕ_t represent the trace operations in Eq. (5.26) (see Appendix A.1). We observe that the dipole moment expresses in terms of the coherent fields $\phi^{'}$ and $\phi^{''}$ is written as follow

$$\boldsymbol{\mu}(t) = \sum_{\mathbf{n}} \; \mu_{\mathbf{n}} \left(\phi_{\mathbf{n}}^{'*}(t) + \phi_{\mathbf{n}}'(t) + \phi_{\mathbf{n}}^{''*}(t) + \phi_{\mathbf{n}}''(t)\right) , \tag{5.29}$$

where $\mu_{\mathbf{n}}$ is the dipole moment associated to the $\mathbf{n}$th-site. The number of field combinations in Eq. (5.28) is $4^4 = 256$, but only some terms are relevant. In order to simplify Eq. (5.28) and reduce the number of correlation functions, we adopt the following approximations:

- the *semi-impulsive limit* for the electronic field, $E_i(t) \approx E_0 \delta(t - t_i^0) \, \sin(\omega t - \mathbf{k_i} \cdot \mathbf{r})$;
- we assume that the system initially is in the *ground state*, $\rho_0 = |0\rangle\langle 0|$;
- we adopt the *Rotating Wave Approximation* (RWA), consisting in neglecting the quickly oscillating frequency terms under the time integral in Eq. (5.28). This approximation is reliable when the carrier frequency of the pulses ω is comparable to the transition energies in the molecule Δe. Therefore, in Eq. (5.28) the frequency of the terms fast oscillating is the sum of $\omega + \Delta e$, while the term that are taken into account they slowly oscillate with frequency $\omega - \Delta e$.

Adopting the change of the time variables t_1, t_2, and t_3 into $\tau_1' = t - t_1 - t_2 - t_3$, $\tau_2' = t - t_2 - t_3$, and $\tau_3' = t - t_3$ and performing the integrations over the new variables in Eq. (5.27), the third-order polarization becomes

$$P^{(3)}(\tau_3, \tau_2, \tau_1) = \theta(\tau_3)\theta(\tau_2)\theta(\tau_1) \; R^{(3)}\left(\tau_3, \tau_2, \tau_1\right) \; E_3(t_3^0) \, E_2(t_2^0) \, E_1(t_1^0) ,$$

where τ_i is the time interval between the i-th and the following pulse. The quantity $R^{(3)}$ is commonly written as the sum of four terms

$$R^{(3)}(\tau_3,\tau_2,\tau_1) = R_1(\tau_3,\tau_2,\tau_1) + R_2(\tau_3,\tau_2,\tau_1) + R_3(\tau_3,\tau_2,\tau_1) + R_4(\tau_3,\tau_2,\tau_1) + c.c. \quad (5.30)$$

With these assumptions, we distinguish among 2D-Photon Echo signals measured in different spatial direction, where the final wave-vector $\mathbf{k}_s$ depends on the relative sign between the incoming pulses[8],

$$\mathbf{k}_s = \pm\mathbf{k}_1 \pm \mathbf{k}_2 \pm \mathbf{k}_3 \ . \quad (5.31)$$

Due to the RWA approximation, the choice of the wave vector sign selects only one component of the dipole moment in Eq. (5.29). In the following we list the three spatial direction $\mathbf{k}_s$ which can be measured by experiments:

- The case of $\mathbf{k}_s = -\mathbf{k}_1+\mathbf{k}_2+\mathbf{k}_3$ is known as *rephasing* experiment, and it is the most studied. In this spatial direction, the third-order response function involves three contributions:

$$\begin{aligned}
R_2^{-++}(\tau_1,\tau_2,\tau_3) &= -\mu_{\mathbf{n_3}}\,\mu_{\mathbf{n_2}}\,\mu_{\mathbf{n_1}}\langle\boldsymbol{\mu}(\tau_1+\tau_2+\tau_3)\phi''^{*}_{\mathbf{n_3}}(\tau_1+\tau_2)\phi'^{*}_{\mathbf{n_2}}(\tau_1)\phi''_{\mathbf{n_1}}(0)\rangle\,,\\
R_3^{-++}(\tau_3,\tau_2,\tau_1) &= -\mu_{\mathbf{n_3}}\,\mu_{\mathbf{n_2}}\,\mu_{\mathbf{n_1}}\langle\boldsymbol{\mu}(\tau_1+\tau_2+\tau_3)\phi'^{*}_{\mathbf{n_3}}(\tau_1+\tau_2)\phi''^{*}_{\mathbf{n_2}}(\tau_1)\phi''_{\mathbf{n_1}}(0)\rangle\,,\\
R_4^{-++}(\tau_3,\tau_2,\tau_1) &= \mu_{\mathbf{n_3}}\,\mu_{\mathbf{n_2}}\,\mu_{\mathbf{n_1}}\,\langle\boldsymbol{\mu}(\tau_1+\tau_2+\tau_3)\phi'^{*}_{\mathbf{n_3}}(\tau_1+\tau_2)\phi'^{*}_{\mathbf{n_2}}(\tau_1)\phi''_{\mathbf{n_1}}(0)\rangle\,.
\end{aligned}$$

- The case of $\mathbf{k}_s = \mathbf{k}_1-\mathbf{k}_2+\mathbf{k}_3$ is known as *non-rephasing* experiment. In this spatial direction, the third-order response function involves three contributions:

$$\begin{aligned}
R_1^{+-+}(\tau_3,\tau_2,\tau_1) &= \mu_{\mathbf{n_3}}\,\mu_{\mathbf{n_2}}\,\mu_{\mathbf{n_1}}\,\langle\boldsymbol{\mu}(\tau_1+\tau_2+\tau_3)\phi'^{*}_{\mathbf{n_3}}(\tau_1+\tau_2)\phi'_{\mathbf{n_2}}(\tau_1)\phi'^{*}_{\mathbf{n_1}}(0)\rangle\,,\\
R_2^{+-+}(\tau_3,\tau_2,\tau_1) &= -\mu_{\mathbf{n_3}}\,\mu_{\mathbf{n_2}}\,\mu_{\mathbf{n_1}}\langle\boldsymbol{\mu}(\tau_1+\tau_2+\tau_3)\phi'^{*}_{\mathbf{n_3}}(\tau_1+\tau_2)\phi''_{\mathbf{n_2}}(\tau_1)\phi'^{*}_{\mathbf{n_1}}(0)\rangle\,,\\
R_4^{+-+}(\tau_3,\tau_2,\tau_1) &= \mu_{\mathbf{n_3}}\,\mu_{\mathbf{n_2}}\,\mu_{\mathbf{n_1}}\,\langle\boldsymbol{\mu}(\tau_1+\tau_2+\tau_3)\phi''^{*}_{\mathbf{n_3}}(\tau_1+\tau_2)\phi''_{\mathbf{n_2}}(\tau_1)\phi'^{*}_{\mathbf{n_1}}(0)\rangle\,,
\end{aligned}$$

- The case of $\mathbf{k}_s = \mathbf{k}_1+\mathbf{k}_2-\mathbf{k}_3$ is known as *two-quantum* experiment. In this spatial direction, the third-order response function involves two contributions:

$$\begin{aligned}
R_1^{++-}(\tau_3,\tau_2,\tau_1) &= \mu_{\mathbf{n_3}}\,\mu_{\mathbf{n_2}}\,\mu_{\mathbf{n_1}}\,\langle\boldsymbol{\mu}(\tau_1+\tau_2+\tau_3)\phi'_{\mathbf{n_3}}(\tau_1+\tau_2)\phi'^{*}_{\mathbf{n_2}}(\tau_1)\phi'^{*}_{\mathbf{n_1}}(0)\rangle\,,\\
R_3^{++-}(\tau_3,\tau_2,\tau_1) &= -\mu_{\mathbf{n_3}}\,\mu_{\mathbf{n_2}}\,\mu_{\mathbf{n_1}}\langle\boldsymbol{\mu}(\tau_1+\tau_2+\tau_3)\phi''_{\mathbf{n_3}}(\tau_1+\tau_2)\phi'^{*}_{\mathbf{n_2}}(\tau_1)\phi'^{*}_{\mathbf{n_1}}(0)\rangle\,.
\end{aligned}$$

[8] Eq. (5.31) derives from the momentum conservation.

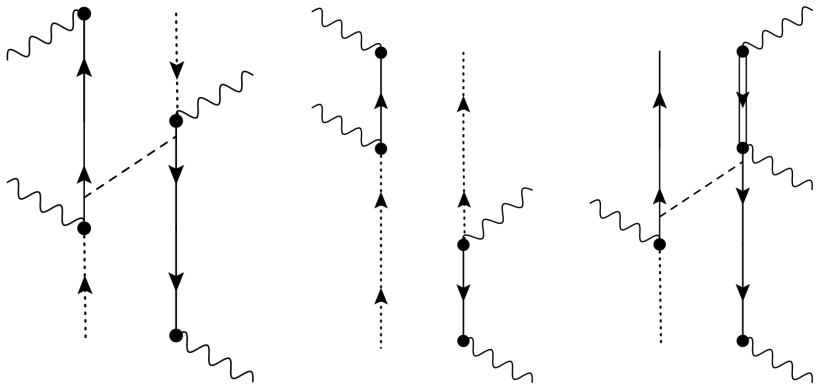

Figure 5.8: Double Feynman diagrams for *rephasing* 2D-Photon Echo experiment. Dotted line represent the ground state, Single line represents the forward or backward propagation of a coherent field, and double line represents the evolution of two electric excitations. The wiggly line represent the incoming laser pulse interacting with the system, and the dashed line the *vibron* propagator interacting between the forward and backward quantum evolution.

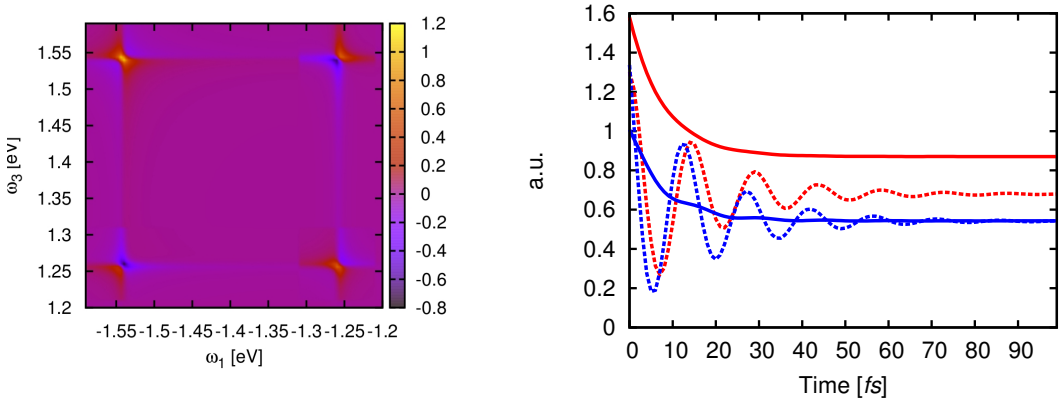

Figure 5.9: **Left panel**: 2DEP map at τ_2 for the model dimer. **Right panel**: time evolution of the four peaks. The full lines correspond to diagonal peaks (in red $(\omega_1, \omega_3) = (-1.54, 1.54)$ eV and in blue $(\omega_1, \omega_3) = (-1.26, 1.26)$ eV), the dashed lines represent off-diagonal peaks (in red $(\omega_1, \omega_3) = (-1.26, 1.54)$ eV and in blue $\omega_1 = \omega_3 = (-1.54, 1.26)$ eV)

A further approximation consists in separating the quantum dynamics between the initial time $t_0 = 0$ and t in three distinct time evolution of the density matrix, i.e. the expectation value in the previous equation is a product of three different correlation functions. In case of the *rephasing* experiment the three components of the third-order response function become

$$\begin{aligned}
R_2^{-++}(\tau_1,\tau_2,\tau_3) =& -\mu_{\mathbf{n_4}}\mu_{\mathbf{n_3}}\mu_{\mathbf{n_2}}\mu_{\mathbf{n_1}}\ \langle\phi''_{\mathbf{n_1}}(0)\phi''^{*}_{\mathbf{k}}(\tau_1)\rangle \times \langle\phi''_{\mathbf{k}}(\tau_1)\phi''^{*}_{\mathbf{n_3}}(\tau_1+\tau_2)\phi'^{*}_{\mathbf{n_2}}(\tau_1)\phi'_{\mathbf{m}}(\tau_1+\tau_2)\rangle\times \\
&\times\langle\phi'^{*}_{\mathbf{m}}(\tau_1+\tau_2)\phi'_{\mathbf{n_4}}(\tau_1+\tau_2+\tau_3)\rangle\,, \\
R_3^{-++}(\tau_1,\tau_2,\tau_3) =& -\mu_{\mathbf{n_4}}\mu_{\mathbf{n_3}}\mu_{\mathbf{n_2}}\mu_{\mathbf{n_1}}\ \langle\phi''_{\mathbf{n_1}}(0)\phi''^{*}_{\mathbf{n_2}}(\tau_1)\rangle \times \langle\phi'^{*}_{\mathbf{n_3}}(\tau_1+\tau_2)\phi'_{\mathbf{n_4}}(\tau_1+\tau_2+\tau_3)\rangle\,, \\
R_4^{-++}(\tau_1,\tau_2,\tau_3) =& \ \mu_{\mathbf{n_4}}\mu_{\mathbf{n_3}}\mu_{\mathbf{n_2}}\mu_{\mathbf{n_1}}\ \langle\phi''_{\mathbf{n_1}}(0)\phi''^{*}_{\mathbf{k}}(\tau_1)\rangle \times \langle\phi''_{\mathbf{k}}(\tau_1)\phi''^{*}_{\mathbf{m}}(\tau_1+\tau_2)\phi'^{*}_{\mathbf{n_2}}(\tau_1)\phi'_{\mathbf{s}}(\tau_1+\tau_2)\rangle\times \\
&\times\langle\phi''_{\mathbf{m}}(\tau_1+\tau_2)\phi''^{*}_{\mathbf{n_4}}(\tau_1+\tau_2+\tau_3)\phi'^{*}_{\mathbf{s}}(\tau_1+\tau_2)\phi''_{\mathbf{n_4}}(\tau_1+\tau_2+\tau_3)\phi'^{*}_{\mathbf{n_3}}(\tau_1+\tau_2)\phi''_{\mathbf{n_4}}(\tau_1+\tau_2+\tau_3)\rangle\,.
\end{aligned}$$

In Fiq. 5.8 we show the relative double Feynman diagrams. For the following we would like to note that it will be advantageous to evaluate the expressions of the third-order response function not in τ_1 and τ_3 but in frequency domain by carrying out the Fourier transformation.

5.3.2 Dimer Model Dynamics in 2D Electronic Spectra

Let us now illustrate the theoretical framework to describe 2DPE spectroscopy introduced above by applying it to the dimer model showed in section 5.2. Even though we need a more accurate solution of Eq. (5.18) to compare our theoretical predictions to experimental results, we stress that our QTFT formalism could be applied to simulate non-linear spectroscopy experiments. To this aim we show this illustrative example.

In Fig. 5.9 we show the 2DEP map at $\tau_2 = 0$, where we can distinguish four peaks, and the time evolution of them, on the right panel. The off-diagonal peaks show the typical coherence beating behavior, which is damped after ~ 50 fs. All the peaks reach an equilibrium value, as it has been observed in the time evolution. In the simulation we used the following values for the site dipolar momentum $\mu_1 = 2$ and $\mu_2 = 1$ [9].

We observe that in order to compare theoretical prediction and experimental data we should average over different configuration, varying the dipolar momentums μ_i, the onsite energies e_i and the hopping coefficient t, reproducing the intrinsic static disorder of the system.

[9] We assume that the laser polarization of the successive pulses is independent of i.

Conclusion

In this thesis, we have developed a formalism to describe quantum transport in macromolecular systems at room temperature. We used a path integral approach, which allows us to deal with the dynamics of the atomic nuclei at the classical level, while keeping a fully quantum description of the dynamics of the electronic excitations. The resultant Quantum Transport Field Theory (QTFT) has been studied in three different time regimes, by means of different techniques used in quantum field theory.

A first important advantage of our QTFT formalism is that it makes it possible to describe real-time dynamics in an open quantum system by computing a vacuum-to-vacuum Green's functions, in a closed system at zero-temperature.

A second important feature of our theory is that the tight-binding parameters can be obtained directly from microscopic ab-initio calculations. The information about the configuration-dependent electronic structure of the molecule is implicitly encoded in the parameters appearing in the QTFT. These are determined once and for all by means of quantum-chemistry calculations.

In short-time and short-distance regime, the mapping of the quantum transport dynamics on four-point correlation functions has proved useful. Indeed, it immediately yields the Feynman rules needed to perturbatively compute the corrections to the density matrix due to the interaction between the propagating excitation, the nuclear motion and the heat bath degrees of freedom.

For illustration purposes, we developed a coarse-grained model and applied this formalism to investigate the intra-chain propagation of holes in a conjugate polymer. We found that the propagation can be perturbatively describe up to about 40-50 fs. Beyond that time scale, non-perturbative approaches are required. An alternative non-perturbative approach consists in directly integrating the quantum and stochastic equation of motions which follow from a functional saddle-point approximation. The comparison with the analytic perturbative calculations has shown that the underlying saddle-point approximation is quite robust. However, a large number of trajectories seems to be necessary in order to resolve the small effects of the interaction with the heat bath and with the vibronic modes.

The possibility of performing analytic calculations opens the door to a detailed investigation of the effects generating quantum decoherence in molecular systems coupled to a heat bath. In the studied example, we have identified a specific Feynman diagram which dominates the dissipation of the quantum coherence, and correlates forward and backward propagating fields.

In order to study the long-time and large-distance regime, we systematically coarse-grained the dynamics using the RG formalism. Starting from the microscopic QTFT, we developed a rigorous "low-energy" effective description of the dissipative quantum propagation in the limit in which the quantum excitation travels for a long time and covers distances which are large compared to its de Broglie's thermal wavelength (λ_B). The RG provides a rigorous framework to vary the degree of space- and time- resolution, thereby gaining access the mesoscopic regime.

We set the spatial and time resolution powers of our EFT, introducing the length cut-off scale λ and the time scale Δt, respectively. Afterwards, we analytically computed the evolution of the probability density, by writing down a perturbative expansion in the small parameter $\xi^2 = \lambda_B^2/\lambda^2$. Our final results show that, in the asymptotically long-time and long-distance regime, the emerging

dynamics of the quantum excitation reduces to a classical diffusion process. At intermediate times, such a diffusive dynamics is modified by quantum corrections.

The advantage of this coarse-grained approach is that the resulting "low-resolution" EFT is much simpler than the corresponding microscopic QTFT and it is analytically solvable. We illustrated our formalism by studying hole propagation in a long homo-DNA molecular wire. Comparison with numerical simulations show that, even at the leading-order level, the effective theory yields very accurate predictions.

In the intermediate regime, we applied the resummation scheme to develop a non-perturbative approach which retains microscopic details. Firstly, we apply the diagrams resummation scheme on the computation of forward and backward time evolution Green's functions. Then we derive a Bethe-Salpeter like equation for the quantum Liouvillian operator. We showed that in the Markovian limit we are able to recover a Lindblad quantum master equation.

In the non-Markovian case we discuss two different physical limits, in which we recover the dephasing and dissipative nature of our quantum Liovillian operator and we find an analytic expression for the time evolution of the density matrix. For illustrative purpose, we applied it to study the exciton dynamics in a dimer model. We find that this solution is able to reproduce the exciton transfer from donor to acceptor. However it is clear that the approximations used to derive these equations are too drastic and in particular the diagonal limit for the tensor expressing the exciton-vibron coupling. Indeed the resulting excitons dissipate all the energy and at long time only the lowest energy is populated.

We review the semiclassical method to study 2DEP spectroscopy experiment, applying our QTFT formalism to describe this experimental problem. Finally, we illustrate the feasibility to predict 2DPE Spectroscopy experiments on a simple model of a dimer.

Even if there was a considerable improvement in the accuracy going from the perturbation approach to the resummation technique introduced in this thesis, the development of new techniques and the refinement of the proposed non-perturbative approaches are needed in order to retain theoretical predictions that can be compared to experimental data. Since the coherent-state path integral is affected by a dynamical sign problem, Monte Carlo approaches would be challenging. An alternative non-perturbative approach not requiring stochastic averages could be provided by a self-consistent saddle-point approximation of our microscopic EFT.

Finally, we conclude that this framework can be used to tackle a variety of problems involving quantum transport, ranging from exciton transfer in natural or artificial photosynthetic complexes to charge transfer in biological or organic polymers, or organic transistors. It would be interesting to apply this EFT to study the decoherence mechanism in the FMO complex, or to more general open quantum systems. The role and the physical interpretation of diagrams in perturbation theory in different systems is still an open question. A further direction could be the development of our EFT formalism to compute the electric current induced by external electric fields, in order to directly investigate the $I-V$ characteristic of organic thin-film transistors and molecular wires.

Appendix A

Details on Chapter 2

A.1 Coherent Path integral representation

In this thesis we used the coherent quantum field path integral representation to describe the quantum transport through a macromolecule. In this Appendix we briefly review some general features of the coherent states, focusing on the formulation of coherent path integrals [124, 125].

Coherent states are a basis of of a many-particle Hilbert space, defined as the eigenstates of the annihilation or creation operators

$$a_{\mathbf{m}}|\Phi\rangle = \phi_{\mathbf{m}}|\Phi\rangle\,, \qquad \text{or} \qquad \langle\Phi|a^{\dagger}_{\mathbf{m}} = \phi^{*}_{\mathbf{m}}\langle\Phi|\,,$$

where $\phi_{\mathbf{m}}$ and $\phi^{*}_{\mathbf{m}}$ are the corresponding complex eigenvalues, and each elements of $\Phi = (\phi_1, \ldots, \phi_N)$ represents the coherent state related to the annihilation of an excitation on the $\mathbf{m}$-site.
By this definition, we can demonstrate the following properties: this definition is equivalent,

$$|\Phi\rangle = e^{\sum_{\mathbf{m}} \phi_{\mathbf{m}} a^{\dagger}_{\mathbf{m}}}|0\rangle\,, \qquad \text{or} \qquad \langle\Phi| = \langle 0|e^{\sum_{\mathbf{m}} \phi_{\mathbf{m}} a_{\mathbf{m}}}\,,$$

they satisfy this relation of overcompletness,

$$\int \prod_{\mathbf{m}} \frac{d\phi_{\mathbf{m}}\, d\phi^{*}_{\mathbf{m}}}{2\pi i}\; e^{-\sum_{\mathbf{m}} \phi_{\mathbf{m}}\phi^{*}_{\mathbf{m}}}|\Phi\rangle\langle\Phi| = 1\,,$$

and these adjoint relations are valid,

$$a^{\dagger}_{\mathbf{m}}|\Phi\rangle = -\frac{\partial}{\partial\phi_{\mathbf{m}}}|\Phi\rangle\,, \quad \text{and} \qquad \langle\Phi|a_{\mathbf{m}} = \langle\Phi|\frac{\partial}{\partial\phi_{\mathbf{m}}}\,.$$

In this thesis we express the reduced density matrix $\rho_{\mathbf{ij}}$ in the site or energy level basis. Here, we show how switch from a complete basis, such as the site basis, to the coherent state basis and viceversa. A generally density matrix formulated in the coherent state basis, reads

$$\begin{aligned}\langle\phi'_t|\rho(t)|\phi''_t\rangle \;&=\; \int d\mu(\phi'_0)d\mu(\phi''_0)\langle\phi'_0|\rho(t)|\phi''_0\rangle \\ &\int \mathcal{D}[\phi', \phi^{'*}, \phi'', \phi^{''*}]\; e^{\phi'^{*}_t\phi'_t + \phi''^{*}_0\phi''_0}\; e^{\frac{i}{\hbar}\mathcal{S}[\phi', \phi^{'*}, \phi'', \phi^{''*}]}\end{aligned}$$

where the integration measure over initial coherent states is defined $d\mu(\phi) = \prod_i e^{-\phi^{*}_i\phi_i} d\phi^{*}_i d\phi_i$. The relations between the coherent basis and the site basis used through this thesis are the following:

$$\begin{aligned}\rho_{\mathbf{ij}} \;&=\; \langle 0|a_{\mathbf{i}}\;\rho\; a^{\dagger}_{\mathbf{j}}|0\rangle = \int d\mu(\phi')d\mu(\phi'')\langle 0|a_{\mathbf{i}}|\phi'\rangle\langle\phi'|\rho|\phi''\rangle\langle\phi''|a^{\dagger}_{\mathbf{j}}|0\rangle \\ &=\; \int d\mu(\phi')d\mu(\phi'')\;\phi'\phi''^{*}\;\langle\phi'|\rho|\phi''\rangle\,, \\ \langle\phi'|\rho|\phi''\rangle \;&=\; \sum_{\mathbf{ij}}\langle\phi'|\mathbf{i}\rangle\langle\mathbf{i}|\rho|\mathbf{j}\rangle\langle\mathbf{j}|\phi''\rangle = \sum_{\mathbf{ij}}\langle\phi'|a^{\dagger}_{\mathbf{i}}|0\rangle\rho_{\mathbf{ij}}\langle 0|a_{\mathbf{j}}|\phi''\rangle = \sum_{\mathbf{ij}}\phi'^{*}\phi''\rho_{\mathbf{ij}}\end{aligned}$$

A.2 Saddle-point Approximation

In sections 2.3 and 2.4 we used the estimation of the path integral (2.17) at mean field level, to derive the classical limit for the molecular dynamics and to derive a set of coupled equations which describe quantum evolution influenced by molecular dynamics. In this Appendix we perform this approximation following Ref.s [78] and [87] .
To implement the saddle-point approximation we introduce this obvious sum-rule:

$$1 = \sum_{\mathbf{k}_f} \rho_{\mathbf{k}_f \mathbf{k}_f}(t) \qquad \forall\, t\,, \tag{A.1}$$

which tell us that the probability to observe the quantum excitation everywhere is one[1]. In order to analyse at mean field level the evolution of the reduced density matrix, we need to introduce a set of tensor fields $\rho^{'}_{lm}(t)$,$\rho^{''}_{lm}(t)$, $\sigma^{'}_{lm}(t)$ and $\sigma^{''}_{lm}(t)$ into the path integral in Eq. (A.1). Exploiting the functional generalization of the following Dirac property

$$\begin{aligned} 1 &= \int \mathcal{D}\rho^{'}\, \delta\left(\rho^{'}_{\mathbf{lm}} - \phi^{'*}_{\mathbf{l}}\phi^{'}_{\mathbf{m}}\right) = \int \mathcal{D}\sigma^{'}\mathcal{D}\rho^{'}\, e^{\frac{i}{\hbar}\int_0^t dt' \sigma^{'}_{\mathbf{lm}}\left(\rho^{'}_{\mathbf{lm}} - \phi^{'*}_{\mathbf{l}}\phi^{'}_{\mathbf{m}}\right)}\,, \\ 1 &= \int \mathcal{D}\rho^{''}\, \delta\left(\rho^{''}_{\mathbf{lm}} - \phi^{''*}_{\mathbf{l}}\phi^{''}_{\mathbf{m}}\right) = \int \mathcal{D}\sigma^{''}\mathcal{D}\rho^{''}\, e^{-\frac{i}{\hbar}\int_0^t dt' \sigma^{''}_{\mathbf{lm}}\left(\rho^{''}_{\mathbf{lm}} - \phi^{''*}_{\mathbf{l}}\phi^{''}_{\mathbf{m}}\right)}\,. \end{aligned}$$

we obtain the new expression for the sum-rule (A.1)

$$1 = \int \mathcal{D}\rho^{'}\mathcal{D}\rho^{''}\mathcal{D}\sigma^{'}\mathcal{D}\sigma^{''} \int_{Q_0}\mathcal{D}R \int_0^0 \mathcal{D}y\; e^{\frac{i}{\hbar}\mathcal{F}[R,y,\rho^{'},\rho^{''},\sigma^{'},\sigma^{''}]}\; e^{\log\left(\sum_{\mathbf{k}_f} g^f_{\mathbf{k}_f}[\sigma^{'}] g^b_{\mathbf{k}_f}[\sigma^{''}]\right)}\,, \tag{A.2}$$

where the functional $\mathcal{F}$ is defined by

$$\begin{aligned} \mathcal{F}[R,y,\rho^{'},\rho^{''},\sigma^{'},\sigma^{''}] = \int_0^t dt' \Big\{ & \sigma^{'}_{\mathbf{lm}}\rho^{'}_{\mathbf{lm}} - \sigma^{'}_{\mathbf{lm}}\rho^{''}_{\mathbf{lm}} + M\dot{R}\dot{y} - V\left[R + y/2\right] + V\left[R - y/2\right] - \\ & \left(f_{\mathbf{lm}}\left[R + y/2\right]\rho^{'}_{\mathbf{lm}} - f_{\mathbf{lm}}\left[r - y/2\right]\rho^{''}_{\mathbf{lm}}\right) + i\left(\frac{M\gamma K_B T}{\hbar} y^2(t') + iM\gamma\; \dot{R}\cdot y\right)\Big\}\,, \end{aligned}$$

and $g^f_{k_f}$ and $g^b_{k_f}$ are the following two point correlation functions:

$$\begin{aligned} g^f_{\mathbf{k}_f}[\sigma^{'}] &= \langle 0|\phi^{'}_{\mathbf{k}_f}(t)\phi^{'*}_{\mathbf{k}_i}(0)|0\rangle = \int \mathcal{D}\phi^{'}\mathcal{D}\phi^{'*}\; \phi^{'}_{\mathbf{k}_f}(t)\phi^{'*}_{\mathbf{k}_i}(0)\; e^{-\phi^{'*}_{\mathbf{m}}(0)\phi^{'}_{\mathbf{m}}(0)}\; e^{\frac{i}{\hbar}\mathcal{S}[\phi'*,\phi',\sigma^{'}]}, \\ g^b_{\mathbf{k}_f}[\sigma^{''}] &= \langle 0|\phi^{''}_{\mathbf{k}_i}(0)\phi^{''*}_{\mathbf{k}_f}(t)|0\rangle = \int \mathcal{D}\phi^{''}\mathcal{D}\phi^{''*}\phi^{''}_{\mathbf{k}_i}(0)\phi^{''*}_{\mathbf{k}_f}(t)\, e^{-\phi^{''*}_{\mathbf{m}}(t)\phi^{''}_{\mathbf{m}}(t)}\; e^{-\frac{i}{\hbar}S_{MF}[\phi^{''},\phi^{''*},\sigma^{''}]}\,, \end{aligned}$$

which correspond to the forward propagator g^f and backward propagator g^b of a system described by this new σ-dependent action

$$\mathcal{S}_{MF}[\phi^*,\phi,\sigma] = \int dt' \phi^*_{\mathbf{l}}(t')\left(i\hbar\,\frac{\partial}{\partial t'}\delta_{\mathbf{lm}} - \sigma_{\mathbf{lm}}(t')\right)\phi_{\mathbf{m}}(t')$$

We note that, until now we have not introduced any approximation, indeed path integral in Eq. (A.2) is still an exact representation of the sum-rule.
In general, the saddle-point solution consists in finding the path $\bar{\psi}$ that minimize the action $\mathcal{S}$, i.e.

$$\int \mathcal{D}\psi\; e^{\frac{i}{\hbar}\mathcal{S}[\psi]} \qquad \longrightarrow \qquad \frac{\delta\mathcal{S}[\bar{\psi}]}{\delta\psi} = 0\,.$$

In our case we implement this approximation by imposing the stationarity of the exponents, in Eq. (A.1), with respect to the tensor fields $\sigma^{'}_{lm}$, $\sigma^{''}_{lm}$, $\rho^{'}_{lm}$ and $\rho^{''}_{lm}$ and with respect to the molecular paths y and R.

[1] We have not introduce in the model (2.1) any operator that model sink or source behavior related to the quantity transported. Therefore, this model conserves the number of "particles"

- Imposing the stationarity with respect to the $R(t')$ and $y(t')$ path leads to the equations

$$M\ddot{y} - M\gamma\dot{y} + 2\frac{\partial}{\partial y}\left(V\left[R+\frac{y}{2}\right] + V\left[R-\frac{y}{2}\right] + f_{\mathbf{lm}}\left[R+\frac{y}{2}\right]\rho^{'}_{\mathbf{lm}} + f_{\mathbf{lm}}\left[R-\frac{y}{2}\right]\rho^{''}_{\mathbf{lm}}\right) = 0$$
$$M\ddot{R} + M\gamma\dot{R} + \frac{1}{2}\frac{\partial}{\partial R}\left(V\left[R+\frac{y}{2}\right] + V\left[R-\frac{y}{2}\right] + f_{\mathbf{lm}}\left[R+\frac{y}{2}\right]\rho^{'}_{\mathbf{lm}} + f_{\mathbf{lm}}\left[R-\frac{y}{2}\right]\rho^{''}_{\mathbf{lm}}\right) = i\frac{M\gamma}{\hbar\beta}y$$

  We remember that in Eq. (A.2) we have the further border constraint $y(0) = y(t) = 0$. Therefore, the saddle-point solution for the fluctuations path y is

$$y(t') = 0 \qquad \forall t' \,.$$

- Imposing the stationarity with respect to the density tensor fields $\rho^{'}_{\mathbf{lm}}(t')$ and $\rho^{''}_{\mathbf{lm}}(t')$, and to the conjugate fields $\sigma^{'}_{\mathbf{lm}}(t')$ and $\sigma^{''}_{\mathbf{lm}}(t')$, leads to the equations

$$\sigma^{'}_{\mathbf{lm}}(t') = f_{\mathbf{lm}}\left[R(t') + \frac{y(t')}{2}\right], \qquad \sigma^{''}_{\mathbf{lm}}(t') = f_{\mathbf{lm}}\left[R(t') - \frac{y(t')}{2}\right], \qquad \text{and}$$

$$\rho^{'}_{\mathbf{lm}}(t') = \langle 0|\phi^{'}_{\mathbf{k}_f}(t)\phi^{'*}_{\mathbf{l}}(t')\phi^{'}_{\mathbf{m}}(t')\phi^{'*}_{\mathbf{k}_i}(0)|0\rangle \;=$$
$$\frac{\sum_{\mathbf{k}_f} g^b[\sigma'']}{\sum_{\mathbf{k}_f} g^f[\sigma']g^b[\sigma'']}\int \mathcal{D}\phi^{'}\mathcal{D}\phi^{'*}\left[\phi^{'}_{\mathbf{k}_f}(t)\phi^{'*}_{\mathbf{l}}(t')\phi^{'}_{\mathbf{m}}(t')\phi^{'*}_{\mathbf{k}_i}(0)\right]e^{-\phi^{'*}_{\mathbf{m}}(0)\phi^{'}_{\mathbf{m}}(0)}e^{\frac{i}{\hbar}\mathcal{S}_{MF}[\phi^{'},\phi^{''*},\sigma^{'}]},$$

$$\rho^{''}_{\mathbf{lm}}(t') = \langle 0|\phi^{''}_{\mathbf{k}_i}(0)\phi^{''*}_{\mathbf{l}}(t')\phi^{''}_{\mathbf{m}}(t')\phi^{''*}_{\mathbf{k}_f}(t)|0\rangle \;=$$
$$\frac{\sum_{\mathbf{k}_f} g^f[\sigma']}{\sum_{\mathbf{k}_f} g^f[\sigma']g^b[\sigma'']}\int \mathcal{D}\phi^{''}\mathcal{D}\phi^{''*}\left[\phi^{''}_{\mathbf{k}_i}(0)\phi^{''*}_{\mathbf{l}}(t')\phi^{''}_{\mathbf{m}}(t')\phi^{''*}_{\mathbf{k}_f}(t)\right]e^{-\phi^{''*}_{\mathbf{m}}(t)\phi^{''}_{\mathbf{m}}(t)}e^{-\frac{i}{\hbar}S_{MF}[\phi^{''},\phi^{''*},\sigma^{''}]},$$

  This set of saddle-point equation for the tensor fields is satisfied by imposing the following identities

$$\sigma^{'}_{\mathbf{lm}}(t') = \sigma^{''}_{\mathbf{lm}}(t') = f_{\mathbf{lm}}[R(t')]\,, \qquad \rho^{'}_{\mathbf{lm}}(t') = \rho^{''}_{\mathbf{lm}}(t') = \rho_{\mathbf{lm}}(t')\,.$$

  Two important consequence of this approximation are that forward and backward evolution in time are the same, and that the tensor field $\rho_{\mathbf{lm}}$ coincides with the reduced density matrix,

$$\rho_{\mathbf{lm}}(t) = \langle\psi(t)|a^{\dagger}_{\mathbf{l}}a_{\mathbf{m}}|\psi(t)\rangle$$

  where the quantum state $|\psi(t)\rangle$ is defined by

$$|\psi(t)\rangle \;\equiv\; T\, e^{-\frac{i}{\hbar}\int_0^t d\tau\left\{f_{\mathbf{lm}}[R(\tau)]a^{\dagger}_{\mathbf{l}}a_{\mathbf{m}}\right\}}\,|\mathbf{k}_i\rangle\,.$$

Finally, we note that the molecular path R is solution of the following deterministic differential equation

$$M\ddot{R}(t') + M\gamma\dot{R}(t') + \frac{\partial}{\partial R}\left(V\left[R(t')\right] + f_{\mathbf{lm}}\left[R(t')\right]\rho^{'}_{\mathbf{lm}}(t')\right) = 0\,, \tag{A.3}$$

with initial condition $R(0) = Q_0$. Only going beyond saddle-point approximation in the variable y, i.e. taking in account fluctuations around the minimal action path $y = 0$, we are able to include thermal noise, obtaining the classical Langevin equation (see Ref. [87]).

A.3 Derivation of Onsager-Machlup functional

In section 2.3 we introduce the Onsager-Machlup action, observing that it corresponds to the statistical weight to the stochastic trajectories in the Langevin dynamics. Here, we review the corresponding path integral formulation of the classical Langevin dynamics. Starting from Langevin equation we derive the conditional probability to reach a configuration Q_f after a time t in the form of a Feynman path integral in Eq. (A.10), that *Adib* proved to be an equivalent formulation of the Onsager-Machlup action [127].

Let us introduce the over-damped Langevin equation[126]:

$$\dot{q}_\alpha = -\frac{1}{M\gamma}\frac{\partial}{\partial q_\alpha}V(Q) + \eta(t), \qquad (\alpha = 1, \ldots, N_p)\,, \tag{A.4}$$

where γ is the friction coefficient, $V(Q)$ is the potential energy function entering in Eq. (2.6) and $\eta(t)$ is delta-correlated Gaussian noise, satisfying the fluctuation-dissipation relationship:

$$\langle \eta^\alpha(t') \cdot \eta^\beta(t) \rangle = \frac{6k_BT}{M\gamma}\ \delta^{\alpha\beta}\ \delta(t-t') \qquad (\alpha, \beta = 1, \ldots, N_p)\,. \tag{A.5}$$

Note that in the original Langevin equation there is a mass term $M\ddot{q}$. However, for macromolecular systems this term is damped at a time scale $10^{-13}\ s$, which much smaller than the time scale associated to local conformational changes.

The stochastic differential Eq. (A.4) generates a time dependent probability distribution $P(Q,t)$ which obeys the well-known Smoluchowski equation:

$$\frac{\partial}{\partial t}P(Q,t) = \frac{k_BT}{M\gamma}\nabla\left[\nabla P(Q,t) + \frac{1}{k_BT}\nabla V(Q)P(Q,t)\right]\,. \tag{A.6}$$

By performing the formal substitution

$$P(Q,t) = e^{-\frac{1}{2k_BT}V(Q)}\ \Psi(Q,t)\,,$$

the Smoluchowski Eq. (A.6) can be recast in the form of an imaginary time Schrödinger equation:

$$-\frac{\partial}{\partial t}\Psi(Q,t) = \hat{H}_{eff}\ \Psi(Q,t)\ ,$$

where

$$\hat{H}_{eff} \ = \ -\frac{k_BT}{M\gamma}\hat{\nabla}^2 + \hat{V}_{eff}(Q)\,, \tag{A.7}$$

is an effective Hamiltonian operator and

$$V_{eff}(Q) = \frac{1}{4k_BTM\gamma}\left((\nabla V(Q))^2 - 2k_BT\nabla^2 V(Q)\right)\ . \tag{A.8}$$

The conditional probability $P(Q_f, t|Q_0)$ to find the system at the configuration Q_f at time t, provided it was prepared in the configuration Q_0 at time $t = 0$ is the Green's function of the Smoluchowski equation, and can be related to the imaginary time propagator of the effective "quantum" Hamiltonian (A.7):

$$P_t(Q_f|Q_0) \ = \ e^{-\frac{1}{2k_BT}(V(Q)-V(Q_0))}\ \langle Q_f|e^{-tH_{eff}}|Q_0\rangle\,. \tag{A.9}$$

Using such a connection, it is immediate to obtain an expression of the conditional probability (A.9) in the form of a Feynman path integral

$$P_t(Q_f|Q_0) = e^{-\frac{V(Q_f)-V(Q_0)}{2k_BT}}\ \int_{Q_0}^{Q_f}\mathcal{D}r\ e^{-S_{eff}[r]}, \tag{A.10}$$

where

$$S_{eff}[r] = \int_0^t dt' \ \left(M\gamma \ \frac{\dot{r}^2}{4k_B T} + V_{eff}[r] \ \right) , \tag{A.11}$$

is called the effective action. The conditional probability $P_t(Q_f|Q_0)$ is sometimes written also in the following equivalent form:

$$P_t(Q_f|Q_0) = \int_{Q_0}^{Q_f} \mathcal{D}r \ e^{-S_{OM}[r]} , \tag{A.12}$$

where $S_{OM}[r]$ is the so-called the Onsager-Machlup functional,

$$S_{OM}[r] = \int_0^t dt' \ \frac{M\gamma}{4k_B T} \left(\dot{r} + \frac{1}{M\gamma} \nabla V(r) \right)^2 , \tag{A.13}$$

Proving the equivalence between the expressions (A.10) and (A.12) is not straightforward, since it involves elements of stochastic calculus [127, 108].

A.4 Details on the vibronic Green's functions structure

In performing the path integral over the δr and y variables, we exploit the standard result for Gaussian functional integrals:

$$\begin{aligned} \int \mathcal{D}\phi \ \exp\left[- \int_0^t dt' dt'' \ \phi_i(t') A_{ij}(t'-t'') \phi_j(t'') + \int_0^t dt' \, B_i(t') \phi_i(t') + C \right] = \\ \sqrt{\frac{\pi}{\det A_{ij}}} \ \exp\left[\ \frac{1}{4} \ \int_0^t dt' dt'' \ B_i(t') \, A^{-1}_{ij}(t'-t'') \, B_j(t'') + C \ \right] \end{aligned} \tag{A.14}$$

The vibronic two-point functions $\Delta_{ij}(t'-t'')$ and $\mathcal{V}_{ij}(t-t')$, which enter in Eq. (2.26) are contracted from the Green's functions of the $\hat{L}^\dagger \hat{L}$, $\hat{L}$ and $\hat{L}^\dagger$ operators:

$$\begin{aligned} \Delta_{ij}(t) &\equiv \left[\hat{L}^\dagger \hat{L} \right]^{-1}(t) = \left[\ \left(M\partial_t^2 \delta_{ij} + \gamma M \partial_t \delta_{ij} + \mathcal{H}_{ij} \right) \ \left(M\partial_t^2 \delta_{ij} - \gamma M \partial_t \delta_{ij} + \mathcal{H}_{ij} \right) \ \right]^{-1} , \\ \mathcal{V}_{ij}(t) &\equiv \left[\hat{L}^\dagger \right]^{-1}(t) + \left[\hat{L} \right]^{-1}(t) = \left[M \left(\partial_t^2 + \gamma \partial_t \right) \delta_{ij} + \mathcal{H}_{ij} \right]^{-1} + \left[M \left(\partial_t^2 - \gamma \partial_t \right) \delta_{ij} + \mathcal{H}_{ij} \right]^{-1} . \end{aligned}$$

In order to compute them it is convenient to consider the Fourier transform to frequency space. We also transform into the normal mode basis, by applying the unitary transformation $\hat{U}$ which diagonalizes the Hessian operators. We obtain:

$$\widetilde{\Delta}_{ij}(\omega) = \frac{1}{M^2} U^\dagger_{in} \left[\ \left(\omega^2 - i\gamma\omega - \Omega_n \right) \ \left(\omega^2 + i\gamma\omega - \Omega_n \right) \ \right]^{-1} U_{nj} , \tag{A.15}$$

$$\widetilde{\mathcal{V}}_{ij}(\omega) = \frac{-1}{M} U^\dagger_{in} \left[\ \left(\omega^2 - i\gamma\omega - \Omega_n \right)^{-1} + \left(\omega^2 + i\gamma\omega - \Omega_n \right)^{-1} \ \right] U_{nj} , \tag{A.16}$$

where $\mathcal{H}_{ij}$ is the Hessian, and Ω_n are the corresponding normal modes. The expressions (2.29) and (2.30) for $\Delta_{ij}(t)$ and $\mathcal{V}_{ij}(t)$ are obtained by Fourier transforming back to the time representation, taking the continuum limit for the Fourier sum.

Appendix B

Details on Chapter 3

B.1 Details on the perturbative calculations

The following traces enter the derivation of the perturbative estimate (3.14):

$$\begin{aligned} \mathrm{tr}\left[\gamma_-\gamma_5\gamma_+\gamma_5\right] &= 1\,, \\ -\mathrm{tr}\left[\gamma_-\gamma_0\right] = \mathrm{tr}\left[\gamma_+\gamma_0\right] &= 1\,, \\ -\mathrm{tr}\left[\gamma_-\gamma_0\gamma_-\gamma_5\gamma_+\gamma_5\right] = \mathrm{tr}\left[\gamma_-\gamma_5\gamma_+\gamma_0\gamma_+\gamma_5\right] &= 1\,, \\ \mathrm{tr}\left[\gamma_-\gamma_5\gamma_+\gamma_0\gamma_+\gamma_0\gamma_+\gamma_5\right] = \mathrm{tr}\left[\gamma_+\gamma_5\gamma_-\gamma_0\gamma_-\gamma_0\gamma_-\gamma_5\right] &= 1\,, \end{aligned}$$

In this thesis we did not introduce spin components for the fermionic excitations, because they are unnecessary for our purposes. We notice that an alternative definition is proposed in Ref. [1], in which the spin components are introduced.

B.2 Quantifying Quantum Decoherence

In this appendix we review the proof that the ratio

$$R(t) = \mathrm{Tr}[\hat{\rho}^2(t)]/\mathrm{Tr}[\hat{\rho}(t)]\,,$$

provides a measurement of the degree of decoherence of the system.

We first consider a pure state, denoted by the vector $|\chi\rangle$, and we represent the corresponding density operator with $\hat{\rho} = |\chi\rangle\langle\chi|$, so that $\mathrm{Tr}[\hat{\rho}] = \langle\chi|\chi\rangle$.

The operator $\hat{\rho}^2$ reads $\hat{\rho}^2 = |\chi\rangle\langle\chi|\chi\rangle\langle\chi|$, while its trace is

$$\mathrm{Tr}[\hat{\rho}^2] = \langle\chi|\chi\rangle = (\mathrm{Tr}[\hat{\rho}])^2,$$

hence $R(t) = 1$. For a mixed state, there is no single state vector describing the system, and $R(t) < 1$.

Appendix C

Details on Chapter 4

C.1 From Second to First quantization formalism

In section 4.2.2, we have shown that the probability density for the quantum excitation at a given time t can be written in the following form

$$P(\mathbf{y},t|\mathbf{x},0)=\int_{\mathbf{x}}^{\mathbf{y}}\mathcal{D}\mathbf{X}\int_{\mathbf{x}}^{\mathbf{y}}\mathcal{D}\mathbf{Y}\;e^{\frac{i}{\hbar}S_{\mathbf{0}}[\mathbf{X}]}e^{-\frac{i}{\hbar}S_{\mathbf{0}}[\mathbf{Y}]}\;e^{\frac{i}{\hbar}(I[\mathbf{X},\mathbf{Y}]+J[\mathbf{X},\mathbf{Y}])}, \tag{C.1}$$

where $\mathbf{X}[\tau]$ and $\mathbf{Y}[\tau]$ denote paths in coordinate space of quantum excitation described by the coherent fields $\phi^{'}$ and $\phi^{''}$. This path integral formulation is originated by the translation into the first quantized formalism the field representation in Eq. (4.9). In this appendix, we explicitly derive the functionals $I[\mathbf{X},\mathbf{Y}]$ and $J[\mathbf{X},\mathbf{Y}]$.

C.1.1 Derivation of the I and J functionals

In order to switch to the first-quantized formalism the field-theoretic function $S^{eff}_{\mathbf{int}}$, in Eq. (4.14), we have to perform the following replacement:

$$\begin{aligned}\phi^{'*}(\mathbf{x},t)\,\phi^{'}(\mathbf{x},t)&\rightarrow\delta_\lambda\left(\mathbf{x}-\mathbf{X}(t)\right),\\ \phi^{''*}(\mathbf{x},t)\,\phi^{''}(\mathbf{x},t)&\rightarrow\delta_\lambda\left(\mathbf{x}-\mathbf{Y}(t)\right),\end{aligned} \tag{C.2}$$

where $\mathbf{X}[\tau]$ and $\mathbf{Y}[\tau]$ are the paths in coordinate space of quantum excitation described by the coherent fields $\phi^{'}$ and $\phi^{''}$, respectively. In Eq. (C.2), we denote with δ_λ the smeared representation of the δ-function, which is defined in Eq. (4.15).

$J[\mathbf{X},\mathbf{Y}]$ functional

The functional J follows from the Hermitian term in Eq. (4.14):

$$\begin{aligned}S_J&\equiv\int dt''\int dt'\int d\mathbf{z}\left\{\bar\psi(\mathbf{z},t')\psi(\mathbf{z},t')\left[A^0_v\delta(t'-t'')-i\hbar A^1_d\frac{d}{d(t'-t'')}\right]\bar\psi(\mathbf{z},t'')\,\gamma_0\,\psi(\mathbf{z},t'')\right\}\\&=\int dT\int d\tau\int d\mathbf{z}\left\{\bar\psi(\mathbf{z},T+\frac{\tau}{2})\psi(\mathbf{z},T+\frac{\tau}{2})\left[A^0_v\delta(\tau)-i\hbar A^1_v\frac{d}{d\tau}\delta(\tau)\right]\bar\psi(\mathbf{z},T-\frac{\tau}{2})\gamma_0\psi(\mathbf{z},T-\frac{\tau}{2})\right\}.\end{aligned}$$

After expanding the ψ and $\bar{\psi}$ fields into their components[1] $\phi^{'}, \phi^{''}$, we obtain two symmetric terms, $S_J = S_{J_1} - S_{J_2}$, where

$$S_{J_1} = \int dT \int d\tau \int d\mathbf{z}\ \phi^{'*}(\mathbf{z}, T + \frac{\tau}{2}) \phi^{'}(\mathbf{z}, T + \frac{\tau}{2}) \left[A_v^0 \delta(\tau) - i\hbar A_v^1 \frac{d}{d\tau} \delta(\tau) \right] \phi^{'*}(\mathbf{z}, T - \frac{\tau}{2}) \phi^{'}(\mathbf{z}, T - \frac{\tau}{2}) \,,$$
$$S_{J_2} = \int dT \int d\tau \int d\mathbf{z}\ \phi^{''*}(\mathbf{z}, T + \frac{\tau}{2}) \phi^{''}(\mathbf{z}, T + \frac{\tau}{2}) \left[A_v^0 \delta(\tau) - i\hbar A_v^1 \frac{d}{d\tau} \delta(\tau) \right] \phi^{''*}(\mathbf{z}, T - \frac{\tau}{2}) \phi^{''}(\mathbf{z}, T - \frac{\tau}{2}) \,.$$

In first quantization representation, applying replacement in Eq. (C.2), they translate into

$$S_{J_1} \ \rightarrow \ J_1 = \int dT \int d\tau \int d\mathbf{z}\ \left\{ \delta_\lambda \Big(\mathbf{z} - \mathbf{X}(T + \frac{\tau}{2}) \Big) \left[A_v^0 \delta(\tau) - i\hbar A_v^1 \frac{d}{d\tau} \delta(\tau) \right] \delta_\lambda \Big(\mathbf{z} - \mathbf{X}(T - \frac{\tau}{2}) \Big) \right\} \,,$$
$$S_{J_2} \ \rightarrow \ J_2 = \int dT \int d\tau \int d\mathbf{z}\ \left\{ \delta_\lambda \Big(\mathbf{z} - \mathbf{Y}(T + \frac{\tau}{2}) \Big) \left[A_v^0 \delta(\tau) - i\hbar A_v^1 \frac{d}{d\tau} \delta(\tau) \right] \delta_\lambda \Big(\mathbf{z} - \mathbf{Y}(T - \frac{\tau}{2}) \Big) \right\} \,.$$

So that $S_J \rightarrow J = J_1 - J_2$.

It is immediate to check that the terms proportional to A_v^1 vanish identically, while the terms proportional to A_d^0 cancel out in the difference between J_1 and J_2. Hence, $J = 0$. This result is expected, indeed the interaction terms in the functional S_J do not couple forward- and backward-propagating excitations, hence only contribute to the dressing of the one-body propagator (see discussion in section 3.1).

$I[\mathbf{X}, \mathbf{Y}]$ functional

The dissipative character of the effective theory comes from the non-Hermitian term in the functional (4.14),

$$\begin{aligned} S_I &\equiv \frac{i}{\beta^2 D\hbar} \int dT \int d\tau \int d\mathbf{z}\ \left\{ \bar{\psi}(\mathbf{z}, t') \psi(\mathbf{z}, t') \left[\left(A_d^0 - i\hbar A_d^1 \frac{d}{d(t' - t'')} \right) \delta(t' - t'') \right] \bar{\psi}(\mathbf{z}, t'') \psi(\mathbf{z}, t'') \right\} \\ &= \frac{i}{\beta^2 D\hbar} \int dT \int d\tau \int d\mathbf{z}\ \bar{\psi}(\mathbf{z}, T + \frac{\tau}{2}) \psi(\mathbf{z}, T + \frac{\tau}{2}) \left[A_d^0 \delta(\tau) - i\hbar A_d^1 \frac{d}{d\tau} \delta(\tau) \right] \bar{\psi}(\mathbf{z}, T - \frac{\tau}{2}) \psi(\mathbf{z}, T - \frac{\tau}{2}) \,. \end{aligned}$$

After expanding the ψ and $\bar{\psi}$ fields into their components $\phi^{'}$ and $\phi^{''}$, we obtain:

$$S_I = \frac{i}{\beta^2 D\hbar} \left(S_{I_1} + S_{I_2} - 2 S_{I_3} \right) \,,$$

where

$$S_{I_1} = \int dT \int d\tau \int d\mathbf{z}\ \phi^{'*}(\mathbf{z}, T + \frac{\tau}{2}) \phi^{'}(\mathbf{z}, T + \frac{\tau}{2}) \left[A_d^0 \delta(\tau) - i\hbar A_d^1 \frac{d}{d\tau} \delta(\tau) \right] \phi^{'*}(\mathbf{z}, T - \frac{\tau}{2}) \phi^{'}(\mathbf{z}, T - \frac{\tau}{2}) \,,$$
$$S_{I_2} = \int dT \int d\tau \int d\mathbf{z}\ \phi^{''*}(\mathbf{z}, T + \frac{\tau}{2}) \phi^{''}(\mathbf{z}, T + \frac{\tau}{2}) \left[A_d^0 \delta(\tau) - i\hbar A_d^1 \frac{d}{d\tau} \delta(\tau) \right] \phi^{''*}(\mathbf{z}, T - \frac{\tau}{2}) \phi^{''}(\mathbf{z}, T - \frac{\tau}{2}) \,,$$
$$S_{I_3} = \int dT \int d\tau \int d\mathbf{z}\ \phi^{'*}(\mathbf{z}, T + \frac{\tau}{2}) \phi^{'}(\mathbf{z}, T + \frac{\tau}{2}) \left[A_d^0 \delta(\tau) - i\hbar A_d^1 \frac{d}{d\tau} \delta(\tau) \right] \phi^{''*}(\mathbf{z}, T - \frac{\tau}{2}) \phi^{''}(\mathbf{z}, T - \frac{\tau}{2}) \,,$$

Let's begin by analyzing the S_{I_1} part. In first quantization representation it translates as

$$\begin{aligned} \frac{i}{\beta^2 D\hbar} S_{I_1} \ \rightarrow \ I_1 \ &= \ \frac{i A_d^0}{\beta^2 D\hbar} \int_0^t dT \int d\mathbf{z}\ \delta_\lambda(\mathbf{X} - \mathbf{z})\ \delta_\lambda(\mathbf{X} - \mathbf{z}) \\ &\quad - \frac{A_d^1}{\beta^2 D} \int_0^t dT \int d\tau \int d\mathbf{z}\ \delta(\tau) \frac{d}{d\tau} \left[\delta_\lambda \Big(\mathbf{z} - \mathbf{X}(T + \frac{\tau}{2}) \Big) \delta_\lambda \Big(\mathbf{z} - \mathbf{X}(T - \frac{\tau}{2}) \Big) \right] \,. \end{aligned}$$

[1] We recall that $\bar{\psi}(\mathbf{x}, t) = (\phi^{'*}(\mathbf{x}, t), -\phi^{''*}(\mathbf{x}, t))$ and $\psi(\mathbf{x}, t) = (\phi^{'}(\mathbf{x}, t), \phi^{''}(\mathbf{x}, t))$

The term proportional to A_d^1 vanishes identically, while the term proportional to A_d^0 is independent on the paths and reads (setting to $d = 3$ the number of spatial dimensions)

$$I_1 = \frac{i}{\beta^2 D\hbar} \frac{\sqrt{\det[m]}}{(4\mathrm{Tr}[m]\ \lambda^2\pi)^{3/2}}\ A_d^0\ t\,.$$

Clearly, by symmetry, we find that $S_{I_2} \to I_2 = I_1$.

Let us now consider the cross-term S_{I_3}, which couples forward and backward propagating paths. Translating into the first quantization form, we obtain

$$\begin{aligned}\frac{-2i}{\beta^2 D\hbar} S_{I_3} \ \to\ I_3 \ &= \frac{-2iA_d^0}{\beta^2 D\hbar}\int_0^t dT \int d\mathbf{z}\ \delta_\lambda(\mathbf{z}-\mathbf{X}(T))\delta_\lambda(\mathbf{z}-\mathbf{Y}(T)) \\ &+ \frac{2A_d^1}{\beta^2 D}\int_0^t dT \int d\tau \int d\mathbf{z}\delta(\tau)\,\frac{d}{d\tau}\Big[\ \delta_\lambda(\mathbf{z}-\mathbf{X}(T+\frac{\tau}{2}))\,\delta_\lambda(\mathbf{z}-\mathbf{Y}(T-\frac{\tau}{2}))\Big]\end{aligned}$$

After writing explicitly the smeared representation of the δ-function and evaluating the corresponding Gaussian integrals we find:

$$I_3 = \frac{-\sqrt{\det[m]}}{\beta^2 D\hbar(4\pi\,\mathrm{Tr}[m]\,\lambda^2)^{3/2}}\int_0^t dT\ e^{\frac{-m_{ij}(X-Y)_i(X-Y)_j}{4\,\mathrm{Tr}[m]\,\lambda^2}}\left(i2A_d^0 - \frac{\hbar A_d^1}{2\,\mathrm{Tr}[m]\,\lambda^2}\,m_{ij}(Y-X)_i(\dot{Y}+\dot{X})_j\right)$$

C.2 Perturbative calculation of the exciton probability density

In this appendix we provide some details on the perturbative calculation of the density $P(\mathbf{x},t|\mathbf{x_i})$ to order ξ^2, which has been introduced in section 4.3.

As a first step, we expand the path integral in Eq. (4.30) to order ξ^2

$$\begin{aligned}P_1(\mathbf{y},t|\mathbf{x},0) \ &= \ \frac{\int_{\mathbf{x}}^{\mathbf{y}}\mathcal{D}\mathbf{R}\ e^{-\mathcal{S}_0-\xi^2\mathcal{S}_1}}{\int d\mathbf{y}\int_{\mathbf{x}}^{\mathbf{y}}\mathcal{D}\mathbf{R}\ e^{-\mathcal{S}_0-\xi^2\mathcal{S}_1}} \ \simeq\ \frac{\int_{\mathbf{x}}^{\mathbf{y}}\mathcal{D}\mathbf{R}\ (1-\xi^2\mathcal{S}_1)e^{-\mathcal{S}_0}}{\int d\mathbf{y}\int_{\mathbf{x}}^{\mathbf{y}}\mathcal{D}\mathbf{R}\ (1-\xi^2\mathcal{S}_1)e^{-\mathcal{S}_0}} \\ &\simeq\ P_0(\mathbf{y},t|\mathbf{x},0) - \xi^2\Delta P_1(\mathbf{y},t|\mathbf{x},0)\,,\end{aligned}$$

where the classical probability density reads

$$P_0(\mathbf{y},t|\mathbf{x},0) \ =\ \frac{\int_{\mathbf{x}}^{\mathbf{y}}\mathcal{D}\mathbf{R}\ e^{-\mathcal{S}_0}}{\int d\mathbf{y}\int_{\mathbf{x}}^{\mathbf{y}}\mathcal{D}\mathbf{R}\ e^{-\mathcal{S}_0}}\,, \tag{C.3}$$

and the leading-order quantum corrections read

$$\Delta P_1(\mathbf{y},t|\mathbf{x},0) \ =\ \frac{\int_{\mathbf{x}}^{\mathbf{y}}\mathcal{D}\mathbf{R}\ \mathcal{S}_1 e^{-\mathcal{S}_0}}{\int d\mathbf{y}\int_{\mathbf{x}}^{\mathbf{y}}\mathcal{D}\mathbf{R}\ e^{-\mathcal{S}_0}} - P_0(\mathbf{y},t|\mathbf{x},0)\frac{\int d\mathbf{y}\int_{\mathbf{x}}^{\mathbf{y}}\mathcal{D}\mathbf{R}\ \mathcal{S}_1 e^{-\mathcal{S}_0}}{\int d\mathbf{y}\int_{\mathbf{x}}^{\mathbf{y}}\mathcal{D}\mathbf{R}\ e^{-\mathcal{S}_0}}\,. \tag{C.4}$$

We recall that in the previous equations $\mathcal{S}_0 = \int_0^t d\tau\,\frac{1}{4D_0^b}\dot{\mathbf{R}}^2$ is the free diffusion action, while $\mathcal{S}_1 = \int_0^t d\tau\,(C_4^b\ \dot{\mathbf{R}}^4 - C_2^b\ \dot{\mathbf{R}}^2)$ are the quantum correction derived in section 4.2.3. To perform integrals in Eq.s (C.3) and (C.4), we discretize the time interval $[0,t]$ in N slices, obtaining the following discrete actions

$$\mathcal{S}_0 \ \simeq\ \sum_{i=1}^{N}\ \frac{1}{4D_2^b}\,\frac{\Delta\mathbf{R}_i^2}{\Delta t}\,, \qquad\qquad \mathcal{S}_1 \ \simeq\ \sum_{i=1}^{N}\left(C_4^b\frac{\Delta\mathbf{R}_i^4}{\Delta t^3} - C_2^b\frac{\Delta\mathbf{R}_i^2}{\Delta t}\right)\,,$$

where $\Delta\mathbf{R}_i = \mathbf{R}_i - \mathbf{R}_{i-1}$. The resulting integrals are

$$\int_{\mathbf{x}}^{\mathbf{y}}\mathcal{D}\mathbf{R}\ e^{-\mathcal{S}_0} \ \to\ P_0^N = \int_{R_0=\mathbf{x}}^{R_N=\mathbf{y}}\ \prod_{i=1}^{N-1} d\mathbf{R}_i\, e^{-\frac{1}{4D_2^b}\sum_{i=1}^{N}\frac{\Delta\mathbf{R}_i^2}{\Delta t}}\,, \tag{C.5}$$

$$\int_{\mathbf{x}}^{\mathbf{y}}\mathcal{D}\mathbf{R}\ \mathcal{S}_1 e^{-\mathcal{S}_0} \ \to\ P_1^N = \int_{R_0=\mathbf{x}}^{R_N=\mathbf{y}}\ \prod_{i=1}^{N-1} d\mathbf{R}_i\ \sum_{i=1}^{N}\left(C_4^b\frac{\Delta\mathbf{R}_i^4}{\Delta t^3} - C_2^b\frac{\Delta\mathbf{R}_i^2}{\Delta t}\right) e^{-\frac{1}{4D_2^b}\sum_{i=1}^{N}\frac{\Delta\mathbf{R}_i^2}{\Delta t}}\,. \tag{C.6}$$

To perform these discrete path integrals, we compute integrals slice by slice. This iteration can be evaluated analytically, thanks to the following property of the Gaussian integral:

$$\int d\mathbf{R}_i \; e^{-\frac{(\mathbf{R}_i-\mathbf{R}_{i-1})^2}{4D_2^b\,\Delta t}} \, e^{-\frac{(\mathbf{R}_{i+1}-\mathbf{R}_i)^2}{4D_2^b\,\Delta t}} \quad = \quad e^{-\frac{(\mathbf{R}_{i+1}-\mathbf{R}_{i-1})^2}{4D_2^b\,(2\Delta t)}} \; \left(\frac{4D_2^b\pi\; dt}{2}\right)^{3/2} .$$

Applying the last formula to compute P_0^N in Eq. (C.5), we obtain

$$P_0^N = e^{-\frac{(\mathbf{y}-\mathbf{x})^2}{4D_2^b\,(N\Delta t)}} \; \left(\frac{4D_2^b\pi\; dt}{N}\right)^{3/2(N-1)} ,$$

and taking the continuous limit $N \to \infty$ with $Ndt = t$ we derive the result written in Eq. (4.33).

Analog procedure has been followed to compute the discrete path integral P_1^N, and derive the quantum leading-order corrections of diffusive time evolution in Eq. (4.32).

Appendix D

Details of Chapter 5

D.1 One-particle self-energy corrections

In the Dyson's Equation derived in section 5.1.1, we introduced the one-particle self-energy Σ. This quantity takes into account the effects due to an exchange of a *vibron* along the quantum evolution of a quantum fields $\phi^{'(')}$. In Fig. D we show the Feynman diagram corresponding this loop correction. In the time domain the forward and backward self-energies read

$$\begin{aligned}
\Sigma^{forw}_{\mathbf{qq'}}(\tau,\tau') &= -f^{l}_{\mathbf{q's'}}\left(\frac{2M\gamma}{\beta\hbar^2}\Delta_{lh}(\tau'-\tau)\; G^{(0)+}_{\mathbf{s's}}(\tau) - \frac{i}{2\hbar}\mathcal{V}^{1}_{lh}(\tau'-\tau)\; G^{(0)+}_{\mathbf{s's}}(\tau)\right) f^{h}_{\mathbf{sq}}\,, \\
\Sigma^{back}_{\mathbf{qq'}}(\tau,\tau') &= -f^{l}_{\mathbf{q's'}}\left(\frac{2M\gamma}{\beta\hbar^2}\Delta_{lh}(\tau-\tau')\; G^{(0)-}_{\mathbf{s's}}(\tau) + \frac{i}{2\hbar}\mathcal{V}^{2}_{lh}(\tau-\tau')\; G^{(0)-}_{\mathbf{s's}}(\tau)\right) f^{h}_{\mathbf{sq}}\,.
\end{aligned}$$

where the Δ and $\mathcal{V}$ are the vibronic Green's function described in Appendix A.4, $G^{(0)+}$ and $G^{(0)-}$ are the forward and backward unperturbed Green's functions introduced in Sec. 3.1.2.
In Sec. 5.1.1 we switch on the frequency space by means of a Fourier transformation. In frequency space, the one-particle self-energies Σ are described by a loop integral that we are able to compute. The expression for the forward self-energy is

$$\begin{aligned}
\Sigma^{forw}_{\mathbf{q'q}}(\omega) &= f^{l}_{\mathbf{q's'}}\left[\int d\nu\;\left(\frac{-2M\gamma}{\beta\hbar^2}\widetilde{\Delta}_{lh}(\nu) - \frac{i}{2\hbar}\widetilde{\mathcal{V}}^{1}_{lh}(\nu)\right)\; G^{forw}_{\mathbf{s's}}(\omega-\nu)\right]\; f^{h}_{\mathbf{sq}}\,, \\
&= f^{l}_{\mathbf{q's'}}\; U^{\dagger}_{ln} V^{\dagger}_{\mathbf{s'm}}\left(\frac{i(\epsilon^{0}_{\mathbf{m}}-\omega)+\gamma+\frac{i}{2}\beta\hbar\Omega^{2}_{n}}{\beta M\Omega^{2}_{n}\hbar^{2}(\Omega^{2}_{n}-(\epsilon^{0}_{\mathbf{m}}-\omega)(\epsilon^{0}_{\mathbf{m}}-i\gamma-\omega))}\right) V_{\mathbf{ms}}U_{nh}\; f^{h}_{\mathbf{sq}}\,, \quad \text{(D.1)}
\end{aligned}$$

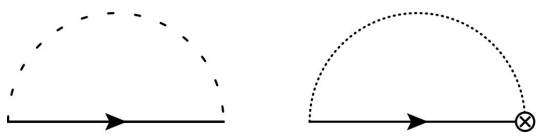

Figure D.1: Diagrammatic representation of Self energy contributions, which enter in Dyson's Equation (5.2) and are computed in Appendix D.1. The single line is the unperturbed Green's function $G^{f0}_{\mathbf{i\ j}}$, the dashed lines represent the two effective interaction terms, Δ_{ij} and $\mathcal{V}_{ij}$, introduced in section 3.1.

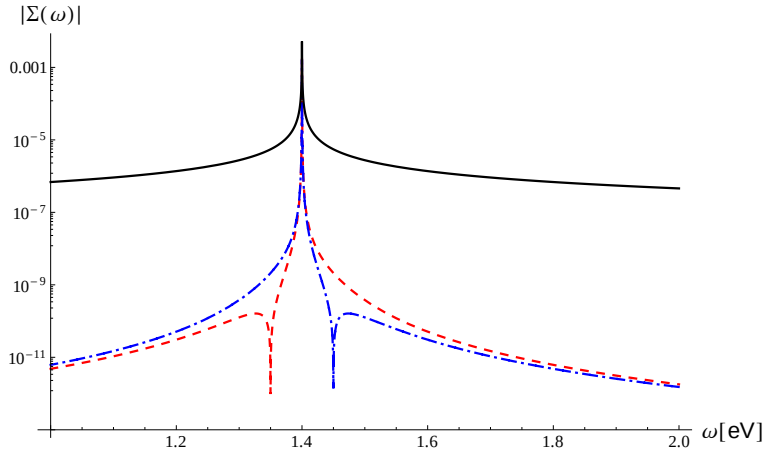

Figure D.2: Absolute value of the real (full line) and imaginary (dashed lines, red forward and blue backward) part of the Self-energy functions in Eq.s (D.1) and (D.2). In the plot we used $\epsilon^0_{\mathbf{m}} = 1.4$ eV, $\Omega_n = 0.001$ eV, $\gamma = 0.1$ eV, $M = 100$ uma, and $T = 300$ K.

while the similar formular for the backward case reads

$$\begin{aligned}\Sigma^{back}_{\mathbf{q'q}}(\omega) &= \int d\nu \left(\frac{-2M\gamma}{\beta\hbar^2}\widetilde{\Delta}_{lh}(\nu) + \frac{i}{2\hbar}\widetilde{\mathcal{V}}^2_{lh}(\nu)\right) f^l_{\mathbf{q's'}}\, G^{back}_{\mathbf{s's}}(\omega-\nu)\, f^h_{\mathbf{sq}}\,, \\ &= f^l_{\mathbf{q's'}}\, U^\dagger_{ln} V^\dagger_{\mathbf{s'm}} \left(\frac{i(\epsilon^0_{\mathbf{m}}-\omega)-\gamma+\frac{i}{2}\beta\hbar\Omega_n^2}{\beta M\Omega_n^2\hbar^2(\Omega_n^2-(\epsilon^0_{\mathbf{m}}-\omega)(\epsilon^0_{\mathbf{m}}+i\gamma-\omega))}\right) V_{\mathbf{ms}}U_{nh}\, f^h_{\mathbf{sq}}\,. \end{aligned} \quad \text{(D.2)}$$

In Fig. D.2 we show the self-energy absolute values in function of the frequencies ω. We notice that these quantity are peaked around the corresponding energy level $\epsilon^0_{\mathbf{m}}$, and the maximum is small in comparison to the energy levels ($\max[\Sigma(\omega)]/\epsilon^0 \sim 10^{-2}$).

D.2 Derivation of Bethe-Salpeter like Equation for Γ

In section D.2, we derived the self-consist Eq. (5.9) for the function Γ. Here, we show the detailed derivation.

Replacing the definition of Γ in Eq. (5.8) in the Ladder expansion (5.7), we obtain

$$\begin{aligned}\int d\omega_1 d\omega_2\, \Gamma_{\mathbf{ij\ kl}}(\omega_1,\ \omega_1-\omega;\ \omega_2,\ \omega_2-\omega) &= \int d\omega_1 \Big\{ G^f_{\mathbf{ik}}(\omega_1)\, G^b_{\mathbf{lj}}(\omega_1-\omega) \\ &+ \int d\nu\, G^f_{\mathbf{ik}}(\omega_1) G^b_{\mathbf{lj}}(\omega_1-\omega)\Delta(\nu) G^f_{\mathbf{ik}}(\omega_1+\nu) G^b_{\mathbf{lj}}(\omega_1-\omega+\nu) \\ &+ \int d\nu d\nu' G^f_{\mathbf{ik}}(\omega_1) G^b_{\mathbf{lj}}(\omega_1-\omega)\Delta(\nu) G^f_{\mathbf{ik}}(\omega_1+\nu) G^b_{\mathbf{lj}}(\omega_1-\omega+\nu)\Delta(\nu') \times \\ &\qquad \times G^f_{\mathbf{ik}}(\omega_1+\nu+\nu') G^b_{\mathbf{lj}}(\omega_1-\omega+\nu+\nu') + \ldots \Big\}\,. \end{aligned} \quad \text{(D.3)}$$

On the right side we introduce a second integral identifying the final frequency ω_2 by means of

dirac deltas,

$$\begin{aligned}\int d\omega_1 d\omega_2\ \Gamma_{\mathbf{ij\ kl}}(\omega_1,\ \omega_1-\omega;\ \omega_2,\ \omega_2-\omega) &= \int d\omega_1 d\omega_2 \Big\{ G^f_{\mathbf{ik}}(\omega_1)\ G^b_{\mathbf{lj}}(\omega_1-\omega)\delta(\omega_1-\omega_2) \\ &+ \int d\nu\ G^f_{\mathbf{ik}}(\omega_1)G^b_{\mathbf{lj}}(\omega_1-\omega)\Delta(\nu)G^f_{\mathbf{ik}}(\omega_1+\nu)G^b_{\mathbf{lj}}(\omega_1-\omega+\nu)\delta(\omega_1+\nu-\omega_2) \\ &+ \int d\nu d\nu' G^f_{\mathbf{ik}}(\omega_1)G^b_{\mathbf{lj}}(\omega_1-\omega)\Delta(\nu)G^f_{\mathbf{ik}}(\omega_1+\nu)G^b_{\mathbf{lj}}(\omega_1-\omega+\nu)\Delta(\nu')\times \\ &\qquad \times G^f_{\mathbf{ik}}(\omega_1+\nu+\nu')G^b_{\mathbf{lj}}(\omega_1-\omega+\nu+\nu')\delta(\omega_1+\nu+\nu'-\omega_2)+\dots\Big\}\,.\end{aligned} \tag{D.4}$$

Then, we collect the interaction term $G^f_{\mathbf{ik}}(\omega_1)G^b_{\mathbf{lj}}(\omega_1-\omega)\Delta(\nu)$:

$$\begin{aligned}\int d\omega_1 d\omega_2\ \Gamma_{\mathbf{ij\ kl}}(\omega_1,\ \omega_1-\omega;\ \omega_2,\ \omega_2-\omega) &= \int d\omega_1 d\omega_2 \Big\{ G^f_{\mathbf{ik}}(\omega_1)\ G^b_{\mathbf{lj}}(\omega_1-\omega)\delta(\omega_1-\omega_2) \\ &+ \int d\nu\ G^f_{\mathbf{ik}}(\omega_1)G^b_{\mathbf{lj}}(\omega_1-\omega)\Delta(\nu)\Big[G^f_{\mathbf{ik}}(\omega_1+\nu)G^b_{\mathbf{lj}}(\omega_1-\omega+\nu)\delta(\omega_1+\nu-\omega_2) \\ &+ \int d\nu' G^f_{\mathbf{ik}}(\omega_1+\nu)G^b_{\mathbf{lj}}(\omega_1-\omega+\nu)\Delta(\nu')G^f_{\mathbf{ik}}(\omega_1+\nu+\nu')G^b_{\mathbf{lj}}(\omega_1-\omega+\nu+\nu')\times \\ &\qquad \times \delta(\omega_1+\nu+\nu'-\omega_2)+\dots\Big]\Big\}\,.\end{aligned} \tag{D.5}$$

Finally, imposing the equivalence between the integrands and identifying the Γ function on the right we obtain Eq. (5.9).

D.3 Lindblad Equation

The most general Markovian and time-homogeneous master equation used to study open quantum system is the Lindblad equation, which reads

$$\frac{d}{dt}\rho_{nm}(t) \;=\; -i\left[H,\rho(t)\right]_{nm} - D_{nm\ ij}\rho_{ij}(t)\,, \tag{D.6}$$

where $D_{nm\ ij}$ is the Redfield tensor which includes the relaxation dynamics [32, 128]. In a simplied manner we can distinguish between four different contribution of the tensor D: (i) $D_{ii\ kk}$ terms describe the incoherent transfer population between i and k quantum states; (ii) $D_{ij\ ij}$ terms describes the dephasing of the $|i\rangle\langle j|$ coherence; (iii) $D_{ij\ kl}$ off-diagonal terms are associated to the coherent motion of the quantum state; (iii) $D_{ii\ kl}$ terms describes the coupling between populations and coherence.

Defining $\rho_{ij}(t) = \mathcal{G}_{ij\ tu}(t)\rho^0_{tu}$ and replacing it in the previous equation, we have the following equation for the corresponding quantum Liouvillian operator

$$\frac{d}{dt}\mathcal{G}_{nm\ tu}(t) \;=\; -iH_{ni}\delta_{jm}\mathcal{G}_{ij\ tu}(t) + iH_{jm}\delta_{ni}\mathcal{G}_{ij\ tu}(t) - D_{nm\ ij}\mathcal{G}_{ij\ tu}(t)\,.$$

Solving this differential, we obtain that time quantum Liouvillian operator for a Lindblad equation reads

$$\mathcal{G}_{nm\ ij}(t) = \int \frac{d\omega}{2\pi} e^{-i\omega t}\ i\Big[\omega\delta_{ni}\delta_{jm} - H_{ni}\delta_{jm} + H_{jm}\delta_{ni} + iD_{nm\ ij}\Big]^{-1}\,.$$

Moving to the energy level basis, where $H_{ab} = \epsilon_a\delta_{ab}$, we obtain

$$\mathcal{G}_{nm\ ij}(t) = \int \frac{d\omega}{2\pi} e^{-i\omega t}\ i\Big[\left(\omega - \epsilon_n + \epsilon_m\right)\delta_{ni}\delta_{jm} + iD_{nm\ ij}\Big]^{-1}$$

Acknowledgments

... In the present context we take the (probably oldfashioned) point of view that the primary purpose of citation is not to allot credit meticulously among one's colleagues but to help the reader to understand the paper, and the references in the text are chosen with this in mind.
Leggett et. all Rev. Mod. Phys. 1989

Non posso che cominciare ringraziando il Prof. Faccioli, ovvero Pietro, a cui va tutta la mia stima accademica per quello che mi ha insegnato in questi intensi tre anni di dottorato, ed umana per la comprensione e la vicinanza mostratami. Lavorare con Pietro è stata un'esperienza unica che mi ha permesso di crescere lavorativamente e umanamente. Non meno importante è stato Silvio, stretto collaboratore con cui ho condiviso tante brillanti discussioni di fisica e non. Inoltre ringrazio tutti i componenti del LISC, tra cui Simone per le interminabili chiacchierate serali, e Giovanni per avermi ricordato con voce gutturale in ogni dove e quando che c'era una tesi da scrivere.

Un libro, o una seconda tesi, servirebbe invece per raccontare gli ultimi 3 anni passati con i colleghi Roberto, Diego, Alessandro, Enrico, Accordini, e Giorgia. Come ad esempio quella volta che qualcuno scrisse ad imperitura memoria questa verita assoluta:

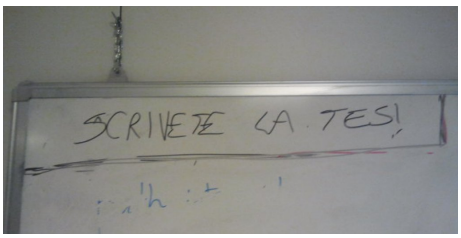

La mia prima impressione di Trento, arrivando da un erasmus a Parigi, fu di un paesello in cui sarebbe stato difficile fare amicizia con i locali e gli altri studenti. Ecco, tale giudizio si è rivelato essere completamente infondanto, dato che la lista degli amici e amiche da ringraziare in questi tre anni si è allungata parecchio.
Inizio partendo dallo Spagnolo sempre pronto a far festa a qualunque ora della notte e del giorno. Sono grato a Fernando e Alessia per essermi stati particolarmente vicini negli ultimi giorni della stesura della tesi come due adorabili "genitori". Non posso immaginare Trento senza l'appuntamento del sabato mattina con Bea, caffè, chiacchiere e puntatina al mercato contadino. Due inseparabili compagni di avvunture, cene, e feste sono stati Manuel e Paolo. Trento sarebbe stata un'altra città se non avessi conosciuto Eleonora, Alessia, Mostarda, Gemma, Roberta, Irena, Nicolò, Luisa ed Elena. Ultimo ma non il meno importante il fratello Giuseppe con cui ho condiviso letti, disavventure e caffè serali.

Sono grato a mammà e papà, che in questi tre lunghi anni mi hanno sostenuto e mi sono stati vicini nei momenti più difficili, ed anche la mia sorellina Mara, che tutti fa disperare ma a cui tutti vogliano bene.

In questi anni ci sono stati anche amici lontani che però mi sono stati vicini: Eugenio che puntualmente ogni Natale è passato a trovarmi, Sandro e Silvia che invece sono stati la mia meta di villeggiatura estiva in questi 3 anni, e Giulia che nei momenti più difficili è sempre stata presente

telematicamente. Concludo con Баба Яга una persona che si è aggiunta solo ultimamente alle persone che meritano di essere citate in questi ringraziamenti ma che nonostante questo ha è letto più della metà delle formule incomprensibili di questa tesi.

Bibliography

[1] E. Schneider, S. a Beccara, and P. Faccioli, *Phys. Rev. B* **88**, 08542 (2013).

[2] E. Schneider, and P. Faccioli, *Phys. Rev. B* **89**, 134305 (2014).

[3] V. May and O. Kühn, *Charge and Energy Transfer in Molecular Systems*, 2nd ed. (WILEY-VCH, Wreinheim, 2004).

[4] H.-P. Breuer and F. Petruccione, *The Theory of Open Quantum Systems*, 2nd ed. (Pearson Education Limited, Harlow, 2001).

[5] Á. Rivas, S.F. Huelga, *Open Quantum Systems: An Introduction*, Springer (2011).

[6] L. A. Pachón, and P. Brumer, *Phys. Chem. Chem. Phys.* **14**, 10094-10108 (2012).

[7] S. Nakajima, *Progr. Theor. Phys.*, **20**, 948-959, (1958).

[8] R. Zwanzig, *J. Chem. Phys.*, **33**, 1338-1341, (1960).

[9] A. Ishizaki, and G. R. Flemig, *J. Chem. Phys.* **130**, 234111 (2009).

[10] A. Ishizaki, and G. R. Flemig, *Proc. Natl. Acad. Sci. USA* **106**, 17255-17260 (2009).

[11] B. Hein, C. Kreisbeck, T. Kramer, and M. Rodríguez, *New J. Phys.* **14**, 023018, (2012).

[12] A. Ishizaki, and G. R. Flemig, *J. Chem. Phys.* **130**, 234110 (2009).

[13] J. Prior, A.W. Chin, S.F. Huelga and M.B. Plenio. *Phys. Rev. Lett.* **105**, 050404 (2010).

[14] A.W. Chin, A. Rivas, S.F. Huelga and M.B. Plenio. *J. Math. Phys.* **51**, 092109 (2010).

[15] N. Makri, and D. E. Makarov, *J. Chem. Phys.* **102**, 4600-4610 (1195).

[16] N. Makri, and D. E. Makarov, *J. Chem. Phys.* **102**, 4611-4618 (1995).

[17] L. Mühlbacher, J. Ankerhold, and C. Escher, *J. Chem. Phys.* **121**, 12696 (2004).

[18] L. Mühlbacher, and J. Ankerhold, *J. Chem. Phys.* **122**, 184715 (2005).

[19] R. P. Feynman and F. L. Vernon, *Ann. Phys.* **24**, 118 (1963).

[20] R. Egger and C. H. Mak, *Phys. Rev. B* **50**, 15210 (1994).

[21] P. Huo, and D. F. Coker, *J. Chem. Phys.* **135**, 201101 (2011).

[22] P. Huo, and D. F. Coker, *Mol. Phys.* **110**, 1035-1052 (2012).

[23] S. Shim, P. Rebentrost, S. Valleau, and A. Aspuru-Guzik, *Biophysical Journal* **102**, 649-662 (2012).

[24] R. Gutiérrez, R. A. Caetano, B. P. Woiczikowski, T. Kubař, M. Elstner, and G. Cuniberti, *Phys. Rev. Lett.* **102**, 208102 (2009).

[25] P. B. Woiczikowski, T. Kubař, R. Gutiérrez, R. A. Caetano, G. Cuniberti, and M. Elstner, *J. Chem. Phys.* **130**, 215104 (2009).

[26] D. Cheung, D. P. McMahon, and A. Troisi, *J. Phys. Chem. B* **113**, 9393 (2009).

[27] N. Lambert, Y.-N. Chen, Y.-C. Cheng, C.-M. Li, G.-Y. Chen, and F. Nori, *Nat. Physics* **9**, 10-18 (2013).

[28] M. Mohseni, Y. Omar, G.S. Engel, and M. B. Plenio, *Quantum effects in biology*, 1st ed. (Cambridge 2014).

[29] A. W. Chin, J. Prior, R. Rosenbach, F. Caycedo-Soler, S. F. Huelga, and M. B. Plenio, *Nature Phys.* **9**, 113 (2013).

[30] G. Panitchayangkoona, D. Hayesa, K. A. Fransteda, J. R. Carama, E. Harela, J. Wenb, R. E. Blankenship, and G. S. Engel, *Proc. Nat. Acad. Soc. USA* **107**, 12766 (2010).

[31] R. J. Cogdell, A. Gall, and J. Köhler, *Q. Rev. Biophys.* **39**, 227 (2006)

[32] E. Collini, *Chem. Soc. Rev.* **42**, 4932 (2013).

[33] G. S. Engel, T. R. Calhoun, E. L. Read, T.-K. Ahn, T. Mancal, Y.-C. Cheng, R. E. Blankenship, and G. R. Fleming, *Nature* **446**, 782 (2007).

[34] E. Collini, C.Y. Wong, K.E. Wilk, P.M.G Curmi, P. Brumer, and G. D. Scholes, *Nature* **463**, 644 (2010).

[35] S. F. Huelga, and M. B. Plenio, *Contemporary Physics* **54**, 181-207 (2013).

[36] P. Rebentrost, M. Mohseni, I. Kassal, S. Llyod, and A. Aspuru-Guzik, *New J. Phys.* **11**, 033003 (2009).

[37] M.B. Plenio and S.F. Huelga, *New J. Phys.* **10**, 113019 (2008).

[38] F. Caruso, A.W. Chin, A. Datta, S.F. Huelga and M.B. Plenio, *J. Chem. Phys.* **131**, 105106 (2009).

[39] P.W. Anderson, *Phys. Rev.* **109**, 1492 (1958).

[40] R. Benzi, A. Sutera, and A. Vulpiani, *J. Phys. A: Math. Gen.* **14**, L453 (1981).

[41] P. Rebentrost, M. Mohseni, and A. Aspuru-Guzik, *J. Phys. Chem. B* **113**, 9942 (2009).

[42] M. Mohseni, A. Shabani, S. Lloyd, and H. Rabitz, *J. Chem. Phys.* **140**, 035102 (2014).

[43] J. Moix, J. Wu, P. Huo, D. Coker, and J. Cao, *J. Phys. Chem. Lett.* **2**, 3045 (2011).

[44] E. Rivera, D. Montemayor, M. Masia, and D. Coker, *J. Phys. Chem. B* **117**, 5510-5521 (2013).

[45] M. Mohseni, P. Rebentrost, S. Lloyd, and A. Aspuru-Guzik, *J. Chem. Phys.* **129**, 174106 (2008).

[46] M.B. Plenio, J. Almeida, and S.F. Huelga, *J. Chem. Phys.* **139**, 235102 (2013).

[47] V. Tiwari, W. K. Peters, and D. M. Jonas, *Proc. Natl. Acad. Sci. USA* **110**, 1203 (2013).

[48] A. Chenu, N. Christensson, H. F. Kauffmann, T. Mančal, *Scientific reports* **3**, 2029 (2013).

[49] M. Ferretti, V. I. Novoderezhkin, E. Romero, R. Augulis, A. Pandit, D. Zigmantasc and R. van Grondelle, *Phys. Chem. Chem. Phys.* **16**, 9930 (2014).

[50] F. Fassioli, A. Olaya-Castro, and G. D. Scholes, *J. Phys. Chem. Lett.* **3**, 3136âĹŠ3142 (2012).

[51] D. B. Turner, P. C. Arpin, S. D. McClure, D. J. Ulness, and G. D. Scholes, *Nature Communications* **4**, 2298 (2013).

[52] R. de J. León-Montiel, and J. P. Torres, *Phys. Rev. Lett.* **110**, 218101 (2013).

[53] E. J. O'Reilly, and A. Olaya-Castro, *Nature Communications* **5**, 3012 (2014).

[54] J. R. Heath, and M. A. Ratner, *Phys. Today* **43**, 1497-1561 (2003).

[55] V. Coropceanu, J. Cornil, D. A. da Silva, Y. Olivier, R. Silbey, and J. L. Brèdas, *Chem. Rev.* **107**, 926 (2007).

[56] R. Gutierrez, and G. Cuniberti, *Journal of Self-Assembly and Molecular Electronics* **1**, 1-39 (2013).

[57] A. Troisi, *Chem. Soc. Rev.* **40**, 2347-2358 (2011).

[58] T. Frederiksen, M. Paulsson, M. Brandbyge, and A.-P. Jauho, *Phys. Rev. B* **75**, 205413 (2007).

[59] N. J. Tao, *Nature Nanotech.* **1**, 173 (2006).

[60] E. A. Weiss, M. R. Wasielewski, and M. A. Ratner, *Top. Curr. Chem.* **257**, 103 (2005).

[61] Y. A. Berlin, A. L. Burin, and M. A. Ratner, *Top. Curr. Chem.* **275**, 61 (2002).

[62] R. Gutiérrez, R. A. Caetano, B. P. Woiczikowski, T. Kubař, M. Elstner, and G. Cuniberti, *New J. Phys.* **12**, 023022 (2010).

[63] C. D. Dimitrakopoulosand P. R. L. Malenfant, *Adv. Mater.* **14**, 99 (2002).

[64] H. Klauk, *Chem. Soc. Rev.* **39**, 2643 (2010).

[65] Y. Yuan, G. Giri, L. Ayzner, A. P. Zoombelt, S. C. B. Mannsfeld, J. Chen, D. Nordlund, M. F. Toney, J. Huang, and Z. Bao, *Nature Communications* **5**, 3005 (2014).

[66] L. Torsi, N. Cioffi, C. Di Franco, L. Sabbatini, P. G. Zambonin,and T. Bleve-Zacheo, *Solid-State Electr.* **45**, 1479 (2001).

[67] L. Torsiand A. Dodabalapur, *Anl. Chem.* **77**, 380 (2005).

[68] H. Sirringhaus, N. Tessler, and H. Friend, *Science* **280**, 17419 (1998).

[69] A. Troisi, and G. Orlandi, *Phys. Rev. Lett.* **96**, 086601 (2006).

[70] A. Troisi, D. L. Cheung, and D. Andrienko, *Phys. Rev. Lett.* **102**, 116602 (2009).

[71] F. Grozema, P. T. van Duijnen, Y. A. Berlin, M.A. Ratner, and L. D. A. Siebbeles, *J. Phys. Chem. C* **111**, 11104 (2007).

[72] P. Prins, F. Grozema, F. Galbrecht, U. Scherf, and L. D. A. Siebbeles, *J. Phys. Chem. C* **111**, 11104 (2007).

[73] D. P. McMahon, D. L. Cheung, F. Goris, F. Dacuña, A. Salleo, and A. Troisi, *J. Phys. Chem. C* **115**, 19386 (2011).

[74] J. E. Northrup, *Phys. Rev. E* **76**, 245202 (2007).

[75] Y.-K. Lan, and C.-I Huang, *J. Phys. Chem. B* **112**, 14857 (2008).

[76] D. P. McMahon, and A. Troisi, *ChemPhysChem* **11**, 2067 (2010).

[77] A. Troisi, and D. L. Cheung, *Phys. Rev. Lett.* **102**, 116602 (2009).

[78] L. Boninsegna and P. Faccioli, *J. Chem. Phys.* **136**, 214111 (2012).

[79] T. Nelson, S. Fernandez-Alberti, A. E. Roitberg, and S. Tretiak, *Accounts of Chemical Research* **47**, 1155 (2014).

[80] B. Baumeier, J. Kirkpatrick, and D. Andrienko, *Phys. Chem. Chem. Phys.* **12**, 11103 (2010).

[81] T. Kubař, P. Woiczikowski, G. Cuniberti, and M. Elstner, *J. Phys. Chem. B* **112**, 7937 (2008).

[82] M. Elstner et all, *Phys. Rev. B* **58**, 7260 (1998).

[83] S. Tretiak, and S. Mukamel, *Chem. Rev.* **102**, 3171 (2002).

[84] T. Minami, S. Tretiak, V. Chernyak, and S. Mukamel, *Journal of luminescence* **87**, 115-118 (2000).

[85] J. Aragó, and A. Troisi, *Phys. Rev. Lett.* **114**, 026402 (2015).

[86] A. O. Caldeira and A. J. Leggett, *Phys. Rev. Lett.* **46**, 211 (1981).

[87] H. Grabert, P. Schramm, and G.-L. Ingold, *Phys. Rep.* **168**, 115 (1988).

[88] A. O. Caldeira and A. J. Leggett, *Ann. Phys.* **149**, 374 (1983).

[89] A. Schmid *J. Low Temp. Phys.* **49**, 609 (1982).

[90] L. Boninsegna, *Microscopic Real-time Dynamics of Molecular Quantum Wires in Solution* (Master Thesis, University of Trento, unpublished, 2012).

[91] L. Onsager and S. Machlup, *Phys. Rev.* **91**, 1505 (1953).

[92] E. Autieri, P. Faccioli, M. Sega, F. Pederiva, and H. Orland, *J Chem Phys* **130**, 064106 (2009).

[93] G. Mazzola, S. A. Beccara, P. Faccioli, and H. Orland, *J Chem Phys* **134**, 164109 (2011).

[94] P. Faccioli, M. Sega, F. Pederiva, and H. Orland, *Phys Rev Lett* **97**, 108101 (2006).

[95] S. a Beccara, T. Škrbić, R. Covino, and P. Faccioli, *Proc Natl Acad Sci USA* **109**, 2330 (2012).

[96] A. Navarra, J. Tribbia, and G. Conti, *PLOS* **8**, 67022 (2013).

[97] F. Scholz, *Conducting Polymers: A New Era in Electrochemistry* (Monographs in Electrochemistry, Springer, Heidelberg, 2008).

[98] A. Assadi, C. Svensson, M. Willander, and O. Inganas, *Appl. Phys. Lett.* **53**, 195 (1988).

[99] B. Aradi, B. Hourahine, and T. Frauenheim, *J. Phys. Chem. A* **111**, 5678 (2007).

[100] D. Alberga, *Modelli molecolari per i semiconduttori polimerici P3HT e PBTTT.* (Master Thesis, University of Bari, unpublished, 2012).

[101] B. Müller and A. Schäfer, *Phys. Rev. C* **73**, 054905 (2006).

[102] A. Diaz-Torres, *Phys. Rev. C* **81**, 041603 (2010).

[103] P. Lepage, arXiv:nucl-th/9706029 (unpublished).

[104] A. Manohar, arXiv:hep-ph/9606222 (unpublished)

[105] P. Faccioli and E. Lipparini, *Phys. Rev. B* **80**, 045405 (2009)

[106] M. Bazzanella, P. Faccioli and E. Lipparini, *Phys. Rev. B* **82**, 205422 (2010)

[107] O. Corradini, P. Faccioli and H. Orland, *Phys. Rev. E* **80**, 061112 (2009).

[108] P. Faccioli, *J. Chem. Phys.* **133**, 164106 (2010).

[109] T. Ichinomiya, *J. Comp. Phys.* **251**, 319 (2013).

[110] L. D. Landau, E. M. Lifšits, *Teoria dei Campi*, (Editori Riuniti, Roma, 2004).

[111] M. Le Bellac, *Quantum and Statistical Field Theory*, (Oxford University Press Inc., New York, 1991).

[112] J. U. Wallace, *Carrier Mobility in Organic Charge Transport Materials: Methods of Measurement, Analysis, and Modulation*, PhD thesis, Department of Chemical Engineering of the University of Rochester (2009) (unpublished).

[113] A. Troisi, *J. Chem. Phys.* **134**, 034702 (2011)

[114] L. Machura, M. Kostur, P. Hänggi, P. Talkner and J. Luczka, *Phys. Rev. E* **70**, 031107 (2004).

[115] W. T. Coffey, Y. P. Kalmykov, S. V. Titov, and B. P. Mulligan, *J. Phys. A* **40**, F91(2007).

[116] W. T. Coffey, Y. P. Kalmykov, S. V. Titov, L. Cleary, *Phys. Rev. E* **78** 031114 (2008).

[117] S. a Beccara, G. Garberoglio, and P. Faccioli, *J. Chem. Phys.* **135**, 034103 (2011).

[118] E. Conwell, S. Rakhmanova, *Proc. Natl. Acad. Sci. USA* 97, 4556 (2000)

[119] M.T.W. Milder, B. Brüggemann, R. van Grondelle, and J.L. Herek, *Photosynthesis Research* **104**, 257 (2010).

[120] J. M. Moix, Y. Zhao, and J. S. Cao, *Phys. Rev. B* **85**, 115412 (2012)

[121] S. Mukamel, *Principles of Nonlinear Optical Spectroscopy*, Oxford Series on Optical and Imaging Sciences (1999).

[122] Minhaeng Cho, *Two-Dimensional Optical Spectroscopy*, (CRC press,New York, 2009).

[123] A.M. Brańczyk, D.B. Turner, and G.D. Scholes, *Annalen der Physik* **526**, 31-49 (2014).

[124] W. M. Zhang H. Feng and R. Gilmore, *Rev. Mod. Phys.* **62**, 867 (1990).

[125] M. W. Y. Tu and W. M. Zhang, *Phys. Rev. B* **78**, 235311 (2008).

[126] F. Schwabl, *Statistical Mechanics* (2nd Ed.). Springer-Verlag. Berlin-Heidelberg, 2006.

[127] A. Adib, *J. Phys. Chem. B* **112** (2008), 5910.

[128] Y.-C. Cheng, and G. Fleming, *Ann. Rev. Phys. Chem.* **60**, 241 (2009).